Apparent inverted temperature gradient across the Lesser Himalayan Sequence: Raman spectroscopy of carbonaceous material in the eastern Bhutan Himalaya

Nicholas Whynot

Submitted in Partial Fulfillment of the Requirements
For the Degree of Bachelor of Sciences, Honours
Department of Earth Sciences
Dalhousie, Halifax, Nova Scotia
March 2010

DALHOUSIE UNIVERSITY
Inspiring Minds

Department of Earth Sciences
Halifax, Nova Scotia
Canada B3H 4J1
(902) 494-2358
FAX (902) 494-6889

DATE: April 26th 2010

AUTHOR: Nicholas Whynot

TITLE: Apparent inverted temperature gradient across the Lesser Himalayan Sequence: Raman spectroscopy of carbonaceous material in the eastern Bhutan Himalaya

Degree: Earth science Convocation: May 27th Year: 2010

TABLE OF FIGURES

TABLE OF TABLES

ABSTRACT

One of the confusing features of the Himalayan Orogen is the inverted metamorphic temperature gradient. Along the orogen the dominant foliation, the lithotectonic units, and the main structures separating them dip dominantly to the north. Therefore, from south to north, one advances into progressively higher structural levels. However, from lowest structural levels of the Lesser Himalayan sequence (LHS) in the south, to the top of the Greater Himalayan sequence (GHS) in the north, the peak metamorphic temperatures increase rather than decrease. In the LHS, which consists dominantly of slates and quartzites, the metamorphic grade ranges from lower to upper greenschist facies conditions. This is shown by index metamorphic minerals, but quantitative thermobarometry is lacking and difficult to do because of absence of suitable mineral assemblages

In this study we apply Raman spectroscopy of carbonaceous material (Beyssac et al. 2002) from samples of slates collected from the LHS in the eastern Bhutan. The 16 samples are evenly distributed between the Main Boundary thrust (MBT) at the base, and the Main Central thrust (MCT) at the top. Results from this study indicate a progressive increase of temperature from south to north. In addition, we observe two jumps in temperature. One in the middle of the LHS is probably due to a younger thrust within the LHS, the Shumar thrust. The second temperature jump is across the MCT separating the LHS and the GHS. The latter jump is determined by combining the Raman spectroscopy data and the published data based on thermobarometry.

These are the first quantitative temperature data for the LHS in the eastern Himalaya; only one equivalent study exists in the central Nepal. The temperature gradient which was determined from this study across the LHS will be combined and compared with field data from Nepal. From the information obtained from this study along with pre-existing numerical models, predictions of potential mechanisms for the inverted metamorphic gradient were determined across the LHS in eastern Bhutan.

Key words: Himalaya, inverted metamorphic gradient, graphite, Raman spectroscopy, RSCM, Lesser Himalayan Sequence, Main Central thrust, Shumar thrust

Acknowledgements

I would like to express my thanks and great appreciation towards my supervisor, Djordje Grujic, whose great enthusiasm and knowledge of the Himalayan Orogen, paired with incredible patience, helped in the understanding of the topic; Dawn Kellett for helping with understanding and utilizing the Raman technique; and Kevin Hewitt for providing help and information about the Raman instrument at Dalhousie.

1.0 INTRODUCTION

The purpose of this study is to analyze the inverted metamorphic gradient across the Lesser Himalayan Sequence (LHS) in eastern Bhutan through structural and metamorphic analyses. There are several conclusions that will be determined from this study: (a) determine the temperature gradient along a N-S transect through the LHS; (b) determine if there is an inverted metamorphic gradient across the LHS; (c) determine if there are any jumps in temperature

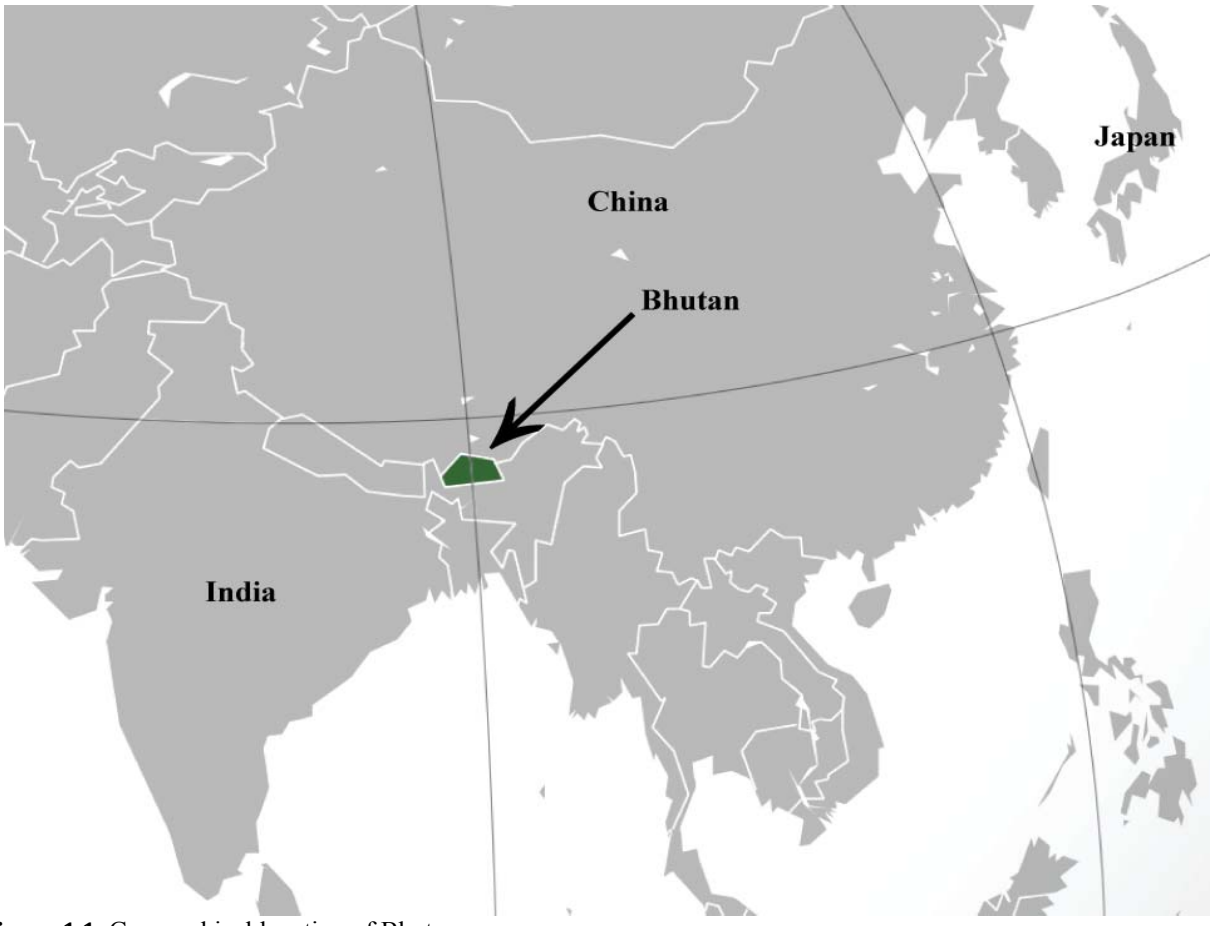

Figure 1.1. Geographical location of Bhutan.

throughout the LHS, and propose a causation for these jumps; and (d) compare observations made in eastern Bhutan to equivalent observations in central Nepal.

1.1 Geography of Bhutan

The Kingdom of Bhutan is a small southern Asian country that is situated between 88°30' - 92°30' E and 26°30' - 28°30' N and is bordered by India to the east, south, and west, and Tibet to the north (Fig 1.1). For a country that is ~38,000 km², which roughly the same size as Switzerland, it has a dramatic relief. In the southern portion of Bhutan the average elevation is ~200 m, but this drastically increases with increasing latitude, with most peaks in northern Bhutan reaching over 7000 m. The highest peak in Bhutan, Kula Kangri, reaches a maximum height of 7,553 m. Climate also varies from the south to the north. In the southern regions the climate is subtropical, but becomes a more alpine-like climate in the northern portions, with the exception of the low-lying valleys in the north, which experience a semi-subtropical climate. Also, throughout Bhutan precipitation is dominated by the Indian Summer Monsoon. The mean annual rainfall along the foothills of the Himalaya ranges from ~6 m/yr in the west to ~4 m/yr in the east (Grujic et al. 2006).

1.2 Previous Work

One of the most influential studies conducted in the Himalaya was undertaken by Gansser (1964). Gansser determined the first order structures of the Himalaya and was the first to propose that the entire Himalaya was composed of metamorphic rocks that had an inverted temperature gradient, in other words with increasing structural level the temperature increases. He deduced this from mineralogical assemblages and mapping the metamorphic isograds. Since then there have been many studies and several models proposed to determine actual causes for the inverted metamorphic sequence in the LHS.

Initially Le Fort (1975) developed a very influential hypothesis that emplacement of the Greater Himalayan allochthon along the Main Central thrust system led to inverted

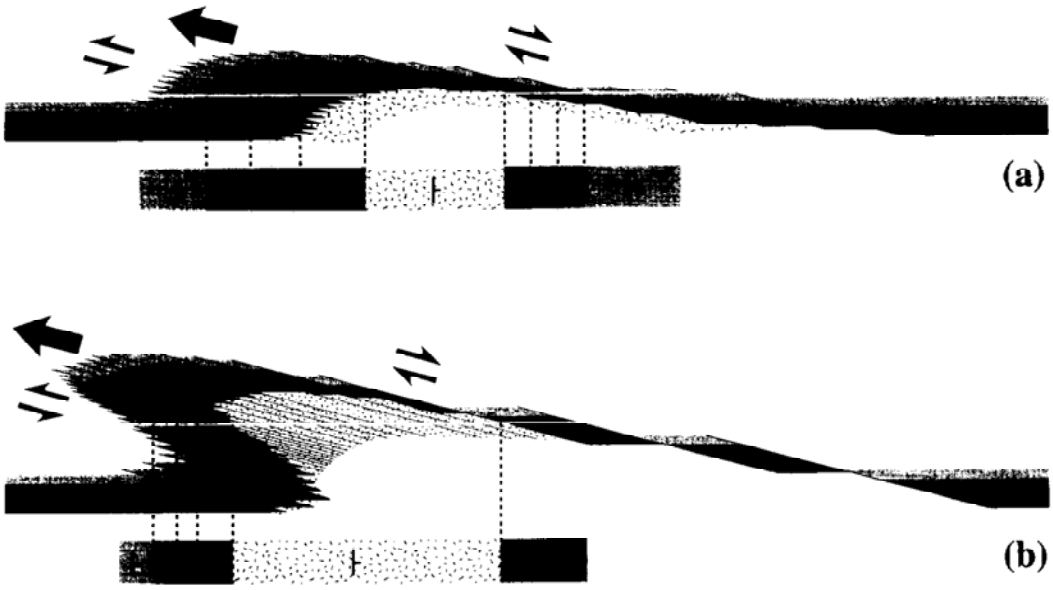

Figure 1.2. This model shows the amount of apparent inverted metamorphic field gradient corresponding to the amount of extrusion of the HHC. Figure (a) corresponds to a low degree of extrusion, and in turn does not produce any visible inverted metamorphic gradients; (b) shows a high degree of extrusion and shows an inverted metamorphic gradient. Image from Gurjic et al. 1996.

metamorphism of the Lesser Himalayan footwall and "refrigeration" of the hanging wall. Eventually, Pêcher (1989) expanded on LeFort's (1975) theory stating that the metamorphic gradient found below the MCT is due to a primary prograde pattern developed during the MCT shearing. In other words, the thrusting of the hot Greater Himalayan Sequence (GHS) over top of the Lesser Himalayan Sequence (LHS) created an "ironing effect." This means that the superimposed GHS heated up the underlying LHS and created an inverted metamorphic sequence structurally downward (Pêcher, 1989). Areas far behind the thrust tip, i.e. closest to the Main Boundary thrust, were not significantly metamorphosed. However, one discrepancy noted by Pêcher (1989) was the absence of low temperature/high pressure parageneses.

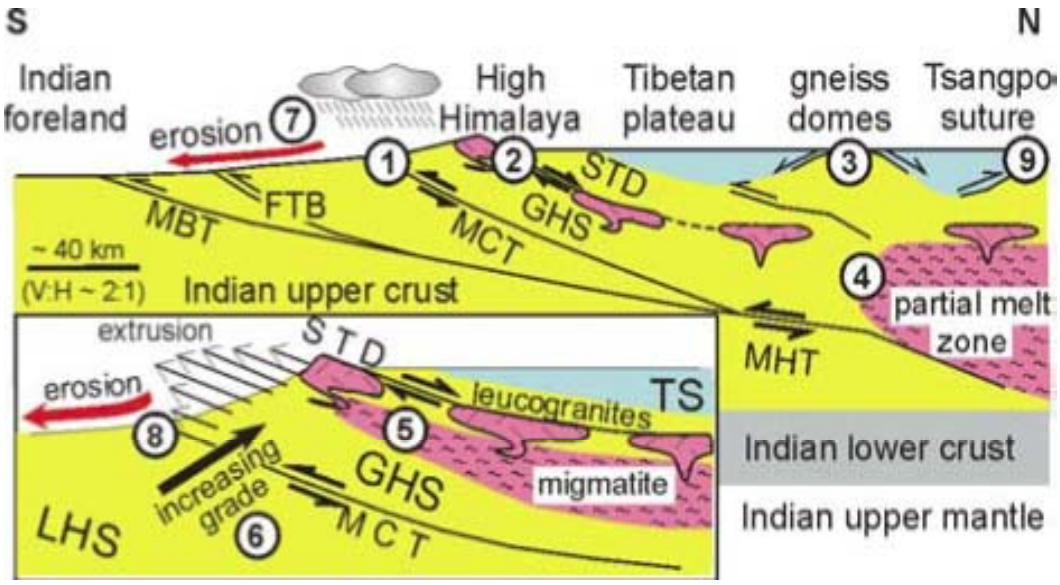

Figure 1.3. A schematic section of the entire Himalaya showing the subduction of the rigid LHS beneath the more ductile GHS. Shown is the sense of shear on the MCT and STD as a result of this extrusion. Figure from Beaumont et al. 2001.

Another main hypothesis for the inverted metamorphic gradient within the LHS and GHS was proposed by Grujic et al. (1996) and Jamieson et al. (1996). The inverted gradient is presumed, in very simplified terms, to be due to pervasive ductile shearing of the isotherms within the Main Central Thrust Zone, and not due to an already existing inverted metamorphic gradient (Grujic et al., 1996). This ductile shearing is thought to be produced by the extrusion of the High Himalaya Crystalline, or the GHS (Fig 1.2). This extrusion of the HHC can be explained by a thrust that is formed above a rigid underthrusting plate (Lesser Himalaya) and a rigid backstop (Tethyan-Tibet Himalaya). The South Tibetan Detachment (STD) therefore forms as a result of the HHC extrusion and not as a result of north-south extension. In relation to the MCT, this extrusion would also create the thrusting-sense of the MCT (Fig 1.3). The main hypothesis for an inverted metamorphic gradient from Grujic et al. 1996, and Jamieson et al. 1996 is directly due to this ductile extrusion of the HHC. This is thought to have occurred by physically altering the isotherms within the lithosphere itself, and creating a sigmoidal relationship between the isotherms. This is interpreted to have occurred by distributed ductile shear within the MCT zone and extrusion of the hot GHS channel above the LHS (Beaumont et

al. 2001). Models produced by Jamieson et al. (2006) show snapshots in time of this ductile extrusion of the GHS and also indicate that the isotherms present in the LHS and GHS do not represent a frozen set of isotherms in time, however, they show a combination of deformation of the isotherms and concurrent shearing along the MCT. This is unlike other theories which have proposed that the metamorphic isograds have become sheared and deformed. Although studies such as Grujic et al. (1996) say that shearing of isograds is possible, they do not believe this is responsible for the inverted metamorphic gradient within the Himalaya.

Hodges (2000) further discusses the inverted metamorphic sequence in the LHS and states that more recent models such as recumbent folding, thrust imbrication, or distributed shearing of a pre-existing, right-way-up metamorphic sequence in the Greater Himalayan zone. However, this does not describe the inverted sequence in the LHS in full. Harrison et al. (1997) discuss that the inverted sequence in the LHS is somehow related to out-of-sequence faulting on the MCT. This theory stated that the currently exposed GHS was once a mid-crustal levels in the hangingwall of a low angle décollment thrust throughout the early- and mid-Miocene. Emplacement of the exposed parts of the GHS, as well as burial metamorphism of the LHS footwall, is related to break-back thrusting on the MCT (Harrison et al. 1997). Although this model produces the results we see in the LHS, it does not predict the inverted metamorphic gradient in the GHS (Hodges, 2000). Hodges (2000) also disagrees with the thrust imbrication model, saying that since the mapped isograds do not correspond with the mapped structural discontinuities (i.e. Shumar thrust, MCT), it would be difficult to argue that deformation of the isograds due to thrust imbrication has occurred.

One of the more recent studies conducted by Bollinger et al. (2004) had proposed yet another theory for the inverted metamorphic sequence. In this study of the LHS in central Nepal, they state that the inverted metamorphic sequence was formed simultaneously from accretion of

the LHS from the Indian plate passive margin onto the Eurasian plate at mid-crustal depths, which is known as underplating, and by postmetamorphic shearing (Bollinger et al. 2004). This underplating and postmetamorphic shearing was dated to have occurred at ~20 Ma (Bollinger et al. 2004). Postmetamorphic shearing would produce an inverted metamorphic sequence in the sense that initially the isograds were flat lying and uniform. Over time as the continental convergence occurred, these isograds became more and more deformed, resulting in recumbent-fold isograds. This would then produce the inverted metamorphic sequence we see today. It would be similar to what is seen in Figure 1.2, however with isograds and not isotherms.

Recently a more quantitative approach was derived, which included the use of a Raman spectrometer for analyzing peak metamorphic temperatures of graphite-bearing rocks. Beyssac et al. (2004); Bollinger et al. (2004); and Célérier et al. (2009) have conducted studies and produced results from this technique, known as Raman spectroscopy of carbonaceous material (RSCM). Their study areas within the Lesser Himalayan Sequence (LHS) ranged from Nepal (Beyssac et al. 2004; Bollinger et al. 2004), to the LHS in India (Célérier et al. 2009), and within the LHS of eastern Bhutan (Daniel et al. 2003). As a combination of all their studies they have concluded that there is in fact an inverted metamorphic sequence within the LHS, and the peak metamorphic temperatures in the LHS range from ~570 °C just below the Main Central thrust (MCT) to ~330 °C at the base of the LHS.

1.3 General Methodology

The RSCM technique has been recently used by Beyssac et al. (2002) as a thermometer in which an empirical formula was derived and used to calculate peak metamorphic temperatures of graphite-bearing rocks. However, one downfall of this thermometer was the range in which it was capable of accurately calculating temperatures, which ranges from 330 to 650 °C (Beyssac et al. 2002). Several years later a second study based around the RSCM technique was conducted

by Rahl et al. (2005), where a second empirical formula was derived and extended the range of temperatures that could be calculated to 100 to 700 °C. This study will be using RSCM to calculate peak metamorphic temperature across the LHS. Also, structural and metamorphic analysis of rock samples using a petrographic microscope will be completed.

2.0 GEOLOGY OF EASTERN BHUTAN

2.1 Background Geology of Eastern Bhutan

The geology of the Bhutan Himalaya consists of packages of rock that are separated along major brittle faults and ductile shear zones. These tectonic boundaries are from the south to the north of the Himalayas the Main Frontal thrust , Main Boundary thrust, Main Central thrust, South Tibetan Detachment system and the Indus-Yalu suture zone. The latter separating the Indian and Tibetan (Asian) plates. The lithotectonic units in between represent the rocks associated with the Indian plate, Quaternary Indo-Gangetic foreland basin, Siwaliks or Subhimalayan (Negeoene foreland basin), Lesser Himalayan sequence (LHS), Greater Himalayan sequence (GHS) and, Tethyan Himalayan strata.

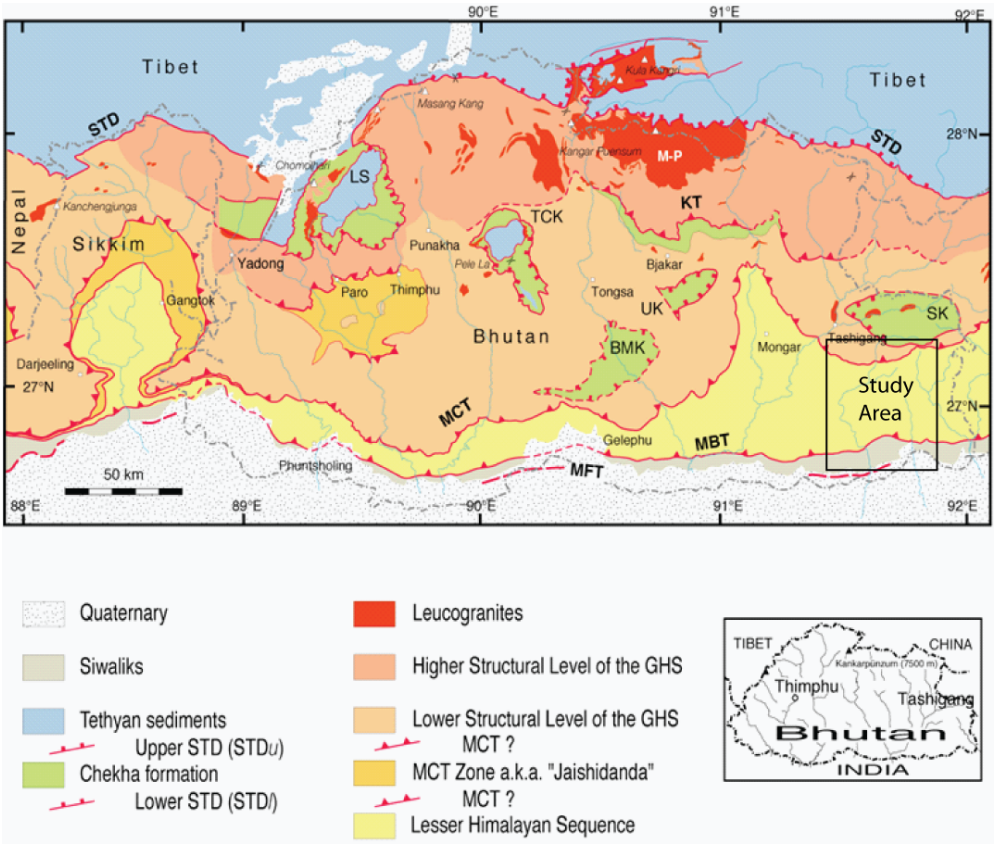

Figure 2.1. Geological map of Bhutan showing the main lithotectonic units, including the Lesser Himalayan Sequence along with the study area indicated. Map modified from Gansser 1983.

The Main Frontal thrust (MFT) is a north dipping thrust fault that separates the Subhimalayan zone from the Indo-Gangetic Plain and represents the toe of the Himalayan orogenic wedge. The geometry of this feature is inferred from the geomorphologcal features, such as defined scarps cutting river terraces, and structural geology of the hanging wall. There are two depictions of the MFT; Yeats and Lillie (1991) state that the MFT is a decollement thrust with no basement involvement as far north as the surface trace of the Main Boundary thrust. The second hypothesis supported by Coward et al. (1988), DeCelles et al. (1998), Molnar (1984), Schelling (1992), and Schelling and Arita (1991) states that the MFT is a low-angle, basal thrust along which the India plate is subducting beneath the Himalaya and southern Tibet (Hodges, 2000). Geodetic measurements indicate that much of the modern convergence between India and Eurasia is occurring on the MFT (Bilham et al., 1997).

The Subhimalaya Zone is part of the Neogene and Quaternary foreland basin of the Himalayas lying between the LHS and the "active" thrust front of the orogen (Hodges, 2000). The most noticeable characteristic of the Subhimalaya of Bhutan is the discontinuity of the Siwalik Group (see Fig 2.1). In Bhutan, this group of synorogenic sediments is discontinuous, with 20-40 km long portions of the Siwalik sediments either covered by Quaternary sediments, overridden by the Main Boundary thrust (MBT), or appear to not have been deposited at all. This entire package generally coarsens upward from clays and silts in the lowest portion, which are exposed just north of the Main Frontal thrust (MFT), to fluvial siltstones and sandstones in the middle sections that eventually grade into gravels deposited by braided rivers in the upper-most section (McQuarrie et al., 2008). The Siwalik Group in the eastern Bhutan is ~4 km thick with its bedding dipping from 25° to 65°, with the mean between 30° and 40° towards the northwest. The section is not repeated by faults, however, meso-scale folds with fold hinges gently plunging to the west are present in the finer-grained units near the base of the group (McQuarrie et al., 2008).

The entire Siwalik Group is uplifted by motion along the MFT. The magnitude of slip along the fault is an estimated minimum of 9 km, which is required to expose the hanging wall cut-off through the erosion surface (McQuarrie et al., 2008).

Along the northern portion of the Indian craton during the Proterozoic and quite possibly early Paleozoic, predominant clastic and carbonate sediments were deposited. These units ranged in thickness from 8 to 12 km thick and are the protoliths of the metasedimentary rocks found in the present day LHS. These LHS rocks in Bhutan vary from south to north ranging from clastic dominated lithologies such as sandstones, siltstones, carbonates and coals in the south (which are typical passive margin sediments on which they were deposited). They become more metamorphosed into siltstones and sandstones along with slate, quartzite and schist the more proximal to the Main Central thrust (MCT) in the north. Overall, the metamorphic grade within the LHS ranges from low-greenschist in the south to high-greenschist facies in the north (Gansser, 1983). Structurally all the planar fabric within the LHS, including the southern MBT and northern shear zone MCT, dip northward. Therefore from south to north, and from structural lower to structurally higher level the peak metamorphic temperature increases. This results in the inverted metamorphic gradient.

The MCT, referred to also as the Main Central Thrust Zone because there is not one distinct surface, but a ~10 km shear zone in Bhutan (Grujic et al., 1996, Daniel et al., 2003) involving the LHS in the footwall and the GHS in the hanging wall. These GHS rocks are composed of paragneisses, orthogneisses (which become migmatitic in the higher structural levels), schist, quartzite, Miocene age leucogranites, and less common marble and amphibolites layers (Gansser, 1983, Grujic et al., 2002, Daniel et al., 2003). This major shear zone also raises questions about the paleogeography. Based on detrital zircon ages the protoliths of the metasedimentary rocks within the GHS have been dated to Proterozoic to early Paleozoic

(McQuarrie et al., 2008). The rocks in the GHS represent either highly metamorphosed equivalents of the LHS, or were once part of an accreted terrane that became tectonically consolidated with Greater India during the early Paleozoic (McQuarrie et al., 2008). A comparison by Decelles et al. (2000) proposes very different ages of deposition of the LHS and GHS units based on U-Pb ages of detrital zircons stating that the rocks in the LHS sequence in Nepal formed at 1.8 Ga, while the sedimentary rocks of the GHS were deposited between 1.3 Ga and 700 Ma. Based on this gap of at least 600 Ma, DeCelles et al. (2000) theorized that predominantly Neoproterozoic GHS rocks could not have been attached to Greater India prior to the early Proterozoic.

At the roof of the GHS is a normal-sense shear zone known as the South Tibetan Detachment (STD) (Burg et al., 1984, Burchfiel et al., 1992, Edwards et al., 1996, Kellet et al., 2009). Located above the STD are Chekha and Tethyan sediments, with the Chekha sediments at the base of the Paleozoic to Mesozoic Tethyan sediments (Grujic et al. 2002, Kellett et al. 2009). The Tethyan and Chekha sediments were deposited on the northern passive margin of the Indian plate, which is similar to present day Nova Scotia's passive margin, although instead of a 200 km shelf, the shelf off the northern margin of India was ~2000 km broad. These strata (Tethyan and Chekha) are a composite of two superimposed rift and passive margin sequences, the first being Permian to Cretaceous and the second early Paleozoic to Carboniferous in age. As a comparison, rocks of time equivalents to the Tethyan strata that are most proximal to India are part of the Gondwana Formation, which will be described later, as one of the most southerly formations in the LHS. These rocks range in age from Permian through Paleocene, or 285 Ma to 55 Ma (McQuarrie et al., 2008). The STD was most active during the Miocene period, and is known as the uppermost limit of the high-grade metamorphic assemblage of the GHS (Kellett et al. 2009). It is thought that movement on the STD was also simultaneous with movement along the MCT,

although a normal-sense of movement on the STD as opposed to reverse-sense of movement on the MCT (Kellett et al. 2009).

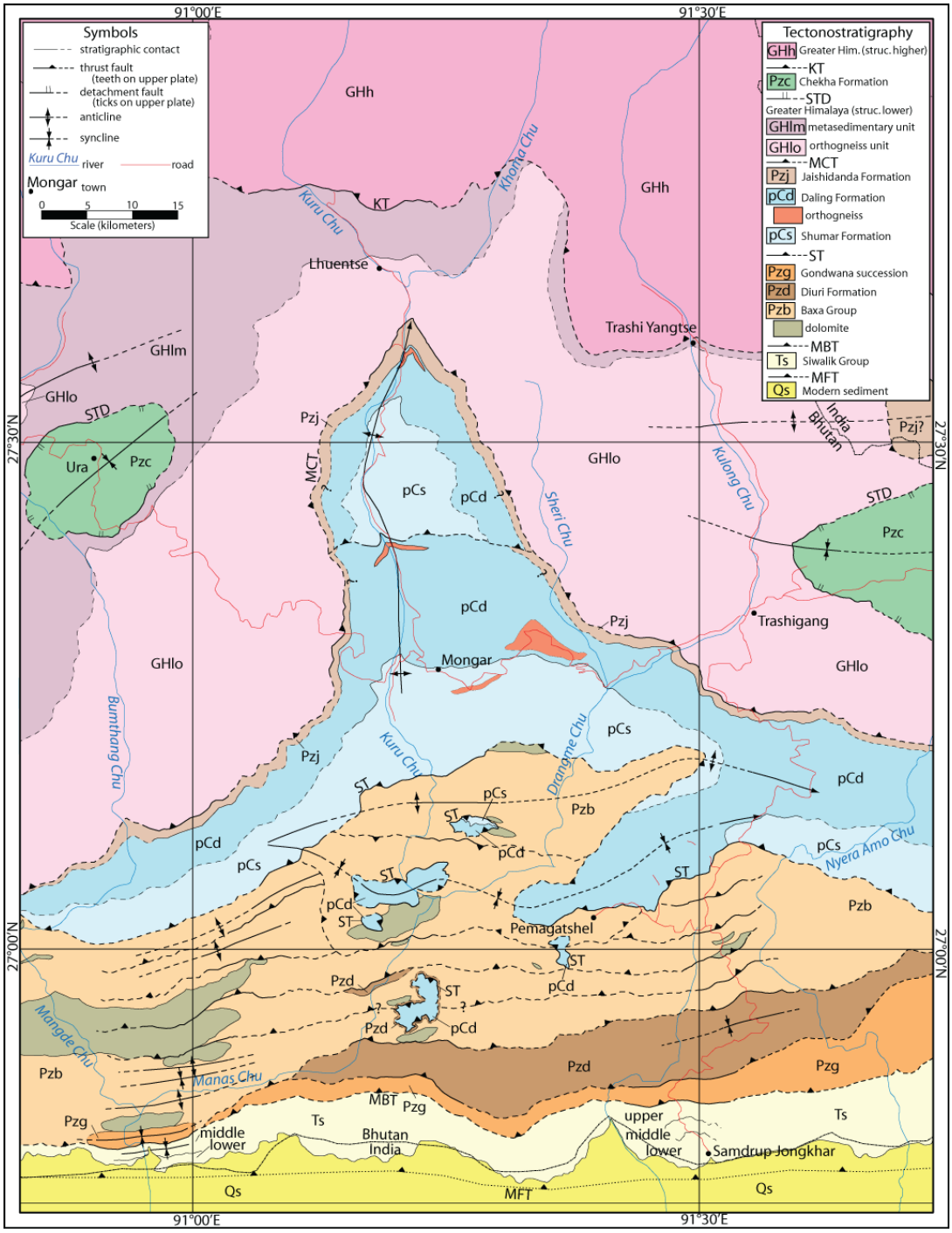

Figure 2.2. Geological map of eastern Bhutan. Image from Long et al. In Press.

2.2 Geology of the Lesser Himalayan Sequence

The Lesser Himalayan sequence is divided into four distinct formations; A) Gondwana Sequence, B) Diuri Formation, C) Baxa Group, D) Daling-Shumar Formation, going from the lowest to highest structural positions (Fig 2.2 and 2.3).

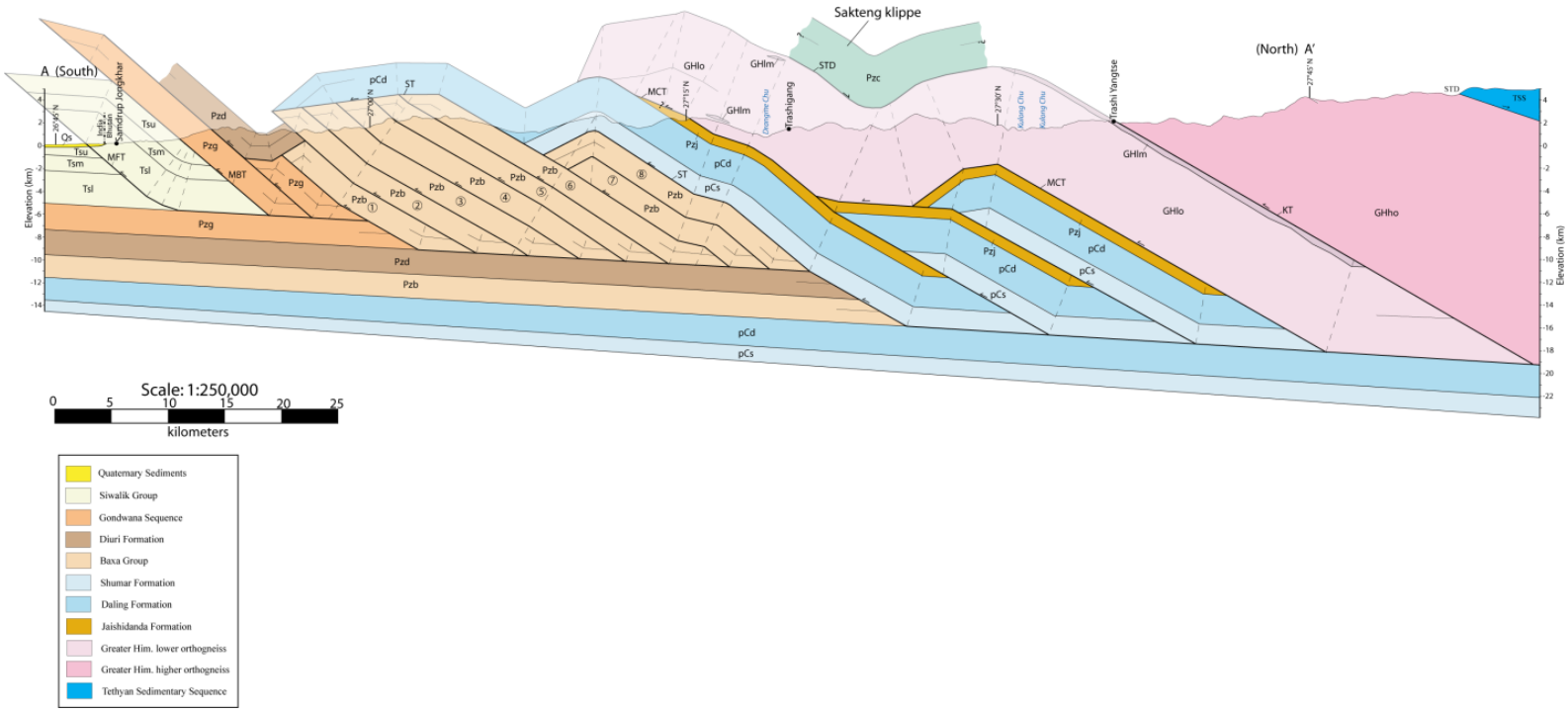

Figure 2.3. A cross section of the LHS and GHS, modified from Long et al. In Press. This section shows the common north-dipping strictures and contacts throughout the LHS and GHS, along with the complicated duplexing of the Jaishidanda, Daling, and Shumar Formations. Legend is the same as Fig 2.2.

2.2.1 Main Boundary Thurst

The Main Boundary thrust (MBT) is a moderate to steeply dipping thrust that dips to the north and joins on to the décollement MHT at depths. This thrust places the structurally higher and older unit of the Lesser Himalayan Sequence (LHS) over the lower and younger Subhimalayan group (Hodges, 2000). Development of the MBT occurred between the mid- to late-Miocene, ~9-11 Ma (Hodges, 2000).

2.2.2 Gondwana Sequence

This sequence is composed of feldspathic sandstone, siltstone, shale, coal lenses, and plant fossils. Both the northern and southern boundaries of this sequence are faulted making its relationship difficult to correlate with the older units (McQuarrie et al. 2008). The stratigraphic age of this unit has been documented as Permian. This sequence also contains finely laminated, dark, salt-and-pepper sandstone, coal seams and carbonaceous shale and slate. Total thickness of the Gondwana Sequence in eastern Bhutan is 1.2 – 2.4 km thick (Long et al., In Press).

The Gondwana Sequence can be broken up into two visibly different lithological units, with the lower section closest to the MBT being composed of medium-grained grey sandstones interbedded with dark-grey thin- to medium-bedded organic rich shale siltstone and shales. The sandstones contain poorly-sorted clasts and are commonly feldspathic and lithic rich (Long et al., In Press). The upper section of the Gondwana Sequence consists of dark-grey, thinly bedded to laminated carbonaceous shale and argillite, interbedded with very fine-grained sandstone and rare black coal beds (Long et al., In Press).

2.2.3 Diuri Formation

This formation is a ~2.3 – 3.1 km thick diamictite, interbedded with slates, that underlies the Baxa Group. It contains pebbly shale, slate, and sandstone with the pebbles ranging in size from 0.5 to 5 cm which are subangular to well-rounded, with a micaceous slate matrix (Long et al., In Press). The diamictite clasts are generally pebble- to cobble-size and consist of grey, red, and green quartzite (Long et al., In Press). Clasts are composed of dark grey quartzite, white vein quartz, and yellowish dolomite quite possibly from the older overlying strata. The ground mass of the diamictite shows schistosity (McQuarrie et al., 2008). All contacts above and below the Diuri Formation have been mapped as tectonic contacts (Long et al., In Press).

2.2.4 Baxa Group

One main observation made by Long et al. (In Press) is the fact that the Baxa Group is laterally variable in lithology. Overall, this group is dominated by grey to white, medium- to thick-bedded quartzite (Long et al., In Press). The quartzite is medium- to coarse-grained with poorly sorted subangular clasts (Long et al., In Press), and locally pebbly to conglomeratic, with distinct clasts of jasper and rose quartz. Sedimentary structures within the quartzite range from trough cross-bedding and lenticular-bedding, along with meter-scale beds swelling and pinching over meters to tens of meters of lateral distance. The less-dominant dolomite horizons are lenticular in map view and represent reefs that were deposited in a deltaic environment. It is thought that the minimum thickness of the Baxa Group is ~2.8 km between the underlying Diuri Formation and the overlying Daling-Shumar Formation (Long et al., In Press).

2.2.5 Daling-Shumar Group

This group was originally named by Gansser (1983) in an attempt to combine the dominantly phyllitic Daling Formation found in Sikkim-Darjeeling to the west, with the quartzite rich Shumar Formation in eastern Bhutan. However, this has led to complications in that the quartzite and phyllite of the Daling-Shumar Group have very similar weathering patterns with the quartzite and slate of the underlying Baxa Group. This group can be therefore broken onto two distinct formations; the Shumar Formation quartzite and the overlying Daling Formation phyllites.

The oldest (but structurally highest) unit of the LHS in Bhutan is the Shumar Formation quartzite. This formation ranges in thickness from west to east Bhutan and reaches a maximum thickness of 6 km in the Kuru Chu valley. The beds are very distinguishable, white to greenish-grey, fine-grained, quartzite (McQuarrie et al., 2008). The Shumar Formation is characterized by continuous planar bedding (McQuarrie et al., 2008). The beds can be medium to thickly bedded, with the layers being separated by thin to three meters thick interbeds of phyllite to schist, with

the phyllitic interbeds becoming more common with closer proximity to the Daling Formation. Foliation planes are defined by mica and sericite.

Overlying the Shumar Formation is the 4 km thick Daling Formation. The contact between the Shumar and Daling Formation is transitional with more quartzite at the base. The Daling Formation is dominated by chloritic to sericitic schist in the north, becoming more phyllitic to the south (McQuarrie et al., 2008). The intercalated quartzite beds range from clean, white, fine-grained rock with 5-10 cm thick beds, to a lithic-rich, thinly-bedded (mm scale) rock, greenish-grey to salt-and-pepper in color (McQuarrie et al., 2008). Some sedimentary structures are present, such as ripple marks along with cross-beds. Quartz veins and blebs are common. Thinly bedded to massive carbonate beds, although rare, range in thickness from 5 to 30 cm thick. Also, bodies (~0.5 km thick) of mylonitized orthogneiss are preserved. These orthogneisses are composed of quartz, orthoclase, plagioclase, muscovite, and biotite. They are lenticular to sheet-like, and contain 1-5 cm scale plagioclase and orthoclase augen. The augen are flattened and sheared as part of a well-developed mylonite S-C fabric with approximate north-south stretching lineation The crystallisation age of these magmatic bodies is ~1.75 Ga (Daniel et al. 2003).

2.2.6 Jaishidanda Formation

The Jaishidanda Formation is thin unit, ~1500 m, and located just beneath the MCT. Consisting of biotite-rich, locally garnet-bearing schist, and interbedded with quartzite from the underlying Daling Formation. This thin unit is found in most areas across Bhutan, however, its absence has been interpreted to either be due to it being interpreted as part of the overlying GHS, or as part of the underlying Daling-Shumar Formation (Long et al. In Press). For this study it will be considered as part of the LHS.

2.2.7 Main Central Thrust

The Main Central thrust (MCT) is the boundary between the LHS to the south and the GHS to the north. Almost along is complete entirety throughout Bhutan, the MCT shows a steep metamorphic gradient from the greenschist-facies rocks of the LHS to the amphibolite-facies rocks of the GHS (Gansser, 1983; Grujic et al., 1996; Daniel et al., 2003). Highly deformed schists and gneisses with a gently north-dipping foliation and strong north-plunging mineral and stretching lineations make up the >10 km thick zone named Main Central Thrust Zone (MCTZ), (Grujic et al., 1996). The main movement on the MCT occurred 15-20 Ma (McQuarrie et al. 2008).

2.2.8 Greater Himlayan Sequence

The Greater Himalayan Sequence (GHS) is the unit of the Himalaya that lies between the north-dipping MCT to the south, and the north dipping normal fault of the South Tibetan Detachment (STD) to the north. It is composed of high-grade metasedimentary and meta-igneous rocks, along with associated leucogranites (Hodges, 2000). In simplified terms, the GHS was described by Le Fort et al. (1994) as follows: from the base upward the three units range from the first unit consisting of clastic metasedimentary rocks such as mica-schists, phyllites, and quartzites. The second unit is described as middle- to upper-amphibolite facies calcareous rocks, and the third unit which is structurally the highest is a nearly homogenous augen orthogneiss. The protoliths of much of these metasedimentary rocks is from the Indian passive margin (Hodges and Parrish, 1996).

2.2.9 South Tibetan Detachment

The top of the GHS is bounded by a shallow north-dipping normal fault known as the South Tibetan Detachment (Grujic et al., 1996, Edwards et al., 1996, 1999, Kellett et al. 2009) and roughly parallels the MCT. This zone typically separates the unmetamorphosed to weakly metamorphosed Tibetan zone strata of the hanging wall from the upper-amphibolite facies

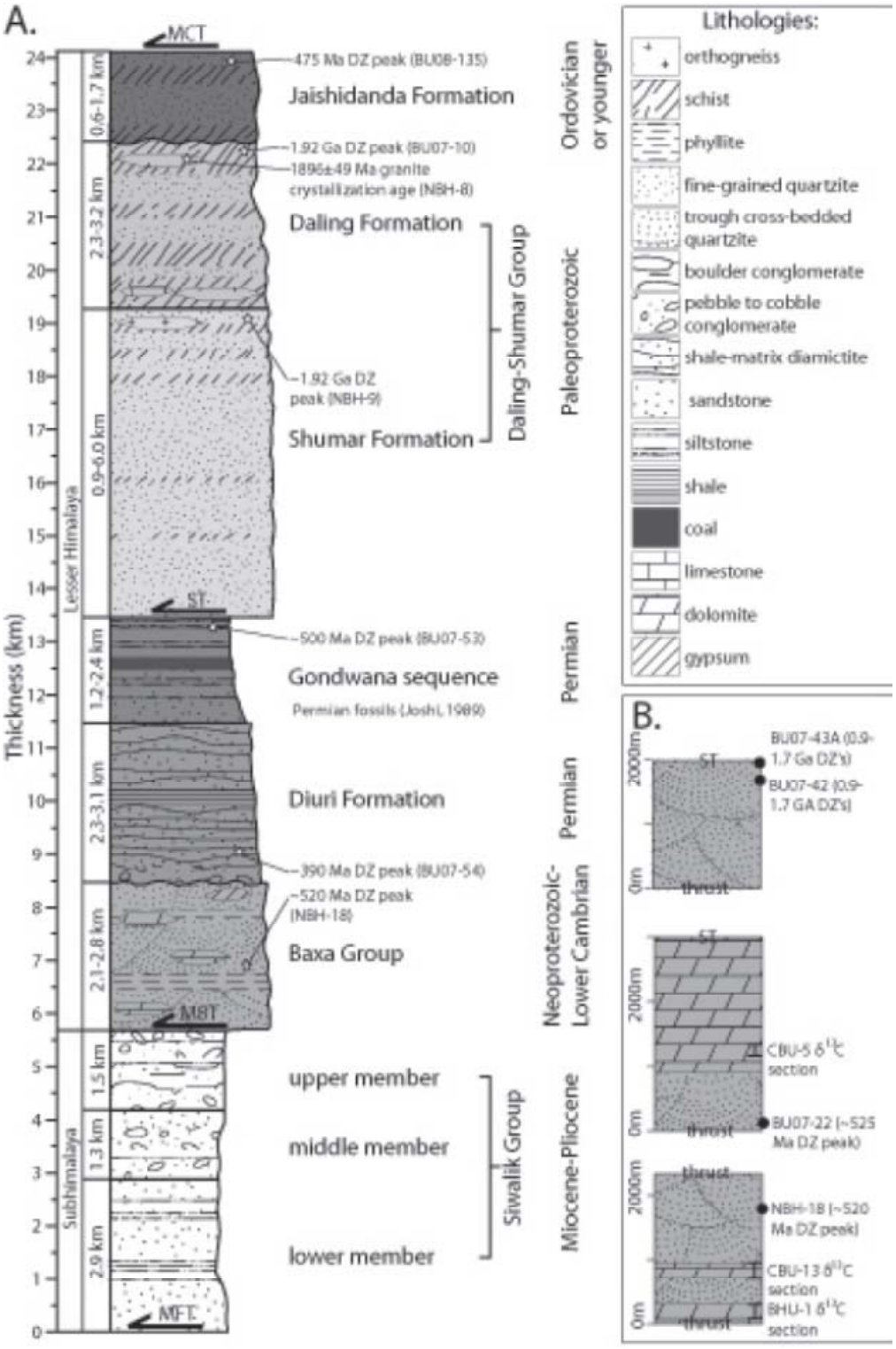

Figure 2.4. A stratigraphic column showing the stratigraphy of the LHS. Note that the LHS is broken up by the Shumar thrust (ST). Below is the Shumar thrust footwall with the different units in order by age from oldest to youngest, bottom to top. Above the ST is the hangingwall with the units ordered the same way as the footwall. Image from Long et al. In Press.

gneisses and leucogranites of the GHS footwall (Hodges et al., 2000). Well developed shear-sense indicators show a northeast or northwest normal sense of motion (Burchfiel et al., 1992). The STD-related foliation is classified as C'-

type shear bands, and overprint previous foliations that indicate top-to-the-south sense of shear (Grujic et al., 2002), this indicates that in its past, the STD experienced differing sense of shear. Also, many Miocene leucogranites dykes and are folded or boudinaged in a north directed shear-sense (Grujic et al., 2002). Based on data from Daniel et al. (2003), and Grujic et al. (2002), the STD was most active from 15 to 22 Ma.

2.3 Previous Work on the Inverted Metamorphic Gradient across the LHS

As early as the 1860's it was known that the LHS had an inverted metamorphic gradient

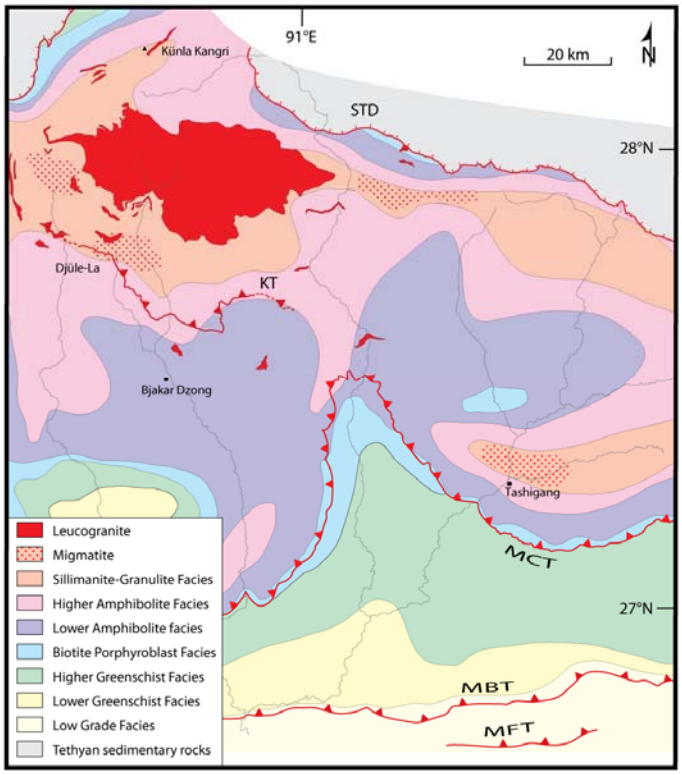

Figure 2.5. A geological map modified by D. Grujic from Gansser (1983). This map shows the metamorphic isograds related to field observations based on metamorphic indicator minerals.

(Bollinger et al. 2004), however, the only evidence available at that time was from metamorphic indicator minerals, and until recently the quantitative numeric values for the peak metamorphic field gradient across the LHS were absent (see Fig 2.5 for a map modified by D. Grujic showing the inverted metamorphic gradient which was determined by indicator minerals).

Pêcher (1989) conducted a study concerning the inverted metamorphic gradient across the LHS and was one of the first to propose possible theories as to how it happened. The study took place in a somewhat easily accessible area of the Himalayas in Central Nepal, with an intense review of previous literature from Garwhal, Kumaun, and Nepal. Since the RSCM technique was not yet available, the peak temperatures were determined based on metamorphic indicator minerals (Fig 2.5). Metamorphism in the LHS is thought to be directly related to the movement along the MCT (Pêcher, 1989). One reason given for the metamorphic zonation is due to the superimposing of two different stages of metamorphism in the overriding Tibetan slab, but this is recorded in the prograde assemblages throughout the LHS, which is linked closely to the thrusting (Pêcher, 1989). It was concluded that heat was supplied to the hanging wall of the MCT shear zone from the overriding Tibetan Slab hanging wall during the MCT shearing and during which the isotherms took on an elongate sigmoidal geometry. Areas far behind the thrust tip (area that is closer to the GHS, which is structurally higher, see Figure 1.2 for geological relationships) received a sufficient amount of heat to metamorphose a several kilometre thick succession of underlying terrane. Closer to the thrust tip the amount of heat supplied was low due to: (1) the thin Tibetan Slab allowed for quick heat loss, (2) it lost a large amount of heat due to the long tectonic transport of the slab, and (3) the cold thermal topographic surface was lowered (Pêcher, 1989), therefore the underlying formations, which would be the LHS, were less metamorphosed. Closer yet to the thrust tip the hot shear belt was replaced by a cold thrust,

which emplaced high-grade gneisses on top of unmetamorphosed formations (described as the Siwaliks in Figure 2.2) (Pêcher, 1989).

Following are two theories for the inverted metamorphic gradient across the LHS based on data collected from RSCM and thermochronology. Figure 2.6 indicates the areas of study from Célérier et al. 2009 (area 1 on Fig 2.6), and Bollinger et al. 2004 (area 2 on Fig 2.6). The other two areas, 3 and 4, are theses studies currently being conducted under the supervision of D. Grujic (Fig 2.6).

As of recently there have been two main hypotheses as to how the actual inverted metamorphism has occurred across the LHS. One study by Célérier et al. 2009 was conducted in the Kumaun and Garwhal Lesser Himalaya in India (area '1' on Fig 2.6). Their analyze rocks based on RSCM for peak metamorphic temperatures, and by thermochronological analysis of white micas. As is the case in the eastern Bhutan LHS, the study area for Célérier et al. 2009 was absent in metamorphic indicator minerals suitable for thermobarometric analyses. They proposed several models with one being most suitable for the data they analyzed: with the spatial association of peaks in the RSCM temperatures, and the proximity to the hanging wall of the MCT, the mechanism for thermal metamorphism as proposed by Célérier et al. 2009 was caused by conduction of heat from the Main Central thrust fault and/or hanging wall to the footwall (Célérier et al. 2009). This was interpreted to have been achieved by a phase of overthrusting during the early Miocene of a hot hanging wall over a down-going footwall which was followed by the initiation of a duplex within the LHS (Célérier et al. 2009).

An earlier study by Bollinger et al. 2004 was conducted on the thermal structure and exhumation history of the LHS in Central Nepal. They use the same techniques for analysis of samples as Célérier et al. 2009 used: RSCM and thermochronology of white micas (Bollinger et

al. 2004). Their main hypothesis for the inverted metamorphic gradient is along the lines of Pêcher 1989, stating that the inverted metamorphic gradient was a direct result of underplating and postmetamorphic deformation of the thermal isograds (Bollinger et al. 2004), in other words the metamorphism took place before deformation of the isotherms occurred. They also show how this inverted metamorphic peak temperatures that were once only documented proximal to the MCT are actually widespread through the entire LHS, and that the LHS units were actually accreted to the range mainly by underplating at midcrustal depths (Bollinger et al. 2009).

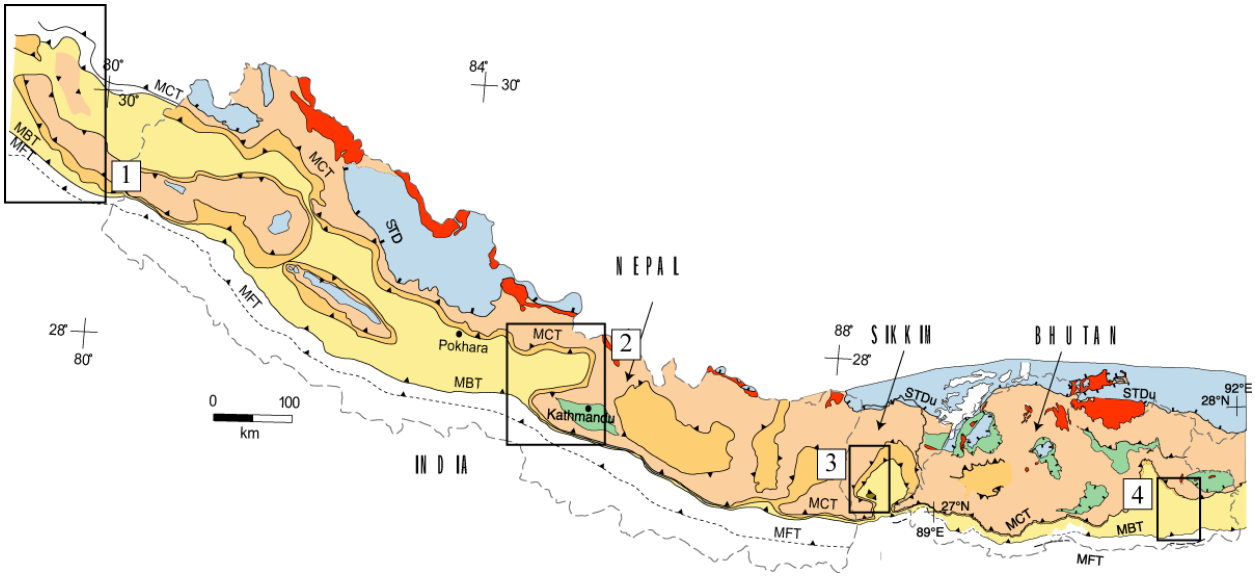

Figure 2.6. Geological map of the Himalaya. Located on the map are the two localities of previous work done in the Himalayas on the inverted metamorphic gradient: (1) Célérier et al. 2009, and (2) Bollinger et al. 2004. Areas (3) and (4) are the localities of two current honours students from M.Doon in the Sikkim window, and the area from this study in the LHS, respectively.

3.0 METHODOLOGY

To obtain and analyze data for this study required a four step procedure, those being (1) sample preparation, (2) measurement of the spectra, (3) use of the program PeakFit® to determine peak of best fit, and finally (4) calculating the peak metamorphic temperatures of the samples using equations derived from Beyssac et al. (2002) and Rahl et al. (2005). I will elaborate on these four steps in the following sections.

3.1 Sample Preparation

The first step was to count, mount, and polish the desired samples. This step was carried out in the thin section facility of the Department of Earth Sciences at Dalhousie University. Rocks slabs were first cut using a diamond-blade rock saw, with the slabs cut perpendicular to foliation and parallel to stretching lineation to best observe the graphite within the kinematic principal plane of the finite strain. From there the samples were mounted on thin section glass and further cut down to the desired thickness of 40 μm by technician Gordon Brown. Once the samples were at the desired thickness they were polished.

3.2 Raman Spectroscopy

When a monochromatic light (i.e. a beam of light with a single frequency) passes through a medium, in the case of this study solid graphite, the majority of the scattered light remains at the same frequency as the incident frequency. However, a small proportion of the scattered light changes its frequency to that of a frequency above or below the incident frequency. This is known as the Raman effect (Potts et al. 1995). This phenomenon was first observed by Raman and Krishnan in 1928.

When a solid, liquid, or gas is illuminated with a monochromatic light, most of this light will pass through the sample without changing. However, a very small proportion will be

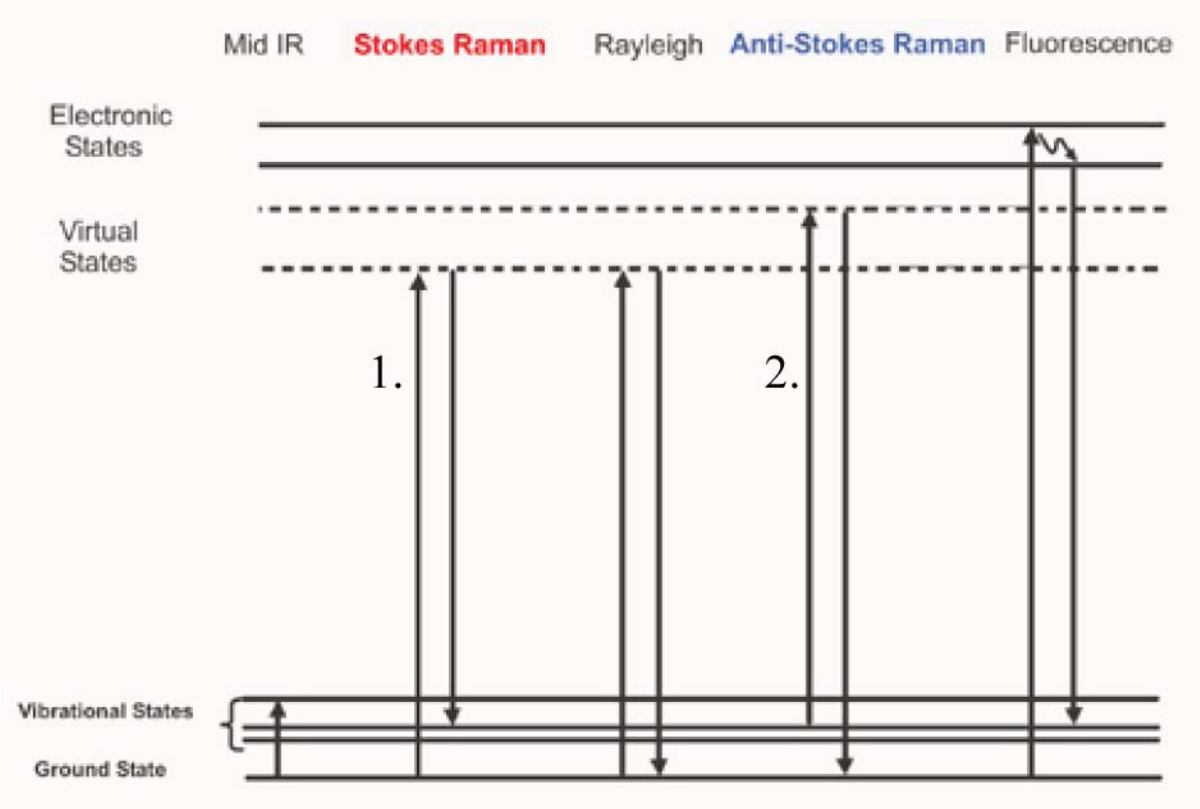

Figure 3.1. Schematic picture of the process behind the Stokes and Antistokes law. In the Stokes law, (labeled 1.) which is also known as the Raman effect, molecules in the material become excited to a virtual state. Once they relax, they relax back to a state that is higher than the initial ground state. This produces the Raman effect. With the Anti-Stokes law (labeled 2.), the excited molecules does not relax back to a higher vibrational state, however, it relaxes back to the ground state, and therefore this frequency shift is below the initial frequency. Image from horiba.com.

scattered by the sample (Potts et al. 1995), about 10^{-3} of the incident intensity will be scattered with the same frequency. This process in which a small proportion of the incident light is scattered with the same intensity is known as Rayleigh scattering (Fig 3.1). In addition to this Rayleigh scattering, about 10^{-6} of the incident intensity is scattered at new frequencies, either above or below the incident frequency. This is known as what was mentioned above as the Raman effect. These shifts in frequency, either above or below the incident frequency, are characteristic of the species in question.

3.2.1 Raman Spectroscopy of Carbonaceous Material

Raman spectroscopy of carbonaceous material (RSCM) provides information of the molecular and structural information at the atomic level. Spectra of natural graphite shows a single Raman line at 1575 cm^{-1}, now more precisely placed at 1580 cm^{-1}, however, carbonaceous material shows additional peaks at 1350 cm^{-1} (Potts et al. 1995) and two others located at 1500 cm^{-1} and 1620 cm^{-1}, known as the'D1', 'D2', and 'D3' peaks respectively. Figure 3.2 shows the locations of these peaks. The intensity of the peak at 1370 cm^{-1} increases as a function of the amount of "unorganized" carbon in the sample – in other words, this peak intensity increases with increasing metamorphic grade. On the contrary, the aforementioned D1 and D2 peaks decrease with increasing metamorphism, and even lower metamorphism creates the almost

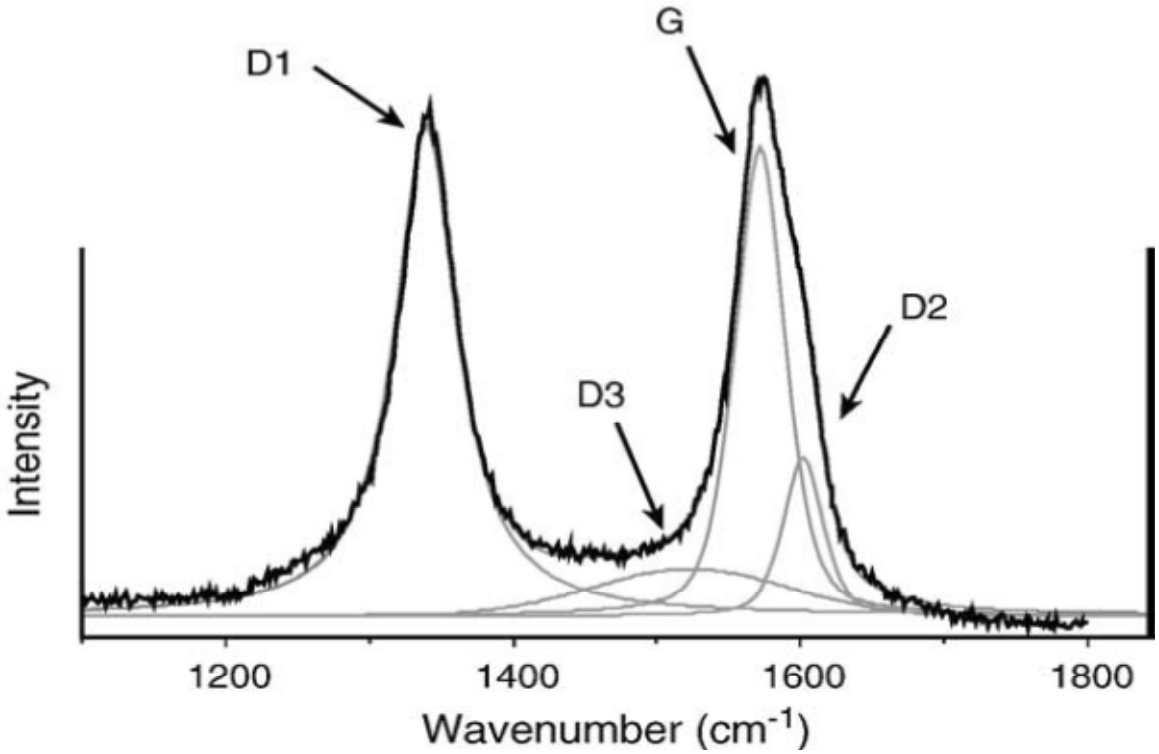

Figure 3.2. A typical Raman spectrum. Within this first order region the position of the graphite peak (G-peak) is located at 1580 cm^{-1} with the other three peaks, D1, D2, and D3, indicating the amount of disorder in the graphite. Image from Rahl et al. 2005.

invisible D3 peak (Beyssac et al. 2002). Using this theory, Wopenka and Pasteris (1993)

proposed that this technique could be into a geothermometer by comparing carbonaceous material of varying metamorphic grades, and correlating these variations in the ratio of the intensities in the 'G' and 'D1' peaks, as seen in Fig. 3.2. These four peaks are contained within the first-order wavenumber, located between 1100 – 1800 cm^{-1} (Beyssac et al. 2002). Wavenumber can also be described as the number of wavelength per unit distance, or a spatial frequency.

3.2.2 Raman Instrument at Dalhousie

The measurement of spectra was completed using the Jobin Yvon 64000 Raman spectrometer located in the Physics and Atmospheric Science Lab, Dalhousie University, and is supervised by Dr. Kevin Hewitt. The measurements were done using a 514.5 nm wavelength Ar laser, 1800 groove/mm grating which creates signal dispersion, and Charge-coupled device detector (see Figure 3.2 for more information). Before each data acquisition session, the instrument was calibrated using a silicon standard, with an 820.7 wavenumber.

3.2.3 Measurement Procedure in this Project

Data acquisition of each spectrum ran a total of four times for a period of 30 seconds per spectrum collection, making the total acquisition time 120 seconds. Polished thin sections were analyzed using a 100x objective ocular. Prior to analyses, it was sometimes necessary to locate areas of graphite using a reflected light microscope due to the fact that some samples contained very dispersed graphite grains. The most distinguishing feature of graphite is its bi-reflectance, ranging from a very light pink to grey as the microscope stage is rotated. During spectra collection graphite grains located under transparent grains, such as quartz, were desired because the high heat caused by the mechanical polishing can retrograde metamorphose the graphite grains and cause inaccurate readings (Wopenka and Pasteris, 1993; Beyssac et al. 2002). However, in samples with very limited amounts of graphite, this option was not always

available. During data acquisition approximately 10-15 spots per thin section were analyzed. This was to limit human error during data acquisition and to also determine a within-sample heterogeneity, meaning that sampling with this technique provides a comprehensive sample analysis.

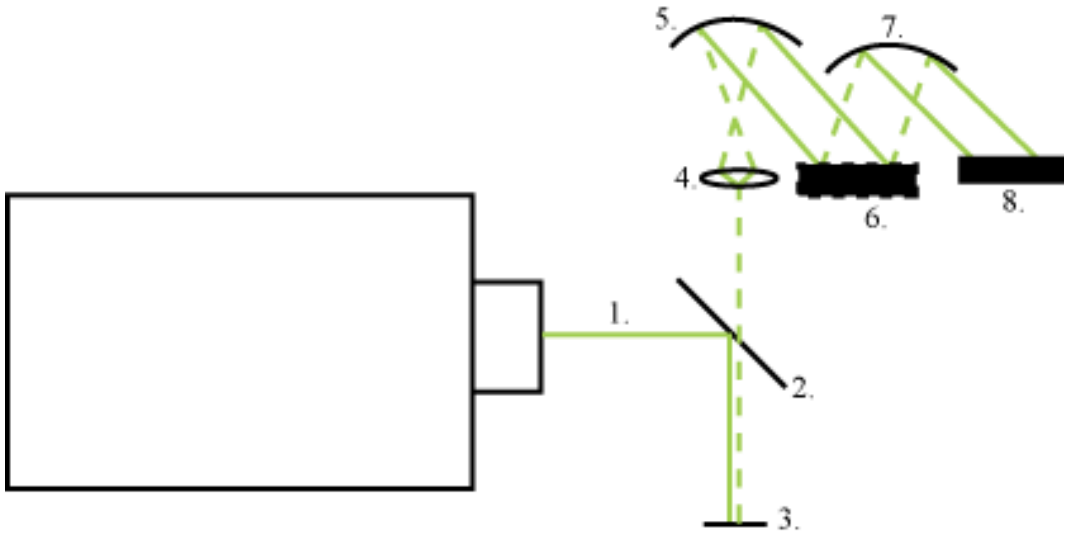

Figure 3.3. A schematic illustration of the main data acquisition and processing unit of the Raman spectrometer. The pathway of the laser beam is as follows: 1. The laser is emitted from the spectrometer, and comes into contact with a beam splitter at location 2. From there the beam makes a 90° turn and is incident on to the prepared thin section at 3. From there a small fraction of the incident beam is returned at a different intensity, known as the Raman effect. It passes through the beam splitter and hits a lens at position 4, and is diffracted until it comes in contact with a mirror at position 5. This mirror allows for the beams to become parallel, and from there is incident on to a diffraction grating, with 1800 grooves per millimeter. The diffraction grating splits the incoming light beams and sends them to another mirror at position 7. This mirror creates parallel beams again which are then incident on to a detector which picks up and displays the signal that can be seen in Figure 3.2.

3.3 Peaks, Ratios, and Previous Raman Work

As stated earlier the two main studies that were used to help in acquiring and understanding the data were studies from Beyssac et al. (2002) and Rahl et al. (2005). These two studies were conducted rather recently and used RS for analyzing peak metamorphic temperatures in graphitic rocks, and each researcher derived their specific ways to calculate the

metamorphic temperatures, such as empirical formulae which utilize certain aspects of the graph as seen in Figure 3.2.

Beyssac et al. (2004) was the first recent researcher to apply this theoretical method to analyze peak metamorphic temperatures from graphitic rocks. Beyssac et al. (2004) derived an empirical formula, which is T(°C) = -445*R2 + 641, with R2 being the ratio of the integrated area of the peaks, found from the simple ratio equation R2 = D1/(D1 + D2 + G), with D1, D2, and G being the peaks shown in Figure 3.2. Looking at the above equation it is a typical y = mx + b, with a linear correlation between the R2 values and the corresponding peak metamorphic temperature. Therefore according to the R2 ratio equation, it could be said that the variable with the most influence on the peak temperature is in fact the area under the G peak, due to the fact that it is in the numerator. The influence of the D1 peak is inversely related to metamorphic grade, in other words as the size of D1 decreases, peak metamorphic temperatures increase. The following figure (Fig 3.3a and b) shows a very good correlation between the R2 ratio and peak metamorphic temperatures, with a correlation value of 0.96. However, the graph below that indicates a very poor correlation between the R2 ratio and the pressure, in kbar. Beyssac et al (2002) had concluded that a similar observation had been made from an earlier study by Bény-Bassez and Rouzand (1985), and in comparison with Beyssac's study shows that they believe the R2 ratio is the best ratio for calculating peak metamorphic grade because although the D1 peaks change due to change in metamorphism, and therefore changing the R1 ratio, the total area under the D1 peak does not change, and therefore the R2 ratio of areas holds no bias and is more suitable.

The study conducted by Rahl et al. (2005) was the second of the two studies that used data from Raman spectroscopy on carbonaceous material. Rahl et al. (2005) stated that although Beyssac's equation held true for most circumstances, that below certain peak

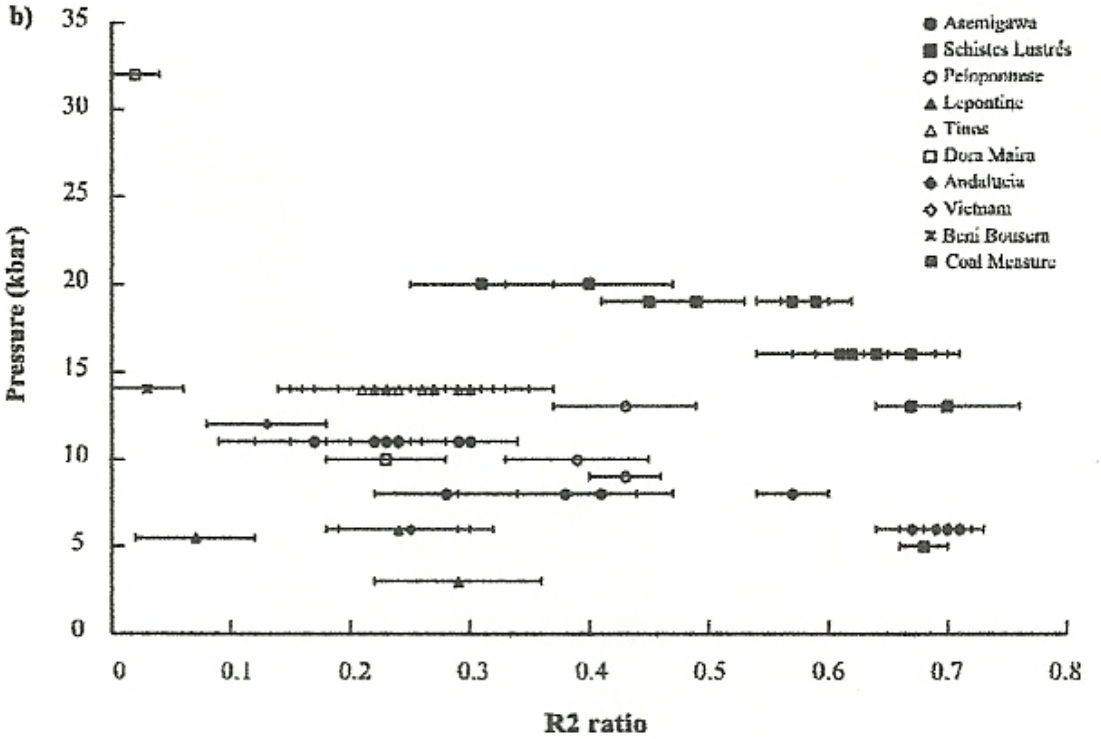

Figure 3.4a. This figure shows a very good correlation between the R2 ratio (x-axis) and peak metamorphic temperature (y-axis). Image from Beyssac et al. 2002.

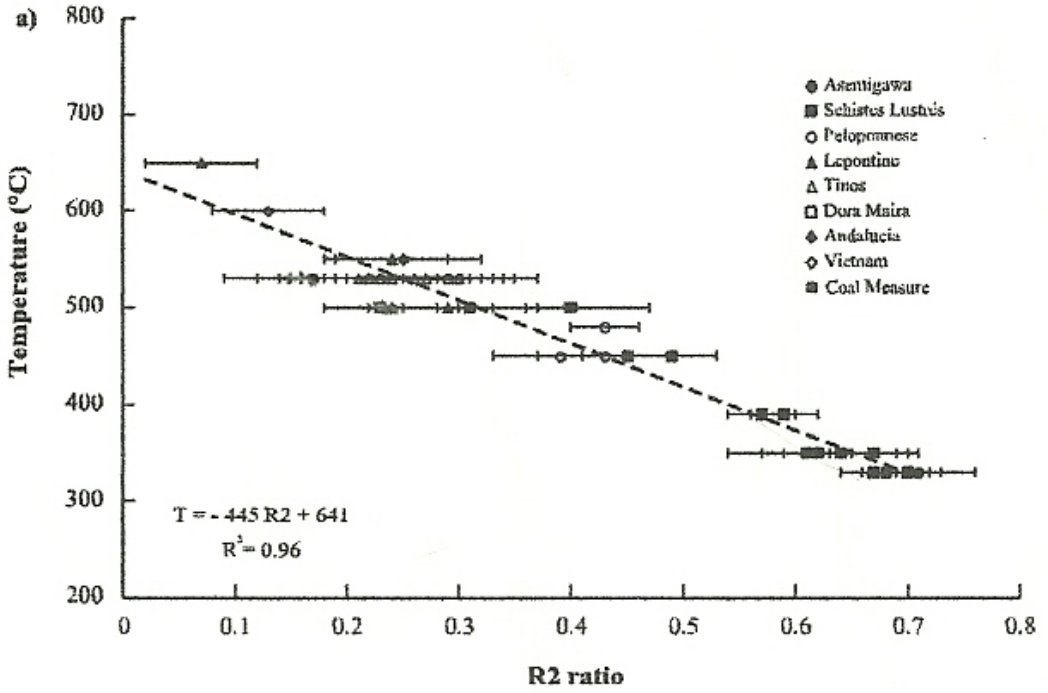

Figure 3.4b. This graph dipicts the R2 ratio in relation to the amount of pressure, showing a low degree of correlation. Image from Beyssac et al. 2002.

metamorphic temperatures lower than 330 °C Beyssac's formula does not hold true. Therefore, they proposed a new empirical formula derived from the fact that within the equation you need to take into account not only the R2 ratio, but also an R1 ratio, where R1 = D1/G. The D1 area, as stated before, decreases with increasing metamorphic temperature, therefore the peak height would decrease with increasing metamorphic temperature. On the contrary, the G peak increases with increasing metamorphic temperature due to the fact that this peak indicates the purity of graphite in the sample. The equation Rahl et al. (2005) derived is as follows: $T(°C) = 737.3 + 320.0*R1 – 1067*R2 – 80.638*R1^2$. Unlike the linear equation proposed by Beyssac with only the R2 ratio, Rahl's equation is a quadratic function of temperature that takes into account both R2 and R1 ratios. Rahl et al. (2005) believed it was necessary to deduce an equation that took both peak area and height into consideration to reduce bias towards one or the other. The applicability of each calibration is to quantify the temperature at which rocks with carbonaceous material were metamorphosed. Each calibration has a distinct temperature range, Beyssac et al. (2002) being 330 – 650 °C, and Rahl et al. (2005) being 100 – 700 °C.

Several studies in the past decade that have used RSCM as a technique to quantify peak metamorphic temperatures. Beyssac et al. (2002, 2004) have conducted studies in the Alps, Japan, and the Himalaya. Bollinger et al. (2004) conducted a study on the thermal structure and exhumation history of the LHS in the Himalaya of central Nepal. Rahl et al. (2005) used a study from Crete, Greece to extend the geothermometre proposed by Beyssac et al. (2002) to a minimum temperature calculation of 100 °C. Most recently the technique has been used in a study by Célérier et al. (2009) to analyze the thermal and deformation histories of the LHS in India.

3.3.1 PeakFit® and Temperature Calculation Procedure

Following the data acquisition on the RS, it was necessary to turn the graphs that were produced into quantitative peak metamorphic temperatures. This was done using a software program called PeakFit®. PeakFit® is a program that allows users to produce a line of best fit to the graphs that were produced by the RS. Once the line of best-fit had been fitted with the lowest error, a text file was saved showing all the data, including the peak heights and integrated area under the peaks. From here, this data was imported into an Excel spreadsheet where the aforementioned R1 and R2 ratios were calculated and placed into the appropriate variables within either Beyssac or Rahl's calibrated formulae. The end result shows the peak metamorphic temperature that the samples had experienced.

4.0 RESULTS

Samples for this study were collected from the LHS between the Main Boundary thrust at the south of the LHS, and the Main Central thrust at the northern limit of the LHS. A total of 16 samples were collected by Djordje Grujic during the 2007 field season. These 16 samples were collected from six (5) lithological units in the LHS: from south to north, (a) Gondwana Formation, (b) Diuri Formation, (c) Baxa Group, (d) Daling Formation, and (e) Jaishidanda Formation. The following is a brief petrographic and structural summary of these samples, more details are in Appendix A.

4.1 Petrographic and Structural Observations

The meta-sedimentary rocks analyzed in this study ranged from low- to high-grade greenschist facies, predominantly composed of graphite + quartz + sericite ± muscovite ± biotite ± calcite ± chlorite ± opaque accessory minerals.

(A) Gondwana Sequence

Three (3) samples from the Gondwana Sequence were analyzed in this study, BH518, BH519, and BH520. Common in all three was a very high amount of graphite, ≥40% of each sample. This graphite was very fine grained, ranging from 5 – 10 μm (Fig 4.1). The graphite is an indicator of low-grade metamorphism. Quartz was also common in these samples, all of which showed some degree of metamorphism with the characteristic undulose extinction. Most quartz grains were subhedral shaped and sub-round. The quartz in these three samples are detrital grains. Another common mineral in these rocks was sericite, a fine grained white mica normally ≤5 μm. The sericite normally occupied the spaces between the graphite. It is also another indicator of low-grade metamorphism in the presence of water. Of these three samples, only one sample contained detrital muscovite, which was BH519. This muscovite was fine grained, (≥10 μm), and dispersed throughout the sample. No porphyroclasts were present in any of

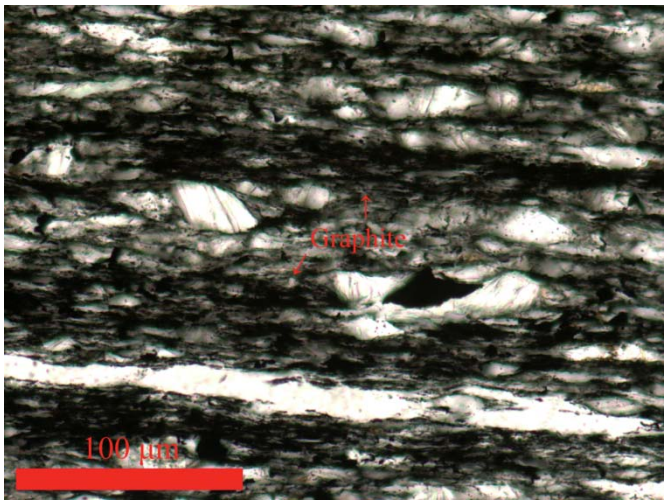

Figure 4.1. A micrograph showing the high concentration and the very fine grained texture of graphite.

the three samples, however, in BH520 there were detrital quartz grains that measured up to 50 µm, and formed a weak Θ-type clast, but without evidence of grain-size reduction it was not possible to label these as porphyroclasts.

Due to the low degree of metamorphism and the characteristics of fine-grained sedimentary rocks, relict sedimentary textures were evident in two of the three samples, BH518 and BH519. In both samples some form of sedimentary layering was visible by alternating layers of quartz and graphite/sericite layers. These layers were wavy, but had no evidence of gradational bedding.

Structures were common and evident in all three samples, with at least one form of foliation in the samples. In all samples there was a dominant foliation S_1 determined to be continuous slaty cleavage defined by alignment of graphite. Within sample BH519 there was a second foliation S_2 determined to be discrete crenulations cleavage overprinting the slaty cleavage. This is defined by the short limb of the crenulated graphite, however, this crenulation was only present in the more graphite-rich zones of BH519. All samples in the Gondwana Formation were named graphitic slate.

(B) Diuri Formation

The next three (3) samples are BH521, BH523, and BH516 which are from the Diuri Formation. Graphite is common among these samples, ranging from 20 – 30% per sample, and ranging in size from 5 – 10 μm. Quartz is also present in these samples, with very similar characteristics from the Gondwana Formation, such as undulose extinction, subidioblastic shaped, and sub-round. Quartz in these samples is also detrital grains that range in size from 10 – 20 μm. Sericite is not as common asin the Gondwana Fm., with it only being common in BH521, and less common in BH516. Several other minerals occurring in these samples that are not present in the Gondwana samples are calcite/dolomite, biotite, and feldspars, all of which are detrital grains. Calcite/dolomite is very common is BH516, with a modal percentage of 65%. The calcite/dolomite is xenoblastic shaped with very irregular grain boundaries. Grains are very fine grained. Biotite is another mineral that was not found in samples from the Gondwana Formation, and was only found in BH521. Since metamorphic grade is not high enough, this biotite would be considered detritus. Feldspar is only found in sample BH523 and exhibits both barcode-twinning and cross-hatching, which indicates both plagioclase and potassium feldspar. Large detrital grains are present in BH523 in three forms: 1) single quartz grains ranging 25 – 50 μm; 2) quartz aggregates ranging in size from 1 – 3 mm, with individual quartz grains ranging from 50 – 100 μm; and 3) quartz aggregate much like the above aggregate but cemented together with calcite/dolomite, and range in size from 50 – 200 μm. There is evidence of Θ-type pressure shadows around the third type of aggregate, but these pressure shadows are very weak. Sample BH516 shows evidence of the first porphyroclasts in these samples, which is a Θ-clast. These porphyroclasts are composed of mm-scale quartz, with very fine grained (≤5 μm) quartz pressure shadows. This fine grained quartz is due to grain size reduction, which occurs due to strain and deformation.

Sedimentary structures are only located within one sample, BH516. This relict sedimentary structure is visible as centimetre scale calcite/dolomite lamina. A calcite-rich lamina is flanked by calcite-poor laminae, with the calcite-poor zones being more quartz rich.

Structures in these samples are evident, and there is at least one form of foliation. Sample BH516 has one foliation: S_1. S_1 is a weak disjunctive wriggly cleavage defined by alignment of graphite. Sample BH521 has two foliations which are oblique to each other. Foliation S_1 is a weak disjunctive cleavage defined by alignment of biotite and elongated quartz. The S_2 foliation is a wriggly crenulation cleavage of S_1, and it also forms parallel to the graphite grains. Sample BH523 has a moderately rough disjunctive cleavage defined by alignment of graphite.

(C) Baxa Group

There are two samples from the Baxa, BH524 and BH511. These two samples are both relatively rich in graphite with a modal percentage of 45% graphite each. Quartz is only present in BH511 and not in BH524 and has the typical undulose extinction, subidioblastic shape, and sub-round grains as was seen in most other samples so far throughout the LHS, being very fine grained ≤5 μm. Biotite is only present in BH524 but not BH511. Sericite is common in both samples, and occupies space between the graphite. Chlorite is visible in same BH511, but is very rare. Rutile is present in BH524 and is only present along edges of micro-fractures and is the classic "beer-bottle brown." No porphyroclasts were visible in either sample.

There was evidence of sedimentary structures in both samples, with both relict sedimentary textures being composed of alternating coarse- and fine-grain zones composed of graphite-rich (fine grained) and quartz-rich (coarse grained) compositional layers.

Structures within these samples varied with BH511 having one foliation and BH524 having two foliations. In BH511, the S_1 foliation is a moderately rough disjunctive cleavage defined by alignment of graphite. Within BH524 there are two foliations, S_1 and S_2. S_1 is a slaty

cleavage defined by alignment of graphite, and S_2 is the crenulations of S_1. There is also evidence of what looks to be a micro-fracture, or what could be called a micro-fault. Curvature of graphite-rich lamina towards the "fault" plane may indicate some form of displacement. This micro-fracture is parallel to S_1.

(D) Daling Formation

Although the map (Fig. 4.3 and 4.4) shows both the Daling and Shumar Formation, the samples that were collected for this study were only collected from the Daling Formation due to ease of access by road. The samples are: BH525, BH513, BH526a, BH526b, BH527, BH528, and BH529. These samples show a larger range of mineralogy within one formation then any of the other formations. Graphite ranges from very high concentrations in BH528-29, with a modal percentage of 60 – 80%, to as low as 5% in sample BH527. All graphite in these samples are similar to all other samples, being very fine grained (≤5 μm). Quartz is also present in all samples, being as high as 60% modal percentage in BH526b and as low as 10% in BH527. All quartz share similar characteristics with undulose extinction, subidioblastic to xenoblastic shaped, and round to sub-round grains. Biotite becomes more abundant in samples BH526 a and b, and BH527, however it is more likely a metamorphic mineral rather than detrital grains in these samples. As with all other samples in this study, sericite is found in all except BH529. Detrital calcite/dolomite is common among samples BH527 and BH525, ranging in percentage from 35 – 60%. Muscovite becomes less common and is absent within the structurally higher samples above BH513. Porphyroclasts are only present in one of the samples, BH513. Within this sample there are two forms of porphyroclasts, Θ-clasts and □-clasts. The Θ-clasts are 20 μm across with very fine grained pressure shadows composed of recrystallized quartz. The □-clasts are very similar aside from the fact that they are larger than the Θ-clasts, being ~50 μm across.

Sedimentary structures were not very common throughout these samples, however BH526 a and b display a form of relict sedimentary structure. BH526a displayed relict cross-bedding, and BH526b displayed relict planar alternating laminae or quartz-rich and quartz-poor laminae. There is a wide range of structure within these samples, ranging from practically structureless in BH529, to strong slaty cleavage in BH513. The most common form of foliation found in these samples was weak to rough disjunctive cleavage.

(E) Jaishidanda Formation

Only one sample from the Jaishidanda Formation was taken, BH507. Graphite within this sample was scarce, and was only present in discrete grains, which were ≤5 μm. Quartz, muscovite, and biotite made up the composition of this sample with accessory opaque minerals. Only the quartz within this sample is thought of as detritus, where as muscovite and biotite are considered metamorphic minerals due to the higher grade of metamorphism of this rock. Of all the samples analyzed in this study, BH507 exhibited the highest amount of deformation. There is a disjunctive slaty cleavage throughout which is highly deformed and is defined by the alignment of muscovite and biotite. One isoclinal micro-fold is present within this sample and is defined by highly deformed muscovite and biotite with opaque accessory minerals found throughout the hinges.

4.2 Sample Locations, Temperatures, and Table of Results

The following figures are two maps showing the location of samples taken by Djordje Grujic and the average peak metamorphic temperature for each sample, a summarized table of results calculated with the equations from Beyssac et al. (2002) and Rahl et al. (2005), and a modified cross-section from Long et al. (In Press) showing samples. For complete data of peak heights, integrated areas, and calculated temperatures for each spot analyzed in the samples, see

Appendix B. Table 4.1 shows the average peak metamorphic temperatures obtained in this study. It is worth pointing out that even though the temperatures calculated using the equation from Beyssac et al. (2004) are at the bottom limit of the calibration (330 °C), when compared with the temperatures obtained from the equation from Rahl et al. (2005), they are within the error, therefore indicating that the Beyssac et al. (2004) equation is still suitable.

Plotted on Figure 4.4 are hypothetical chlorite and biotite isograds determined from the presence of chlorite and biotite from petrographic observations. These isograds do not correspond with Gansser (1983) (Fig 2.5). However, it is worth noting that the samples collected for this study were collected for their graphite content rather than their metamorphic indicator minerals. Figure 4.2 shows a cross section with the plotted sample locations.

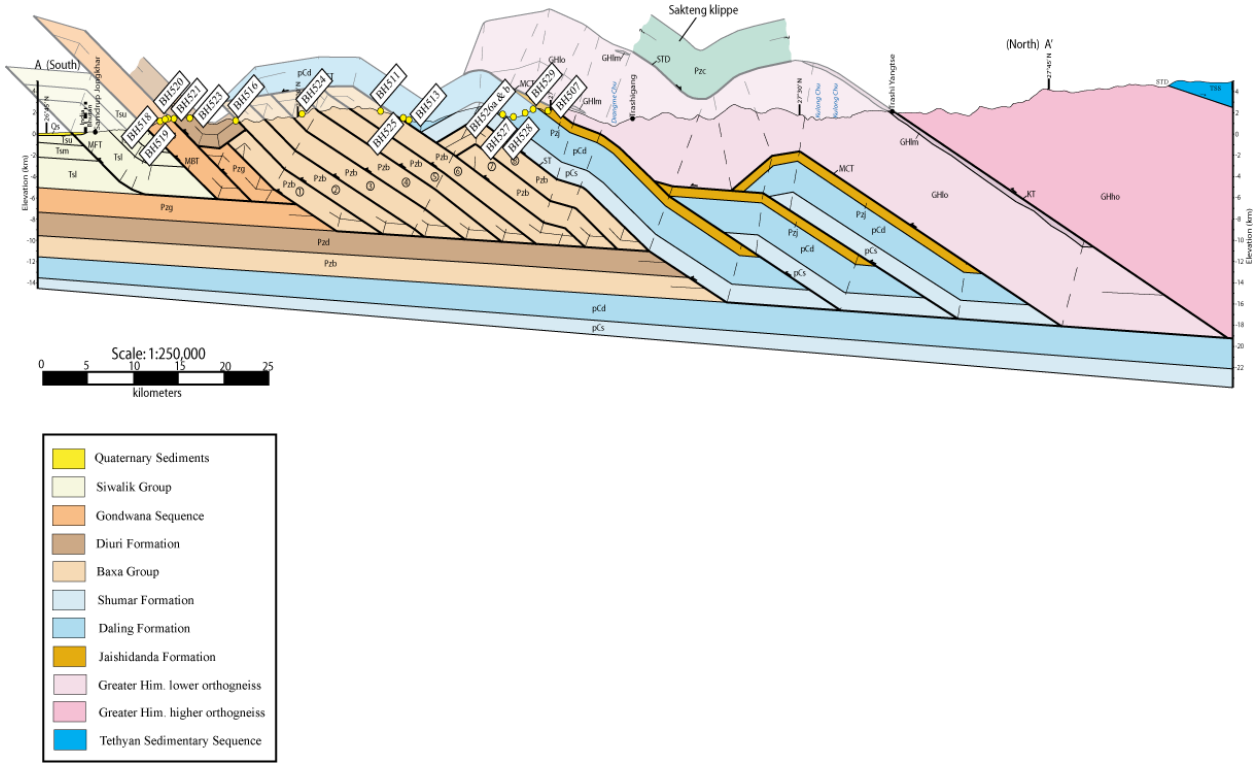

Figure 4.2. Cross section modified from Long et al. (In Press) showing the position of the samples analyzed in this study.

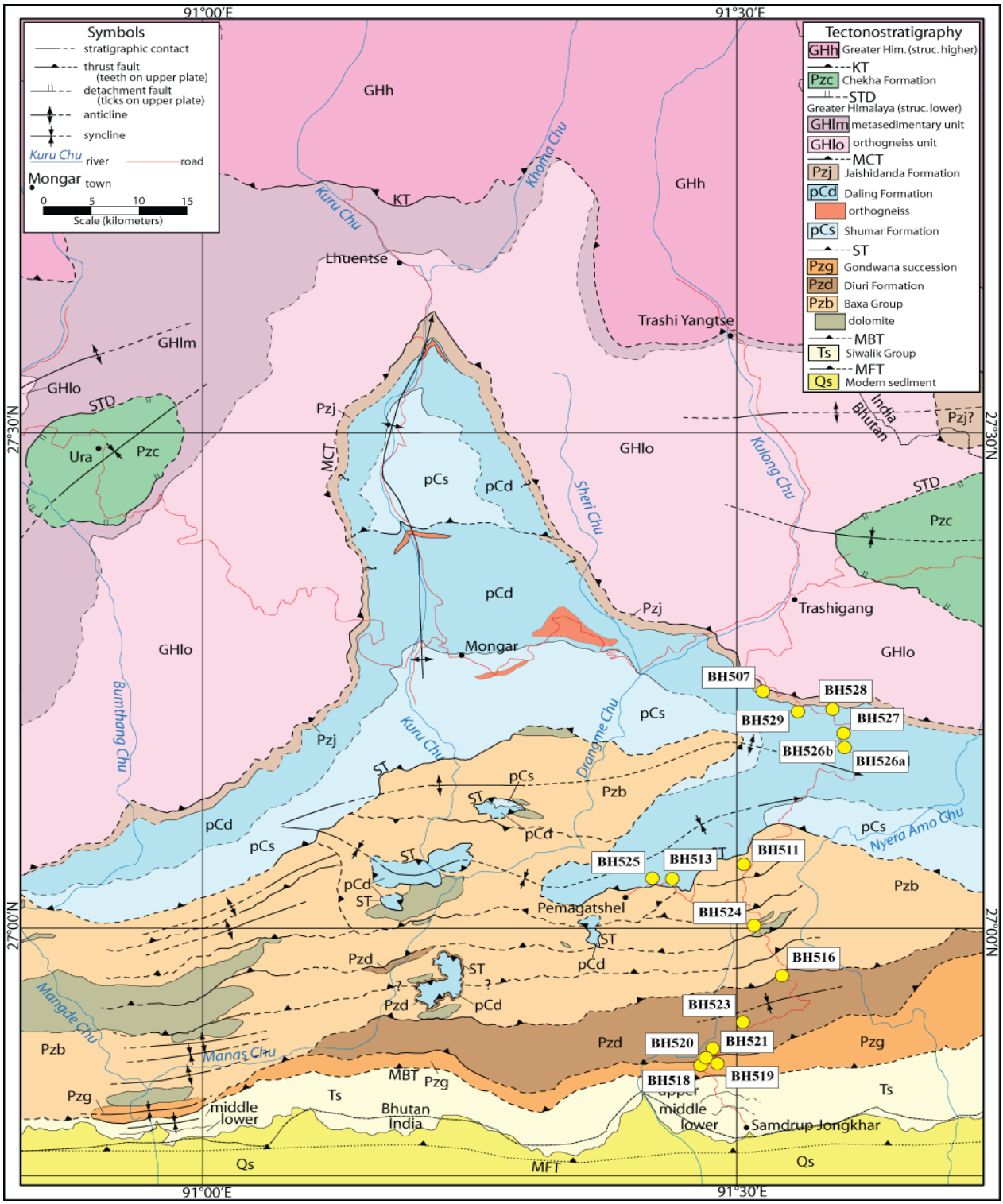

Figure 4.3. A geological map of the study area, located in eastern Bhutan. Plotted on the map are the locations of the 16 samples collected by Djordje Grujic. Image modified from Long et al. (In Press).

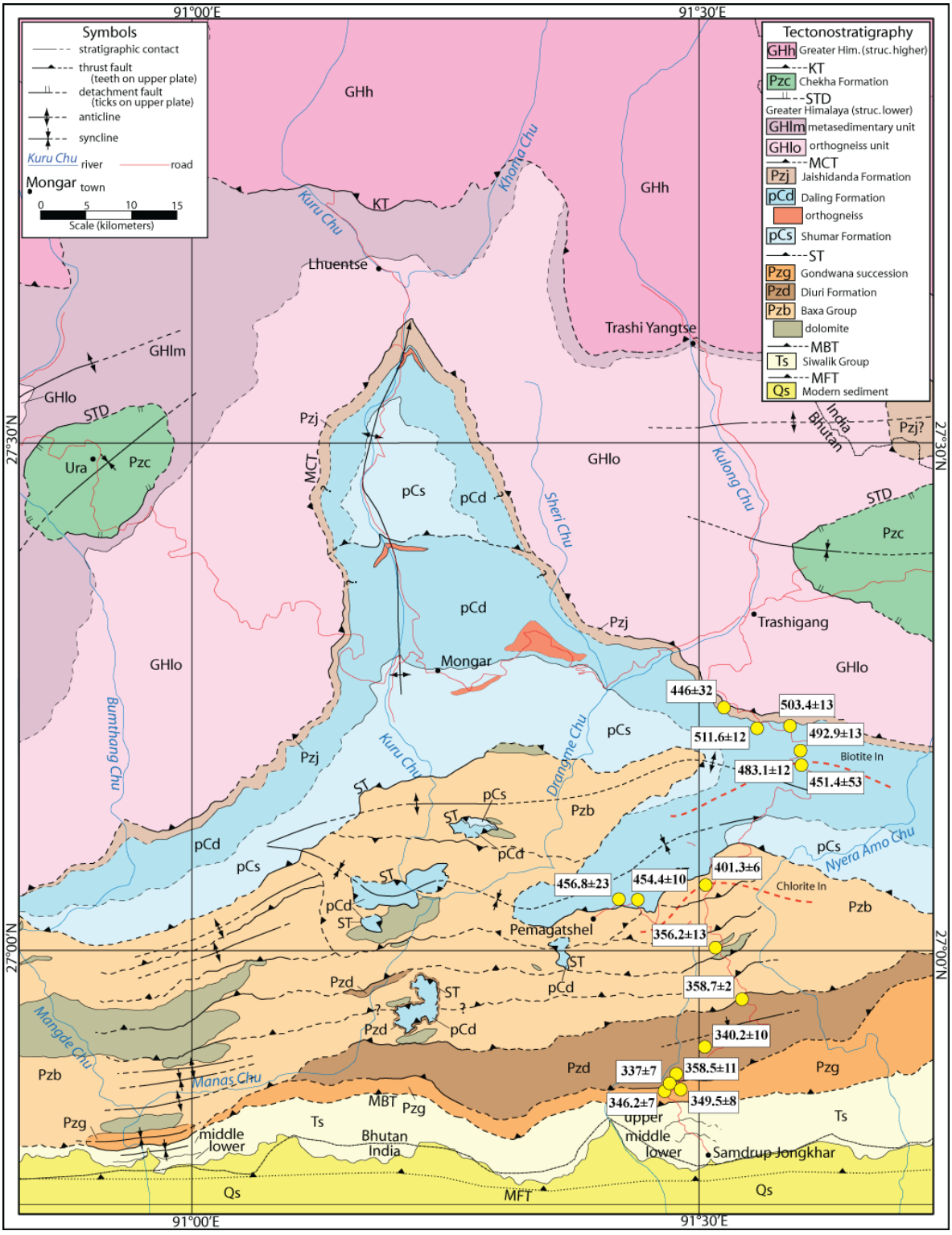

Figure 4.4. This figure is the same geological map as Figure 4.3 except plotted are the average peak metamorphic temperatures for each sample in °C as calculated from the equation by Beyssac et al (2002). Also plotted are the hypothetical chlorite and biotite isograds as determined from presence of metamorphic chlorite and biotie. Image modified from Long et al. (In Press).

Sample	Latitude (°N)	Longitude (°E)	*R1* Ratio (Avg.)	*R2* Ratio (Avg.)	Beyssac Temperature (°C)	Rahl Temperature (°C)	Unit
BH507	27.24321306	91.52034044	0.495	0.438	446±32	406.8±42	Jaishidanda Fm.
BH511	27.06050634	91.51492238	1.139	0.539	401.3±6	421.8±7	Baxa Group
BH513	27.03971386	91.44392967	0.582	0.419	454.4±10	448.9±13	Daling Fm.
BH516	26.95792258	91.54864311	1.758	0.634	358.7±2	373.7±3	Diuri Fm.
BH518	26.86454415	91.48038089	1.648	0.655	349.5±8	344.8±17	Gondwana Fm.
BH519	26.8701607	91.48000002	1.543	0.635	358.5±11	357.9±20	Gondwana Fm.
BH520	26.8712765	91.4795655	2.043	0.663	346.2±7	342.4±25	Gondwana Fm.
BH521	26.87759042	91.47975862	2.012	0.683	337±7	322.4±20	Gondwana Fm.
BH523	26.89226747	91.50638223	1.798	0.676	340.2±10	324.5±22	Gondwana Fm.
BH524	27.00565517	91.52882695	1.659	0.640	356.2±13	361.7±27	Baxa Group
BH525	27.04032004	91.42777741	0.565	0.414	456.8±23	449.7±29	Daling Fm.
BH526A	27.17793882	91.59824789	0.580	0.426	451.4±53	430.3±65	Daling Fm
BH526B	27.17793882	91.59824789	0.401	0.355	483.1±12	473.9±17	Daling Fm
BH527	27.19395697	91.59814596	0.354	0.333	492.9±13	485.4±22	Daling Fm
BH528	27.21914828	91.58370495	0.288	0.309	503.4±13	492.6±23	Daling Fm.
BH529	27.22383678	91.55382514	0.264	0.281	511.6±12	505.9±21	Daling Fm.

Table 4.1. This table shows each sample with their northing and easting coordinates, R1 and R2 ratios, average temperature with error in °C, and the lithological unit from which the samples were taken. Full data found in Appendix B.

5.0 DISCUSSION

5.1 Discussion of Inverted Metamorphic Gradient in the Lesser Himalayan Sequence

For the purpose of this discussion, the sample localities will be broken up into three areas. Looking at Figure 5.1 we see all of the samples plotted on a structural distance-temperature diagram. As stated above, this diagram will be broken into two segments to be

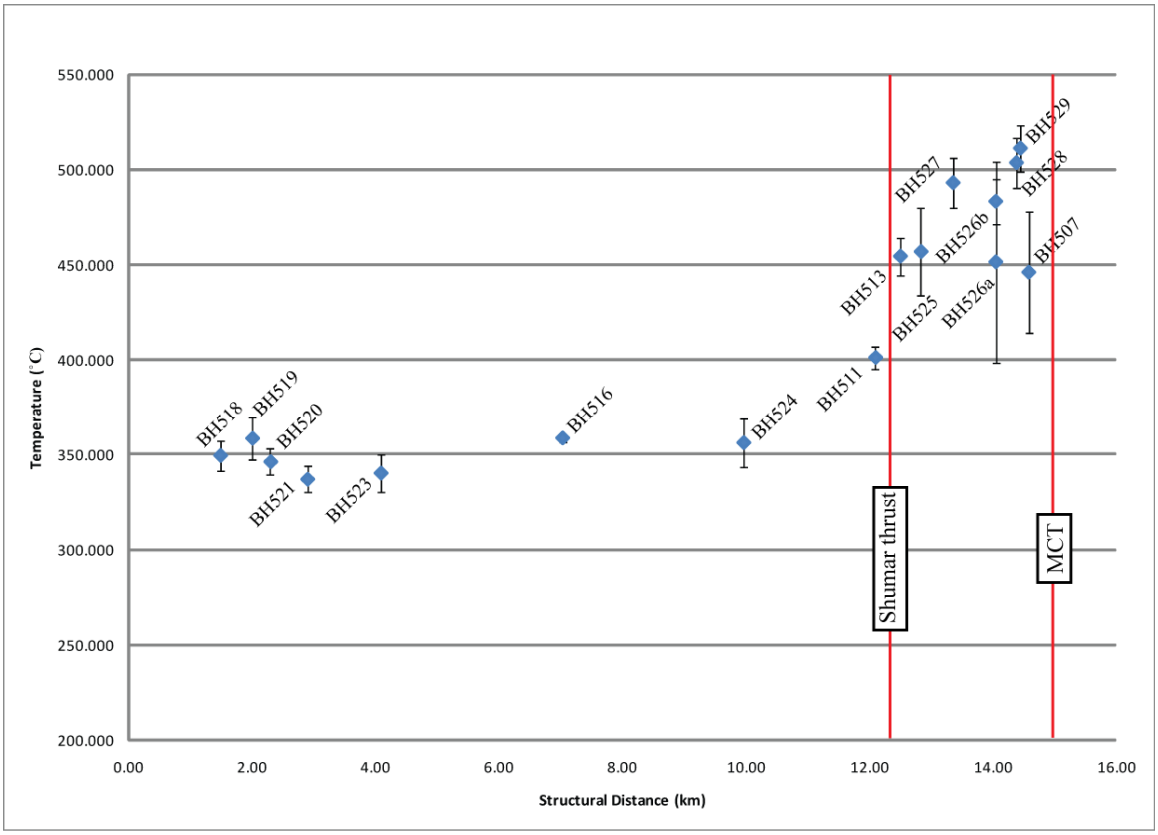

Figure 5.1. Structural distance-temperature diagram for all the samples collected and analyzed. MBT is at the origin, with the Shumar thrust and Main Central thrust labelled. Although in map view BH527 is closer to the MCT than BH526 a & b, samples 526 a & b are structurally further away than 527.

analyzed with the first segment ranging from BH518 to BH524. The second segment will include samples BH525 through to BH529, excluding sample BH507. Sample 507 yielded an RSCM temperature of 446 °C, which is lower than expected. Sample BH507 will be disregarded from further discussion. First there is a sudden drop in an otherwise constant trend of increasing

temperatures. Second it comes from the Jaishidanda Formation. The metamorphism of this unit has been well studied recently (Daniel et al., 2003). The metamorphic temperatures of four samples in the vicinity of 507 range from 650 – 675 °C (Daniel et al., 2003). This is much higher than 507. There are two possible reasons for this disagreement. The first reason being that the Raman spectroscopy of carbonaceous material has range of 330 – 650 °C and that this sample is at the uppermost limit of this technique causing problems

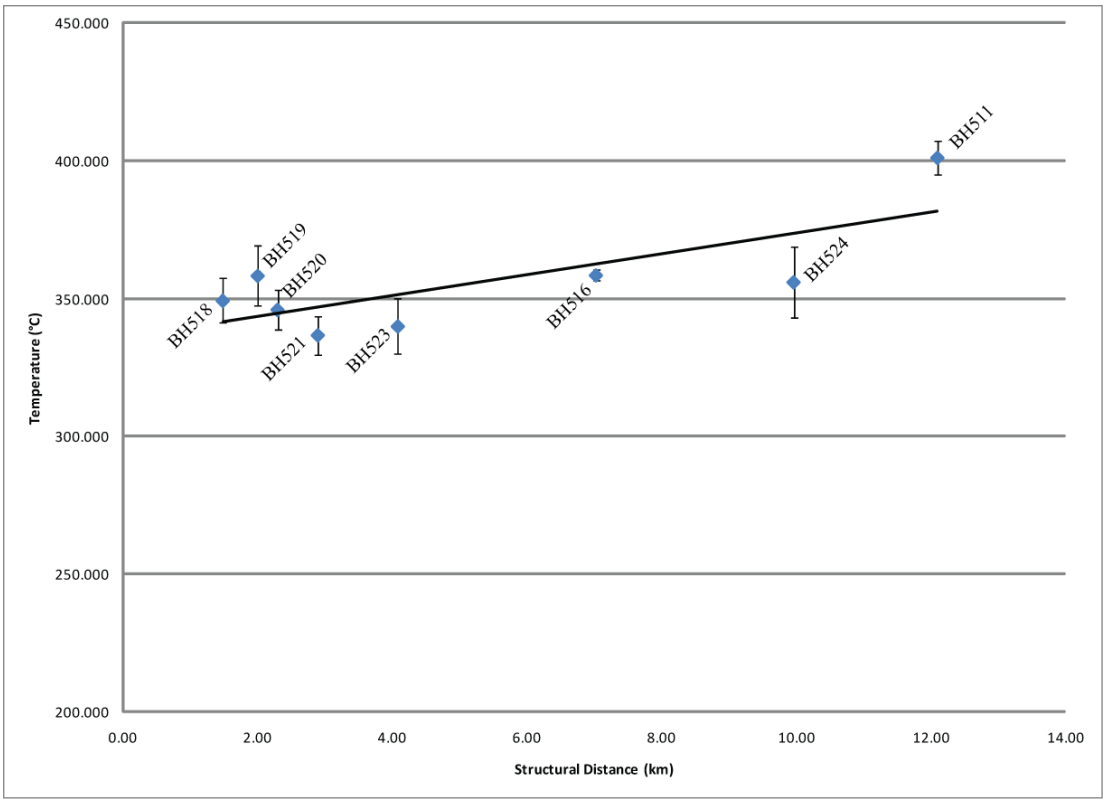

Figure 5.2. Structural distance-temperature diagram of the footwall of the Sumar thrust in the Lesser Himalayan Sequence. The Main Boundary thrust is at the origin of the diagram. This group contains samples BH518 through to BH511. They are from Gondwana, Buxa and Diuri formations.

stemming from the calibration of the Raman spectrometer. The second problem could arise from the scarcity of carbonaceous material within the sample itself, causing a very inaccurate analysis of the sample.

The first segment that will be analyzed contain samples BH518 through to BH524 (Fig 5.2), sample BH511 will be left out of discussion until later. This area does not indicate the inverted metamorphic temperature, and actually has a very low slope, being only 0.63 °C/km for samples BH518 to BH524. The mean value for the first seven samples is 349.4 ± 6.9 °C. This indicates virtually constant peak temperature for the 10 km in the hanging wall of the Main

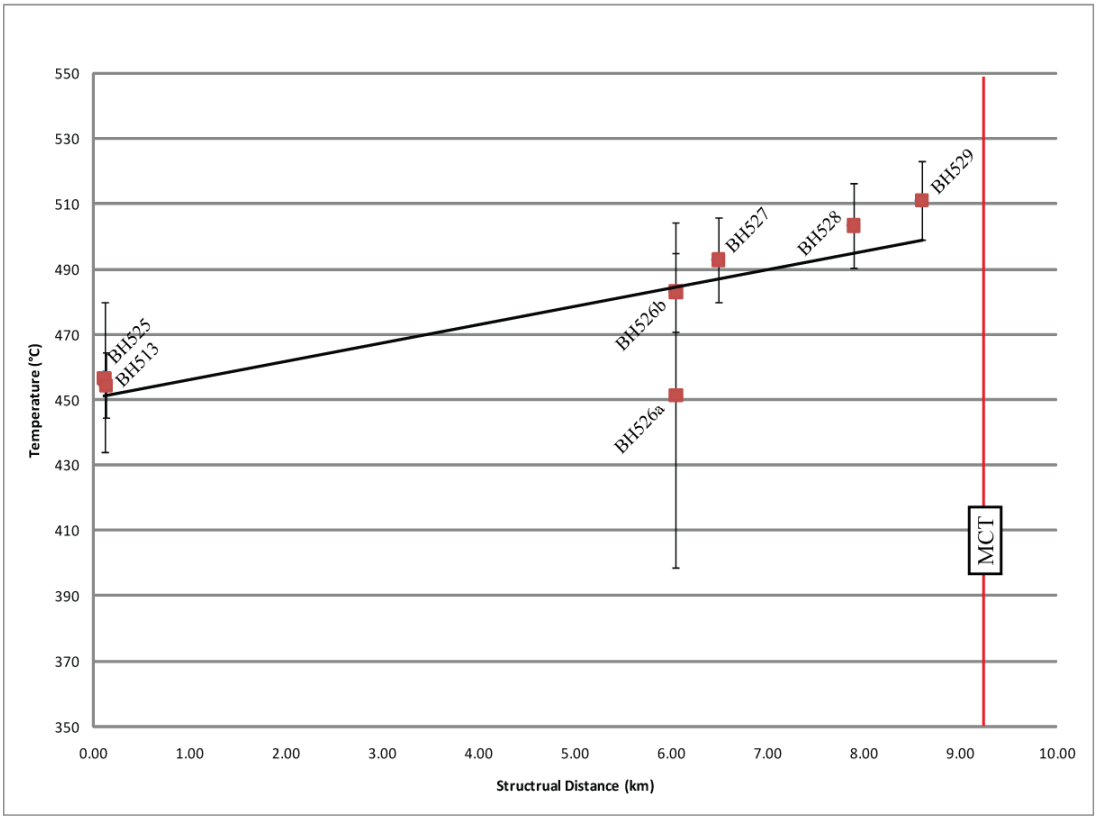

Figure 5.3. Structural distance-temperature diagram showing the seven structurally highest samples from the Shumar thrust (at the origin) to the Main Central thrust, indicated on the diagram.

Boundary thrust. The highest sample in this group, BH511, yields ~400 °C. It is however not clear if this increase is due to the onset of progressive inverted temperature gradient within the LHS or is the heating at the site due to overthrusting of the hotter Shumar thrust. This will be discussed later in chapter 6.

The next segment is located in the hanging wall of the Shumar thrust and includes samples BH525 to BH529, (Fig 5.3). Structural distance of these Samples were measured

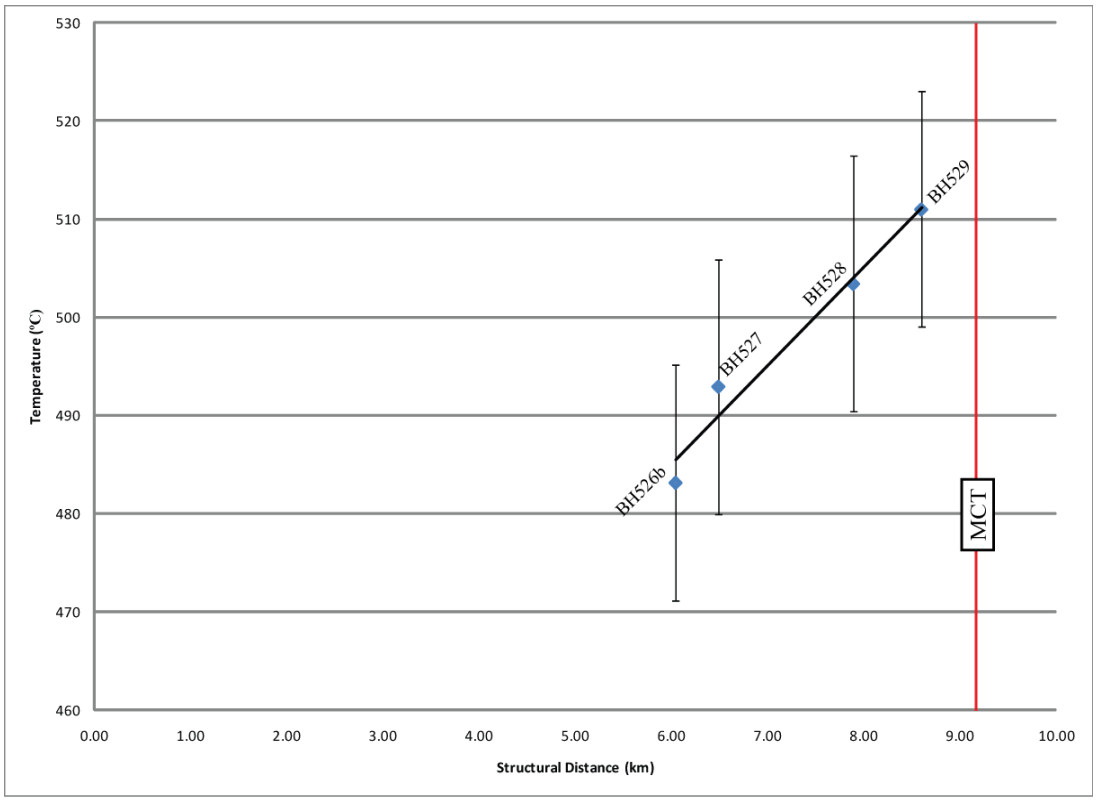

Figure 5.4. Structural distance-termperature diagram showing the four highest samples in the Shumar thrust hanging wall located just below the Main Central thrust, indicated on diagram in red.

from the surface to the Shumar thrust, and in this sense provides a more accurate measurement then the measurement of the entire section from the MBT distance to the Shumar thrust due to no errors from underlying structures such as antiforms. These samples, which range from the Shumar thrust to the Main Central thrust, show an inverted temperature gradient of 6.68 °C/km. This will be discussed later in chapter 6.

Taking a closer look at the four highest samples (BH526b, BH527, BH528, and BH529) the inverted temperature gradient is 10.94 °C/km (Fig 5.4a). The correlation of these two subsets gives an R^2 value of 0.94 for Figure 5.3, and 0.96 for Figure 5.4. In other published data of RSCM in the Lesser Himalayan Sequence similar temperature ranges were observed between 340 °C at the base of the sequence and 510 °C at the top of it (Bollinger et al. (2004), Beysac et al. (2004), Célérier et al. (2009)). Both Bollinger et al. (2004) and Célérier et al. (2009) have

calculated temperature gradients across the LHS from a minimum of 25 °C/km to a maximum of 50 °C/km (Fig 5.5). These gradients are quite different from the ones obtained in this study, which have been estimated between ~ 11 and ~ 7 °C/km. Compared with the distances from the LHS in this study, samples from Bollinger et al. (2004) were not taken from the entire LHS, providing a low degree of constraint for the temperature gradient. Also, temperatures from the hanging wall of the MCT, which is in the Greater Himalayan Sequence, were used in calculating

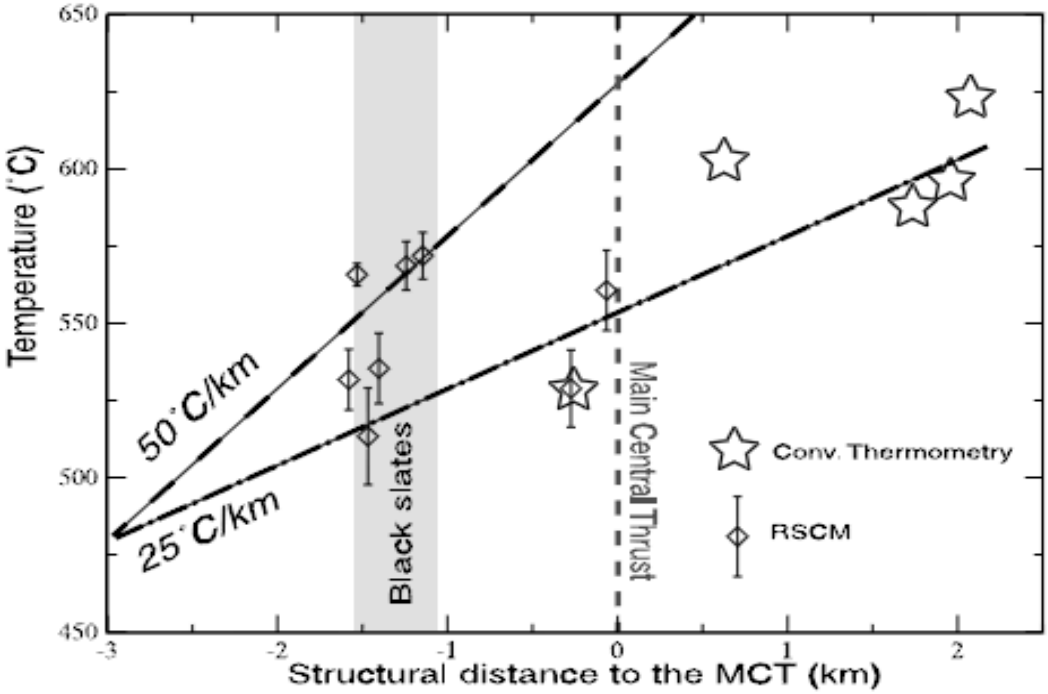

Figure 5.5. This is a structural distance-temperature diagram from Bollinger et al. (2004). Compared with the distances from the MCT in this study, samples from Bollinger were not taken from the entire Shumar thrust hanging wall, providing a low degree of constraint for the temperature gradient.

the temperature gradient, which would provide an inaccurate temperature gradient for the LHS. The analysis in this work indicates that a forward propagation of the line of best fit for the samples from the Shumar hanging wall (Fig 5.3) does not include the samples in Jaishidanda Formation and the base of the GHS in the eastern Bhutan (Fig. 5.5). One main reason the

gradients obtained in this study prove to be more reliable is due to the structural distance constraint of these samples. In the study done by Célérier et al. (2009), they only covered a minimum structural distance of ~1.5 km below the MCT, whereas in this study a structural distance of ~9 km was covered in the Shumar hanging wall. This constrains the samples taken and provides a more accurate structural distance-temperature gradient.

The next observations that will be discussed are the jumps in temperature within the LHS. The first jump, which can be clearly seen in Figure 5.1 at ~12 km, is on the scale of 50 ºC within a few hundred metres, which also crosses the Shumar thrust. Two possible reasons for this jump include overthrusting of the Shumar hanging wall placing hotter rock over the Shumar footwall, or, the thrusting itself propagated the inverted thermal gradient to the south. This then indicates that the minimum temperature jump across the Shumar thrust is ~50 °C if BH511 was originally located within the Shumar hanging wall. On the other hand, if the onset of the thrusting heated up the top of the Shumar footwall, then that would indicate BH511 was originally in the footwall and experienced metamorphism due to the Shumar thrust activation. This would then indicate BH511 had an initial cooler temperature, and would make the jump across the Shumar on the scale of ~100 °C. This will be further discussed in the chapter 6.

The next two jumps occur just below, and across the MCT, respectively. One noticeable jump occurs again within the LHS, and is situated hypothetically across the boundary between the Daling Formation and the Jaishidanda Formation. This jump can be seen from a combination of the data from this study along with data from Daniel et al. (2003). In the Daling Formation, max peak temperatures of ~510 °C were reached, and from Daniel et al. (2003) temperatures of ~650 °C. This indicates a temperature jump across the Daling-Jaishidanda contact of ~140 °C. The third and final notable jump occurs across the MCT. Daniel et al. (2003) also analyzed samples above the MCT in the GHS, and from conventional thermobarometry obtained

minimum peak metamorphic temperatures of ~750 – 800 °C just some 500 m above the MCT. This indicates a second jump occurring across the MCT, and is further evidence for inverted metamorphic temperatures.

5.2 Comparison of Data with Previous Models

Gansser (1983) suggested that the inverted metamorphic gradient trough the LHS and GHS is smooth and continuous transition (Fig 2.3). Similarly the detailed metamorphic study of the MCT zone in the eastern Bhutan by Daniel et al. (2003) indicated a steep temperature gradient across the MCT and small pressure increase. I could not conclude if there is a steep continuous gradient or a sudden metamorphic jump across the MCT. However, the data that were presented in this study shows that; there can be both a smooth gradient along with local jumps in peak metamorphic temperature. For at least 10 km of structural thickness, the temperatures in the footwall of the Shumar thrust show a rather flat slope (Fig 5.2), however, near the Shumar thrust there is a temperature increase from ~350 °C to ~400 °C, from samples BH524 to BH511. This may show evidence for LeFort's (1975) and Pêcher's (1989) theory about the "ironing-effect" in a sense that the Shumar thrust could have superimposed hotter rock (≥450 °C) on top of the Shumar thrust footwall rock (~350 °C). This would cause a structurally downward minimum temperature increase of ~50 °C at ~700 m beneath the thrust. Alternatively, the temperature increase from 350 °C to 400 °C, from sample BH524 to BH511, may be the onset of the trend of inverted metamorphism. Across the Shumar thrust there is a minimum temperature jump of 50 °C (from 400 °C to ~ 450 °C). However, if there was a uniformly inverted temperature gradient in the footwall of ~350 °C, this temperature jump would increase to a minimum of 100 °C (350 °C to 450 °C) before thrusting. Evidence to support this is if the line of best fit is propagated backward from the Shumar hangingwall to the footwall, the gradient of the hangingwall does not intersect the 400 °C mark until well below the Shumar thrust. This would indicate that sample

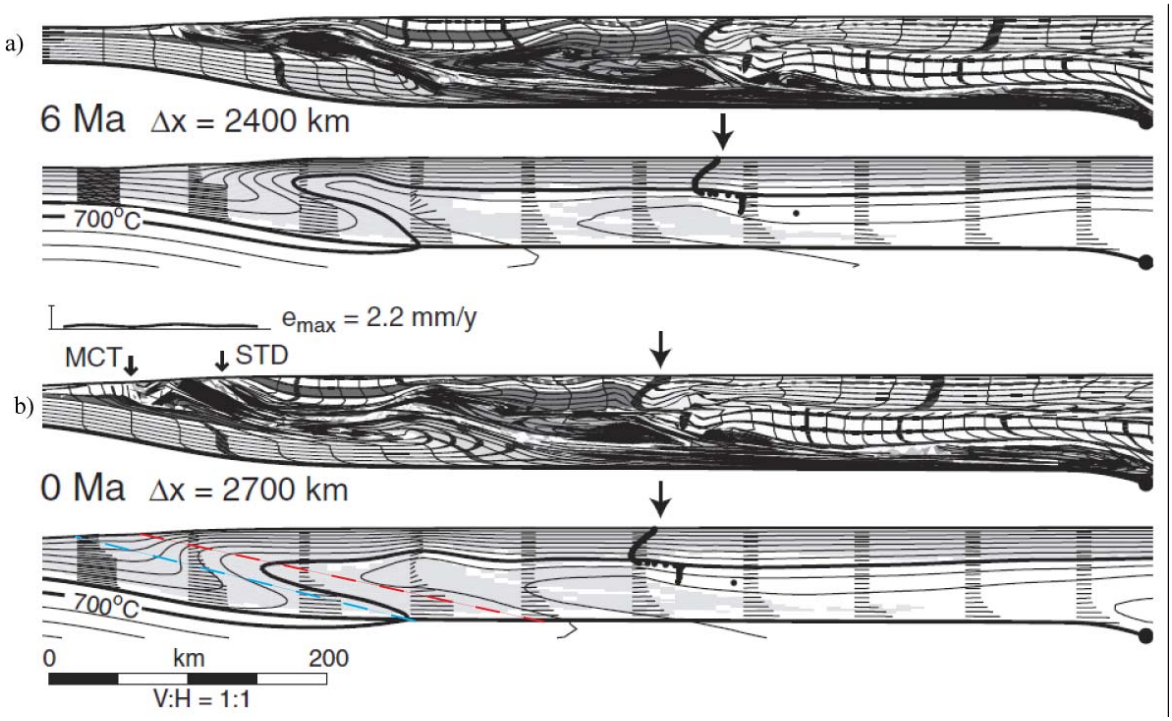

Figure 5.6. Model HT111 from Jamieson et al. 2006 showing the deformation of the isotherms due to the ductile extrusion of the GHS. These two images show snapshots in time at a) 6 Ma, and b) 0 Ma, or present day. The temperature gradient as calculated from 0 Ma corresponds to the temperature gradient calculated from this study, which is ~11 °C/km. A hypothetical MCT is labelled in red, and Shumar thrust in blue.

BH511 is indeed not part of the Shumar hangingwall metamorphic gradient. In the Shumar hangingwall there is indeed an inverted metamorphic gradient (Fig 5.3). Causes for this can be explained by two alternative models. According to theory proposed by Bollinger et al. (2004) postmetamorphic deformation of originally flat lying isograds has produced the inverted metamorphic gradient. According to Beaumont (2001, 2004, 2006 and Jamieson et al., 2004, 2006) the isotherms in the LHS could have been inverted due to the southward flow of a weak mid crustal layer, known as the channel flow hypothesis. The advection of isotherms could cause inversion of the isotherms beneath the GHS (Fig 5.6). In the entire Shumar hangingwall there is a continuous and smooth temperature gradient of ~7 – 11 °C/km (Fig 5.8). Bollinger e al., (2004) and Célerier et al. (2009) infer a temperature gradient of 20 – 50 °Cékm (Fig 5.5). However, they

combine the temperature data from different geothermometric techniques and the data from the LHS and the GHS, which produces a much steeper temperature gradient. In the published channel flow models the temperature gradient has not been described. However, using published figures, a thermal gradient can be estimated. Jamieson et al. (2006) present two models that can be applied to the Himalayas, HT1 and HT111. The former is the simpler model while the latter has a more complex history, and may be more representative of the tectonics of the eastern Himalayas (Fig. 5.6). Temperature gradients have been measured in the area of steep or inverted isotherms beneath the model MCT for the time step at 6 Ma before the present (Fig 5.6). Between isotherms of 400 and 600 °C the model HT1

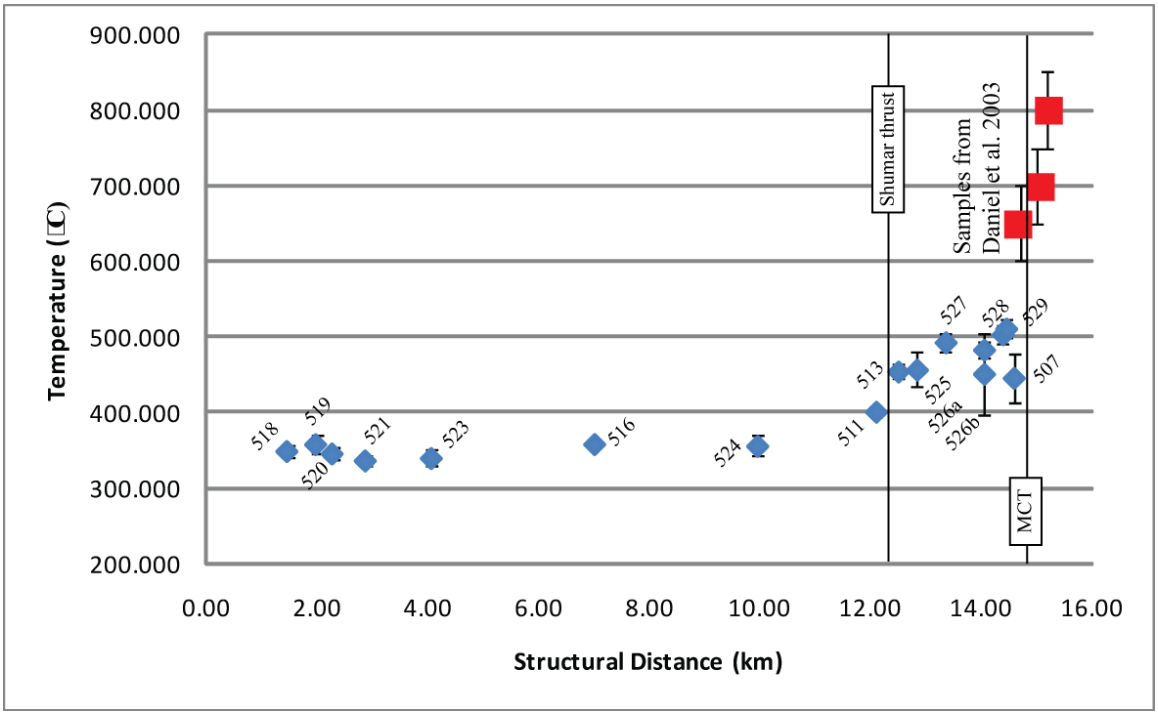

Figure 5.7. A structural distance-temperature diagram showing all samples analyzed in this study along with three samples from Daniel et al. 2003 (in red), with one sample located beneath the MCT and two above. The MBT is at the origin.

yields the gradient of 3 – 5 °C / km and the model HT111 9- 11 °C / km. The latter model therefore predicts the temperature gradient observed in the eastern Bhutan obtained from this

study. However the natural gradient is not necessarily a snapshot of the isotherms at a given time but most likely the result of deformed isotherms and pervasive shearing in the entire measured section. Another interesting area lies at the top of the Shumar hangingwall and across the MCT. Work here by Daniel et al. (2003) and from this study show that within several hundred metres beneath and above the MCT there is a large jump in temperature of ~150 °C (Fig 5.7). This large jump across the MCT could result from a combination of multiple events. The large jump we see in temperature could be a result of the "ironing-effect" theory, with the much hotter GHS being thrust on top of the cooler LHS. The channel flow theory model proposed by Grujic et al. (1996) and Jamieson et al. (2006) would also explain this jump. Looking at Figure 5.6, the pinnacles of the folded isotherms show the ~150 °C jump across the MCT over such a short distance. Also, further work by Daniel et al. (2003) shows that once above 800 °C, the temperature gradient levels out. The HT111 model in Figure 5.6 shows the hypothesized isotherms flattening out rather quickly above the MCT. One observation to note is the lack of a line of best fit in Figure 5.6. This is due to the fact that the entire LHS and lower part of the GHS (data from Daniel et al. 2003, Fig 5.7) is composed of multiple peak metamorphic gradients, and cannot be justified by having one single gradient throughout. This indicates that the LHS and lower part of the GHS are not part of a continuous inverted metamorphic gradient.

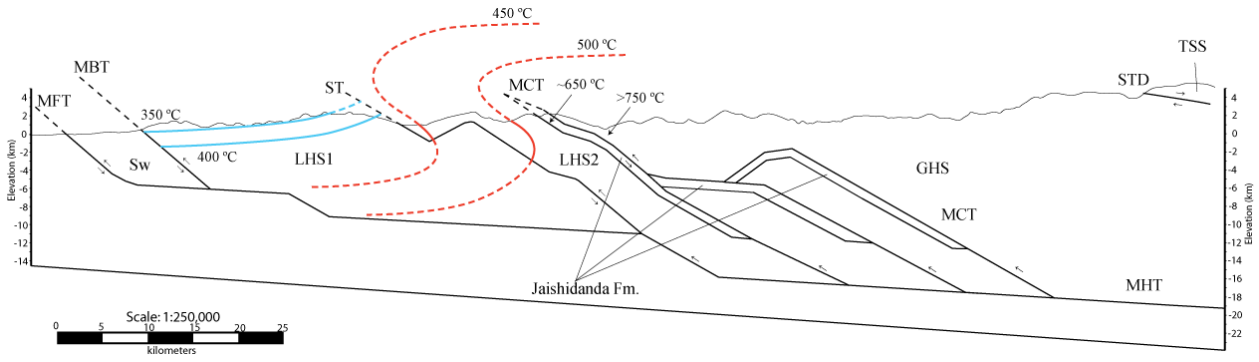

Figure 5.8. A schematic illustration of the potential isotherms located in the Shumar footwall (blue) and the Shumar hangingwall (red). As discussed earlier, the temperature gradient in the footwall is nearly flat with a slight increase at the Shumar thrust. However, once above the ST the temperature gradient jumps to ~450 °C and then smoothly progresses towards the MCT, where another steep jump of ~150 °C occurs across the MCT zone. Image modified from Long et al. In Press.

6.0 CONCLUSION

In this study, samples of carbonaceous slates from a transect across the LHS of eastern Bhutan have been analysed in order to determine the peak metamorphic temperatures. The samples were collected between the MBT and the MCT. The total structural thickness of the section is ~15 km but it has been apparently duplicated along the Shumar thrust (McQuarrie et al., 2008). Of the 16 analysed samples, 8 are in the Shumar footwall and 8 are in the Shumar hanginwall. Analysis of the samples by RSCM from this study has given several conclusions:

(a) There is an inverted metamorphic gradient across the LHS. However, it is composed of two structural parts: it is not evident in the Shumar thrust footwall, but is obvious in the hangingwall.

(b) Temperature gradient in the upper LHS thrust sheet calculated in this study ranged from a minimum of ~7 °C/km, to a max of ~11 °C/km. This are much lower than what was calculated by Bollinger et al. (2004) and Célérier et al. (2010).

(c) Two jumps in temperature have been noticed. The jump across the Shumar thrust is between 50 °C and 100 °C. The jump across the MCT is on the order of ~150 °C. This confirms that the Shumar thrust is a major structure within the LHS and that the metamorphic histories in the LHS and GHS should be considered separately, rather then one continuous zone of inverted metamorphism.

This study provides better constraint on temperature gradient in the LHS than Bollinger et al. 2004 and Célérier et al. 2009. The previous studies have considered samples in the hanging wall of the MCT as well in the GHS order to calculate the temperature gradient. The samples in this study are from the LHS only. As shown here there is no linear correlation between the samples in the LHS to those in the GHS, therefore it is considered that only the samples in the

LHS should be taken into account. A smooth temperature gradient is present in the upper 6 km of the section, while the lower 10 km of the section has attained same temperature. Analysis from this study has also shown how multiple theories of inverted metamorphic gradient can be combined to illustrate the larger picture. Of these theories, the channel flow model gives the most precise prediction of inverted metamorphic gradient in LHS, with a hypothesized temperature gradient equal to that obtained in this study. However later discrete thrusting has apparently dissected and modified the initial smooth temperature and metamorphic gradient. Furthermore, difference in timing and space of metamorphism in the LHS could have affected the discrepancy between Eastern and Central Himalaya. Detailed thermochronological study would be required to determine timing of metamorphism in both areas and comparison between the field data.

REFERENCES

Beaumont, C., Jamieson, R.A., Nguyen, M.H., Lee, B., 2001. Himalayan tectonics explained by extrusion of a low-viscosity crustal channel coupled to focused surface denudation, Nature 414, 738 – 742.

Beaumont, C., Jamieson, R.A., Nguyen, M.H., and Medvedev, S., 2004, Crustal channel flows: 1. Numerical models with applications to the tectonics of the Himalayan-Tibetan orogen: Journal of Geophysical Research, v.109, doi: 10.1029/2003JB002809.

Bény-Bassez, C. & Rouzaud, J. N., 1985. Characterization of carbonaceous materials by correlated electron and optical microscopy and Raman microspectroscopy. In: Scanning Electron Microscopy, p. 119–132, SEM Inc, Chicago.

Beyssac, O., Goffe, B., Chopin, C., Rouzand N., 2002. Raman spectra of carbonaceous material in metasediments: a new geothermometer. Journal of Metamorphic Geology, 20: 859-871.

Beyssac, O., Bollinger, L., Avouac, J-P., Goffe, B., 2004. Thermal metamorphism in the lesser Himalaya of Nepal determined from Raman spectroscopy of carbonaceous material. Earth and Planetary Science Letters, 225: 233-241

Bilham, R., Larson, K., Freymuller, J., and Members, P. I., 1997, GPS measurements of presentday convergence across the Nepal Himalaya: Nature, v. 386, p. 61–64.

Bollinger, L., Avouac, J. P., Beyssac, O., Catlos, E. J., Harrison, T. M., Grove, M., Goffe, B., and Sapkota., S. 2004. Thermal structure and exhumation history of the Lesser Himalaya in central Nepal. Tectonics, vol. 23, TC5015, doi:10.1029/2003TC001564, 2004

Burchfiel, B.C., Chen, Z., Hodges, K.V., Liu, Y., Royden, L.H., Deng, C., and Xu, J. 1992. The South Tibetan detachment system, Himalayan orogen: Extension contemporaneous with and parallel to shortening in a collisional mountain belt. Geological Society of America Special Paper, 41.

Burg, J. P., and Chen, G. M., 1984, Tectonics and structural zonation of southern Tibet, China: Nature, v. 311, p. 219–223.

Célérier, J., Harrison, T.M., Beyssac, O., Herman, F., Dunlap, W.J., Webb, A.G.A., 2009, The Kumaun and Garwhal Lesser Himalaya, India: Part 2. Thermal and deformation histories. GSA Bulletin; 121; 1281 – 1297.

Coward, M. P., Butler, R. W. H., Chambers, A. F., Graham, R. H., Izatt, C. N., Khan, M. A., Knipe, R. J., Prior, D. J., Treloar, P. J., and Williams, M. P., 1988, Folding and imbrications of the Indian crust during Himalayan collision, *in* Shackleton, R. M.,

Dewey, J. F., and Windley, B. F., eds., Tectonic evolution of the Himalayas and Tibet: London, The Royal Society, p. 89–115.

Daniel, C.G., Hollister, L.S., Parrish, R.R., and Grujic, D. 2003. Exhumation of the Main Central Thrust from Lower Crustal Depths, Eastern Bhutan Himalaya. Journal of Metamorphic Petrology, 21: 317-334.

DeCelles, P.G., Gehrels, G.E., Quade. J., Ojha, T.P., 1998. Eocene early Miocene foreland basin development and the history of Himalayan thrusting, western and central Nepal. Tectonics, 17: 741-765

DeCelles, P. G., Gehrels, G. E., Quade, J., LaReau, B., Spurlin, M., 2000. Tectonic Implications of U-Pb Zircon Ages of the Himalayan Orogenic Belt in Nepal. Science, vol. 288, Issue 5465

DeCelles, P.G., 2001. Stratigraphy, structure, and tectonic evolution of the Himalayan fold-thrust belt in western Nepal. Tectonics, 20: 487-509.

Edwards, M.A., Kidd, W.S.F., Li, J., Yue, Y., Clark, M., 1996, Multi-stage development of the southern Tibet detachment system near Khula Kangri. New data from Gonto La; Tectonophysics 260, 1-19.

Gansser, A., 1964, Geology of the Himalayas: London,Wiley Interscience, 289 p.

Gansser, A. 1983. Geology of the Bhutan Himalaya. Birkhäuser, Basel, pp. 181.

Grujic, D., Casey, M., Davidson, C., Hollister, L.S., Kündig, R., Pavlis, T., and Schmid, S. 1996. Ductile extrusion of the Higher Himalayan Crystalline in Bhutan: evidence from quartz microfabrics. Tectonophysics, 260: 21-43.

Grujic, D., Hollister, L.S., and Parrish, R.R. 2002. Himalayan metamorphic sequence as an orogenic channel: insight from Bhutan. Earth and Planetary Science Letters, 198: 177-191.

Grujic, D., Coutand, I., Bookhagen, B., Bonnet, S., Blythe, A., Duncan, C., 2006. Climatic forcing of erosion, landscape, and tectonics in the Bhutan Himalayas. Geology, October 2006, p. 800 – 804.

Harrison, T. M., Ryerson, F. J., Le Fort, P.,Yin, A., Lovera, O., and Catlos, E. J., 1997, A late Miocene–Pliocene origin for the central Himalayan inverted metamorphism: Earth and Planetary Science Letters, v. 146, p. E1–E7.

Hodges, K.V., and Parrish, R.R, 1996. Isotopic constraints on the age and provenance of the Lesser and Greater Himalayan sequences, Nepalese Himalaya. Geological Society of America Bulletin, 108: 904-911.

Hodges, K.V. 2000. Tectonics of the Himalaya and southern Tibet from two perspectives. Geological Society of America Bulletin, 112: 324-350.

Horiba Scientific: Raman spectroscopy. Retrieved from http://www.horiba.com/scientific/products/raman-spectroscopy/

Jamieson, R.A., Beaumont, C., Hamilton, J., Fullsack, P. 1996, Tectonic assembly of inverted metamorphic sequences, Geology; 24, 839 – 842, doi: 10.1130/0091-7613.

Jamieson, R.A., Beaumont, C., Medvedev, S. & Nguyen, M.H. 2004. Crustal channel flows: 2. Numerical models with implications for metamorphism in the Himalayan–Tibetan Orogen. Journal of Geophysical Research, 109, doi:10.1029/2003JB002811.

Jamieson, R.A., Beaumont, C., Nguyen, M.H., Grujic, D. 2006, Provenance of the Greater Himalayan Sequence and associated rocks: Predictions of the channel flow models. Geological Society of London Special Publication, Channel Flow Conference, 1 – 24.

Kellett, D.A., Godin, L., Grujic, D. 2009. Pre-Miocene deformation of the Himalayan superstructure, Hidden valley, central Nepal. *Journal of the Geological Society*. vol. 166: issue.2: 261-275; DOI: 10.1144/0016-76492008-097

Le Fort, P., 1975, Himalayas: The collided range. Present knowledge of the continental arc: American, Journal of Science, v. 275-A, p. 1–44.

Le Fort, P., 1994, French earth sciences research in the Himalaya regions: Kathmandu, Nepal, Alliance Française, p. 174.

Long, S., McQuarrie, N., Tobgay, T., Rose, C., Gehrels, G., Grujic, D. In Press. Tectonostratigraphy of the Lesser Himalaya of Bhutan: Implications for the Along-Strike Stratigraphic Continuity of the Northern Indian Margin

McQuarrie, N. & Davis, G. H. 2002. Crossing the several scales of strainaccomplishing mechanisms in the hinterland of the central Andean fold–thrust belt, Bolivia. Journal of Structural Geology, 24, 1587–1602.

Molnar, P. 1984. Structure and Tectonics of the Himalaya: Constraints and Implications of Geophysical DataAnnual Review of Earth and Planetary Sciences, vol. 12: 489-516.

Pêcher, A., 1989. The metamorphism in the central Himalaya: Journal of Metamorphic Geology, v. 7, p. 31–41.

Potts, P.J., Cave, M.R., Microprobe techniques in the earth sciences, Volume 6 of Mineralogical Society series, Springer 1995.

Ralh, J.M., Anderson, K.M., Brandon, M.T., Fassoulas, C. 2005. Raman spectroscopic carbonaceous material thermometry of low-grade metamorphic rocks: Calibration and application to tectonic exhumation in Crete, Greece.

Schelling, D., Arita, K., 1991. Thrust tectonics, crustal shortening, and the structure of the far-eastern Nepal Himalaya. Tectonics, 10: 851-862.

Schelling, D., 1992. The tectonostratigraphy and structure of the eastern Nepal Himalaya. Tectonics, 11: 925-943.

Wopenka, B., and Pasteris, J.D. 1993. Structural characterization of kerogens to granulite-facies graphite: Applicability of Raman microprobe spectroscopy. American Mineralogist, 78: 533-557.

Yeats, R. S., and Lillie, R. J., 1991, Contemporary tectonics of the Himalayan frontal fault system: Folds, blind thrusts and the 1905 Kangra earthquake: Journal of Structural Geology, v. 13, p. 215–225.

APPENDIX A – PETROGRAPHIC DESCRIPTIONS

Sample: BH507 – muscovite-biotite schist
Location: 27.2432130580N, 91.5203404427E
Rock Unit: Jaishidanda Formation

HAND SAMPLE

- Overall a very fine grained texture, light grey in colour. Alternating bands of compositional layering of biotite and quartz/muscovite (~1 mm). These layers are deformed with small tight folds with a wavelength of 5 mm. These folds are composed mostly of biotite and muscovite. No porphyroclasts present in the sample.

THIN SECTION

Mineralogy:

- Quartz: (dynamically recrystallized grains), 40% of sample, fine grained (10 – 25 μm), equigranular, subidioblastic, sub-angular, undulose extinction and sub-grain formations are common.
- Muscovite: (metamorphic mineral), 35% of sample, fine to medium grained (10 – 100 μm), subidioblastic, defines foliation.
- Biotite: (metamorphic mineral), 20%, fine grained (10 – 30 μm), subidioblastic grains, defines foliation with muscovite.
- Opaque: (metamorphic mineral), 4% of sample, dispersed throughout muscovite and biotite rich zones, dominantly found in axis of folds, possibly Ti-Fe oxide.
- Graphite: (metamorphic mineral), 1% of sample, very fine grained (≤1 μm), very rare and dispersed throughout sample, grains are elongate with no preferred orientation.

Structure:

- Two foliations in this sample: S_1 and S_2.
- S_1: strong disjunctive cleavage defined by the alignment of biotite and muscovite.
- S_2: ≥5 mm crenulation fold of S_1 foliation.
- Hinges of folds are dominated by opaque mineral.

a) 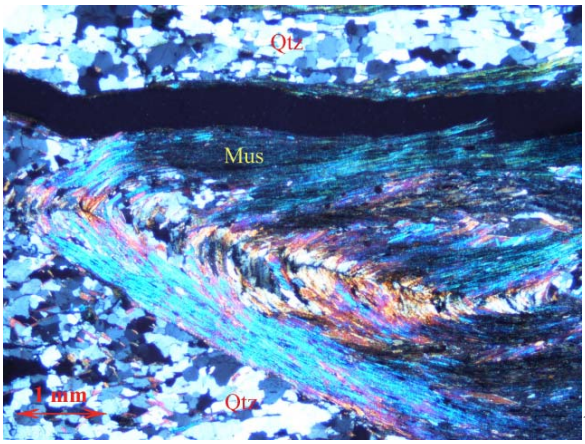

b) 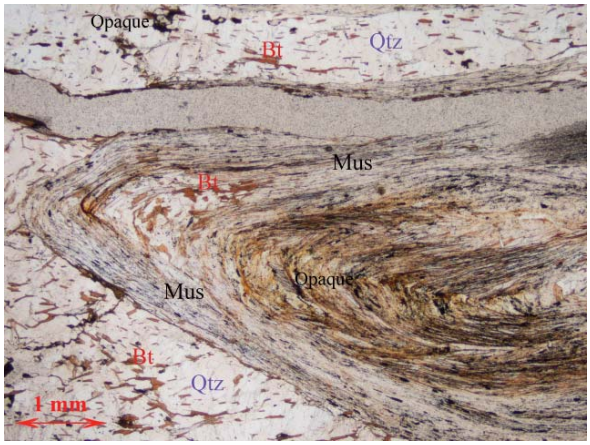

c) 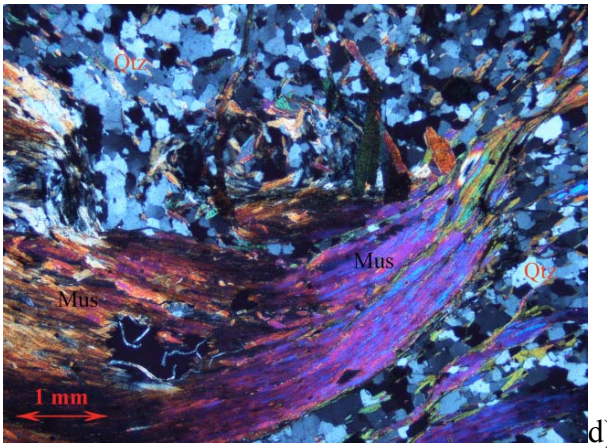

d) 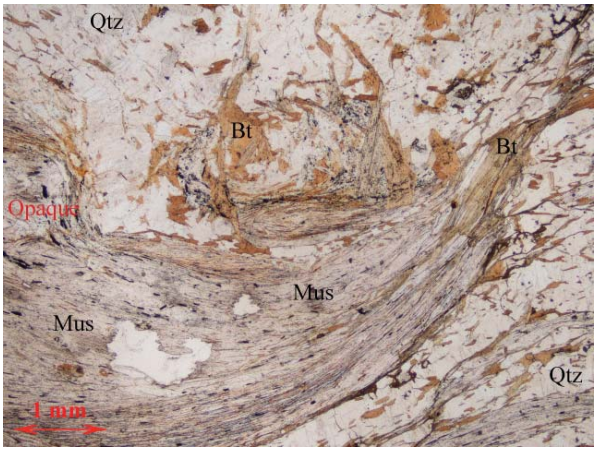

Micrographs for sample BH507. Micrographs a) and b) show the millimetre scale tight fold dominated by biotite and muscovite. Micrographs c) and d) show the slight crenulations of the S_1 foliation.

Sample: BH511 – graphitic slate
Location: 27.0605063440N, 91.5149223804E
Rock Unit: Baxa Group

HAND SAMPLE

- Very fine grained composition, grey in colour. Relict sedimentary structure is present as alternating laminae of dark grey and light grey minerals that are too fine grained to determine. A weak foliation is visible, but no porphyroclasts are present.

THIN SECTION
Mineralogy:

- Graphite: (metamorphic mineral), 45% of sample, very fine grained (≤5 μm), elongate, defines foliation.
- Quartz: (detrital grains), 45% of sample, very fine to fine grained (5 – 50 μm), subidioblastic to xenoblastic, undulose extinction is common, grains are elongate to foliation.
- Sericite: (metamorphic mineral), ~10% of sample, occupies area between graphite and is parallel to foliation.
- Chlorite: (metamorphic mineral), <1% of sample, fine grained (10 – 20 μm), fibrous with an irregular extinction pattern, presence of chlorite might indicate lower degree of metamorphism (lower greenschist).

Sedimentary Structure:

- Relict sedimentary laminae defined by alternating coarse and fine grained zones of quartz.
- Layering is oblique to S_1 foliation.

Structure:

- One foliation present: S_1.
- S_1 is a moderately rough disjunctive cleavage defined by the alignment of graphite.

a) 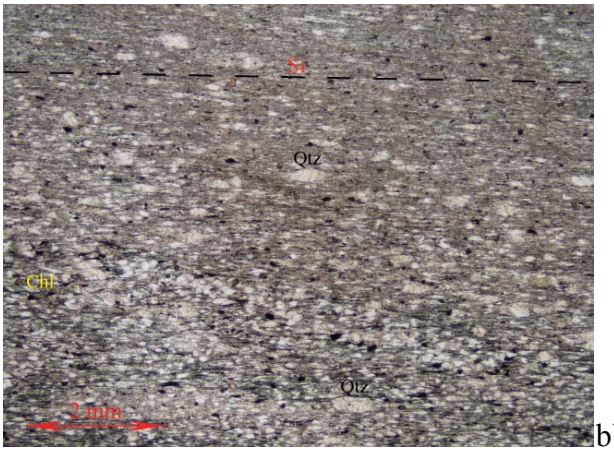

b) 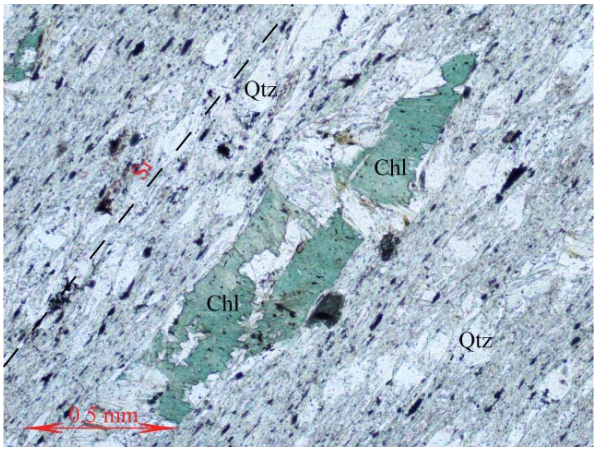

Micrographs for sample BH511. Micrograph a) is a zoomed out view showing the fine grained texture and the disjunctive cleavage. Micrograph b) shows a chlorite grain with very irregular boundaries.

Sample: BH513 – graphitic siltsone
Location: 27.0397138600N, 91.4439296722E
Rock Unit: Daling Formation

HAND SAMPLE

- Very fine grained composition, dark grey in colour. Very high graphite volume percentage with thin lensoid aggregates of quartz with a larger grain size that the groundmass (~1 – 2 mm). Lensoid aggregates are planar to semi-wavy and parallel the foliation. Also present are small 1 mm pits, maybe evidence of weathered away secondary sulphides.

THIN SECTION
Mineralogy:

- Graphite: (metamorphic mineral), 40%, very fine grained, elongate, defines foliation.
- Quartz: (detrital grains), 30% of sample, recrystallized from larger grains (polyginisation), grains show undulose extinction with some clearly formed subgrain boundaries, range from very fine grained to medium grained (<5 µm – 10 µm), composes two different areas:
  1) Lenticular shaped medium grained quartz aggregates
  2) Porphyroclasts with finer grained pressure shadows

- Muscovite: (metamorphic mineral), 30% of sample, fine grained, elongate, high birefringence (2nd order), detectable at low magnification therefore probably not sericite.

Porphyroclasts:

- Two types of porphyroclasts present:

1) Θ-type clasts, fine grained pressure shadows (≤5 μm), composed of dynamically recrystallized quartz, porphyroclast itself is ~20 μm.
2) □-type clasts, larger than Θ-clasts (~50 μm), pressure shadows tails are composed of a finer grained dynamically recrystallized quartz (≤5 μm).

Structure:

- One dominant foliation, pervasive throughout, defined by the alignment of graphite and muscovite (S_1).
- S_1: A very strong continuous cleavage
- Quartz lenses run parallel to the slaty cleavage and may show a competence contrast between the mica/graphite and the quartz.
- Pressure shadows around □-clasts curve until they become parallel to cleavage.

a) 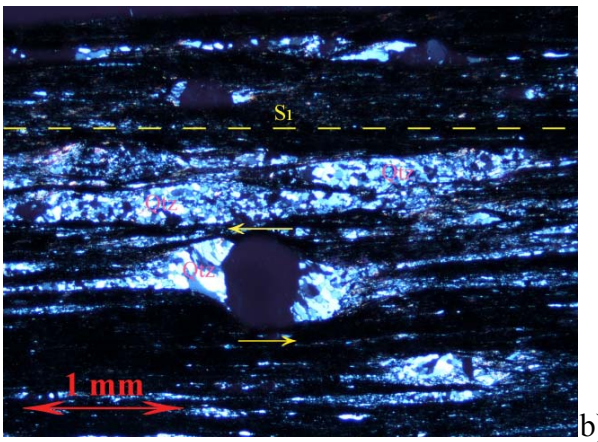

b) 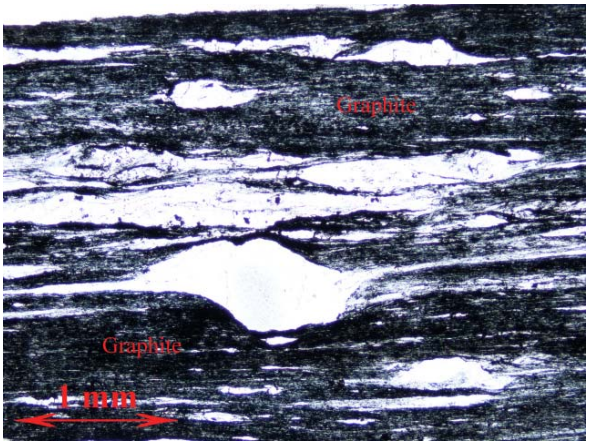

c) 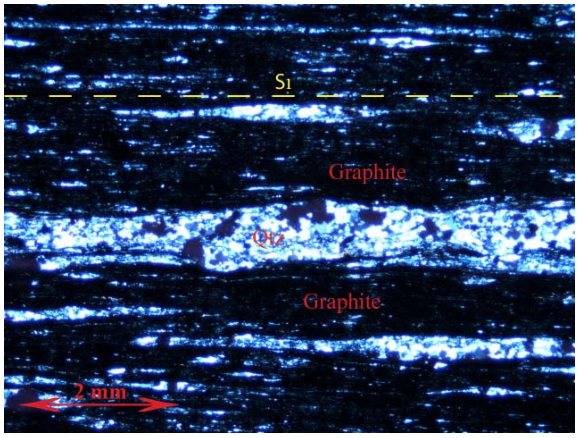

Micrographs for sample 513. Micrograph a) and b) show the □-clast of quartz with the dynamically recrystallized quartz pressure shadows in X-Nicols and PPL. Micrograph c) shows the quartz-rich lenticular shaped aggregates.

Sample: BH516 – graphitic limestone mylonite
Location: 26.9579225780N, 91.5486431122E
Rock Unit: Diuri Formation

HAND SAMPLE

- Overall very fine grained, dark grey in colour, rich in white mica and graphite, no evidence of of relict sedimentary structure, no porphyroclasts or foliations visible.

THIN SECTION

Mineralogy:

- Calcite/dolomite: 60% of sample, xenoblastic shape, grain size ranges from <1 – 10 μm, grain boundaries are very irregular and difficult to distinguish.
- Graphite: (metamorphic mineral), 20% of sample, very fine grained (≤5 μm), grains are xenoblastic and elongate shaped, occupies space between calcite grains, parallel to foliation.
- Quartz: (detrital grains), 10% of sample, grain size ranged from 5 μm – 1 mm, sub-angular to sub-round, subidioblastic shape, undulose extinction, evidence of dynamic resrystallisation by subgrain rotation.
- Sericite: (metamorphic mineral), 5% of sample, very fine grained, typically located in pressure shadows of porphyroclasts.

Sedimentary Structure:

- Calcite-rich section is flanked by calcite-poor areas.
- Calcite-poor areas are more quartz rich with quartz ranging in size from 5 μm – 1mm.

Structure:

- One main foliation in this sample, S_1.
- S_1: weak disjunctive wriggly disjunctive cleavage defined by alignment of graphite and elongate "ribbon quartz."
- Both foliations in calcite-rich and calcite-poor areas are parallel to each other.

Porphyroblasts:

- Porphyroclasts are only present in calcite-poor areas.
- Composed of millimetre scale quartz θ-type clasts, with flanking areas of very fine grained (≤1 μm) quartz and sericite.

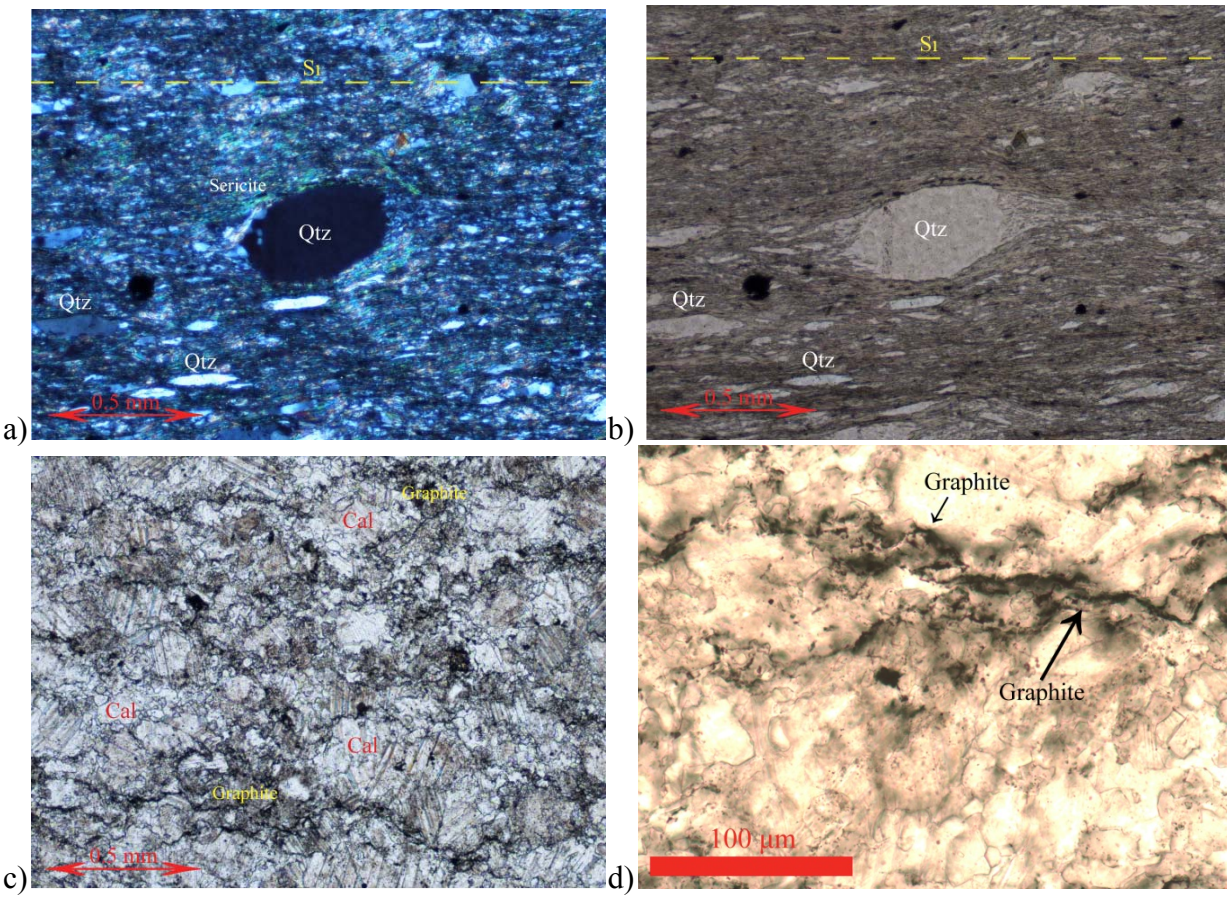

Micrographs for sample BH516. Micrograph a) and b) showing a quartz porphyroclast in X-Nicols and PPL. Micrograph c) shows the calcite-rich area and the irregular grain boundaries. Micrograph d) shows a 40x view of discrete graphite grains between calcite/dolomite grains.

Sample: BH518 – graphitic slate
Location: 26.86454415N, 91.48038089E
Rock unit: Gondwana Formation

HAND SAMPLE

- Very fine grained and charcoal grey in colour. Dominated by a very fine grained mineral, graphite, and very fine grained white micas. Foliation is visible through and is defined by lighter coloured white micas, however, the foliation is not pervasive. Planar laminae are visible as relict sedimentary structures.

THIN SECTION

Mineralogy:

- Graphite: (metamorphic mineral): 40% of sample, very fine grained (≤5 µm), defines the foliation.

- Quartz: (detrital grains): 25% of sample, ranges from very dispersed fine grained to lenses of fine grained (5 – 50 μm), undulose extinction, some have sub-grain boundaries forming, grains are subidioblastic shaped and sub-round.
- Biotite: (detrital grains): 25% of sample, fine grained (≤5 μm), elongate, defines foliation, not constrained to any specific compositional layers.
- Sericite: (metamorphic mineral): 10% of sample, very fine grained (<5 μm), occupies spaces graphite, parallel to foliation.

Sedimentary Structures:

- Straight compositional layering composed of alternating quartz-rich/graphite-poor and graphite-rich/quartz-poor layers.

Structures:

- S_1: continuous slaty cleavage defined by alignment of graphite, biotite, and sericite.

a) 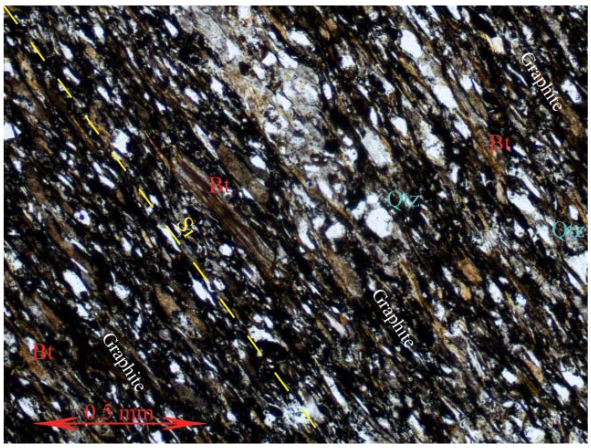

Micrograph for sample BH518. This micrograph shows the continuous slaty cleavage and abundance of graphite.

Sample: BH519 – graphitic slate to quartz arenite
Location: 26.8701606990N, 91.4800000191E
Rock Unit: Gondwana Formation

HAND SAMPLE

- Very fine grained texture with evidence of wavy lamina defined by quartz and white mica. This gives the rock a slight foliation, however, it is weak. Dominantly graphite with no porphyroclasts present.

THIN SECTION
Mineralogy:

- Graphite: (metamorphic mineral), 40% of sample, very fine grained, defines slaty cleavage.
- Quartz: (detrital grains), 40% of sample, very fine grained (~15 μm), occupies space between slaty cleavage, grains are subidioblastic, sub-round, and show undulose extinction.
- Sericite: (metamorphic mineral), 10% of sample, very fine grained, defines foliation although not as pervasive as graphite or muscovite.
- Muscovite: (metamorphic mineral), 8% of sample, relatively high birefringence, fine grained (~10 μm), located dispersed throughout entire sample.
- Rutile: (accessory mineral), 1% of sample, occupies areas along edges of micro-fractures, typical beer-bottle brown.
- Plagioclase: (detrital grains), 1% of the sample, distinct parallel barcode twinning, fine grained (<5 μm), sub-round, and subidioblastic shaped.

Sedimentary Textures:

- Evidence of compositional layering defined by alternating layers of quartz and graphite/sericite/muscovite.
- Compositional layers are wavy.

Structures:

- S_1: Defined by alignment of graphite, muscovite, and sericite, continuous slaty cleavage, areas of disjunctive cleavage within the quartz-rich zones.
- S_2: Defined by the short limbs of the crenulated graphite, crenulations are not pervasive and are only present in the more graphite-rich areas
- Discrete crenulations cleavage overprinting slaty cleavage.

a) 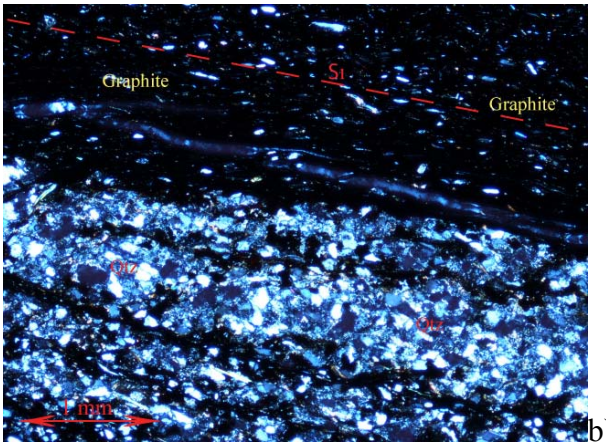

b) 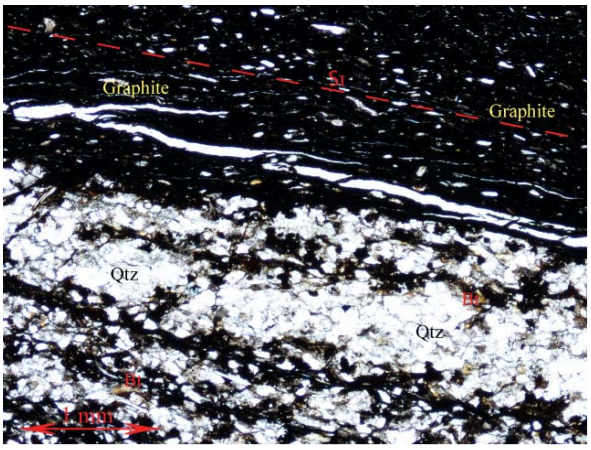

Micrographs for sample BH519. These micrographs show the compositional laminae defined by graphite-rich/quartz-rich zones. Also shows the high abundance of graphite.

Sample: BH520 – graphitic slate
Location: 26.8712765N, 91.4795655E
Rock unit: Gondwana Formation

HAND SAMPLE

- Very fine grained texture and dominantly graphite. A weak foliation is present defined by alignment of lighter coloured minerals, maybe white mica. Several larger quartz detrital grains are present.

THIN SECTION

Mineralogy:

- Graphite: (metamorphic mineral): 70% of sample, alignment defines foliation, very fine grained ~5 μm.
- Quartz: (detrital grains): 15% of sample, undulose extinction, xenoblastic shape, sub-round, grain size ranges from 5 – 1000 μm.
- Sericite: (metamorphic): 10% of sample, occupies space between graphite grains, defines foliation.
- Pyrite: (secondary): 5% of sample, forms in clusters, "raspberry-like" texture, located only in groundmass.

Porphyroclasts:

- Although not very common in this sample there was a presence of Θ-clasts, composed of pyrite.
- Porphyroclasts range in size from 0.5 – 1 mm.
- Pressure shadows are very weak and were composed of the same mineral composition as the groundmass, however, larger grained (10 μm) and fibrous.

Structure:

- S_1: continuous slaty cleavage, defined by alignment of graphite and sericite.
- Pressure shadows of porphyroclasts are parallel to foliation, porphyroclast has no inclusions or relict S_1 fabric therefore indicating they were pre-deformation.

a) 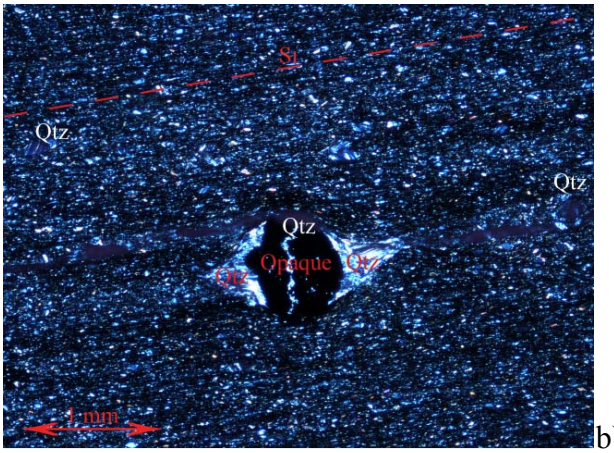

b) 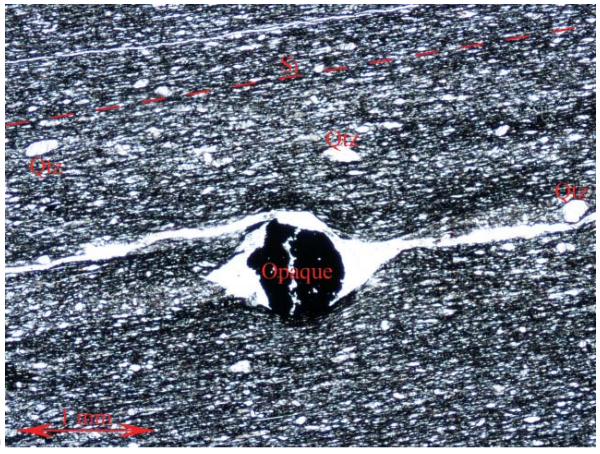

c) 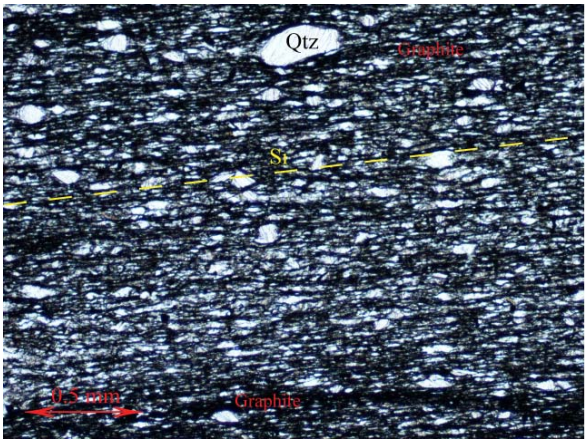

d) 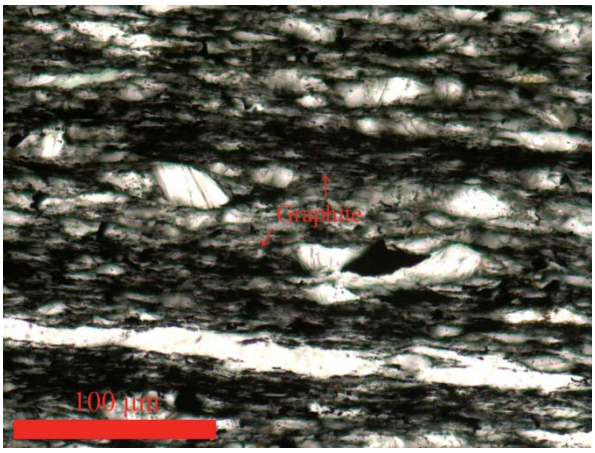

Micrographs for sample BH520. Micrographs a) and b) show the continuous slaty cleavage along with Θ-clasts of pyrite. Micrograph c) is a view of the continuous slaty cleavage. Micrograph d) shows a 40x view of highly concentrated graphite grains.

Sample: BH521 – graphitic slate
Location: 26.8775904180N, 91.4797586203E
Rock Unit: Diuri Formation

HAND SAMPLE

- Very fine grained, light grey colour, dominated by biotite, weak foliation throughout cross-cut by small scale (≤1 mm) fractures, foliation defined by alignment of opaque mineral (graphite), fractures filled with quartz, no visible porphyroclasts.

THIN SECTION
Mineralogy:

- Biotite: (detrital grains), 40% of sample, very fine grained, elongated grains (≤5 µm), defines foliation.
- Sericite: (metamorphic mineral), 20% of sample, very fine grained (≤1 µm), occupies space between graphite and quartz, parallel to main foliation.
- Graphite: **(**metamorphic mineral), 20% of sample, very fine grained (5 – 10 µm) and elongated, defines secondary foliation.
- Quartz: (detrital grains), 10% of sample, fine grained (≥10 µm), undulose extinction, xenoblastic shape, round to sub-round, grains are elongated towards main foliation.

Porphyroclats:

- One visible type of porphyroclast present, □-type clasts. Composed of quartz grains, 0.5 – 1 mm in size. Pressure shadows are composed of a finer grained quartz and sericite (10 – 20 µm).

Structure:

- S_1: Weak disjunctive cleavage defined by alignment of biotite, elongate quartz, and sericite.
- S_2: Crenulation cleavage define by alignment of graphite and a crenulation of S_1.
- S_1 foliation is more pervasive than S_2.

a) 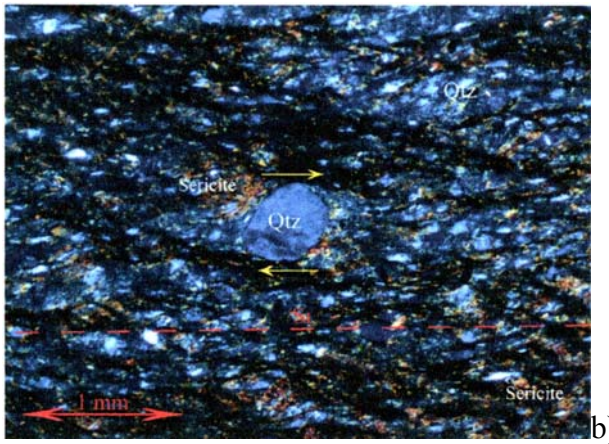

b) 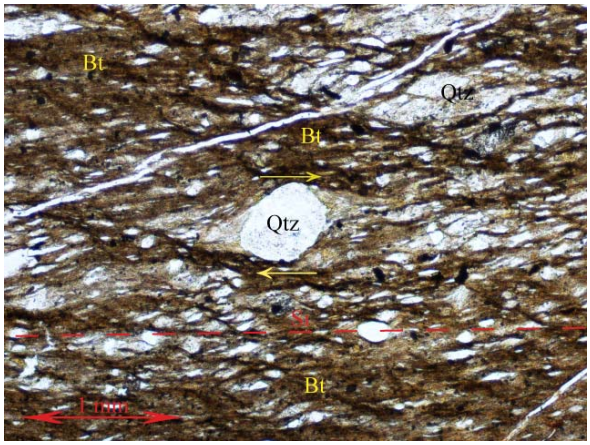

c) 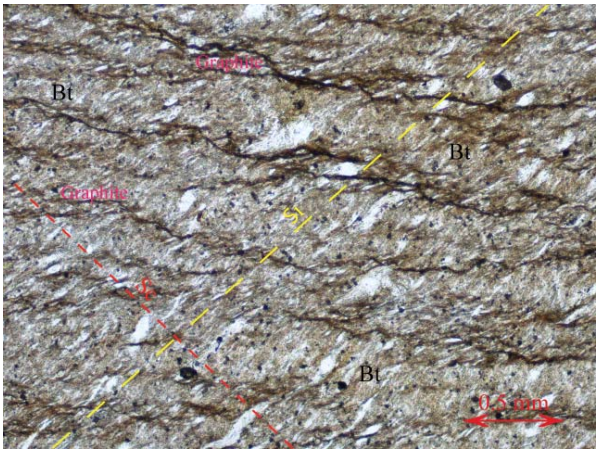

Micrographs for sample BH521. Micrographs a) and b) show the □-clasts of quartz with the finer grained quartz and sericite in the pressure shadows. Micrograph c) shows the discrete crenulation cleavage.

Sample: BH523 – graphitic siltstone
Location: 26.89226747N, 91.50638223E
Rock unit: Gondwana Formation

HAND SAMPLE

- Very fine grained texture and light grey in colour. Mineralogy is dominated by white micas and graphite. Large (~3 mm) quartz vein runs parallel to foliation. Foliation is defined by alignment of white micas. Few porphyroclasts of feldslpar (2 mm) and quartz (3 mm) are present.

THIN SECTION
Mineralogy:

- Quartz: (detrital grains), 35% of sample, composed both the matrix, porphyroclasts, and quartz grain aggregates, range from sub-angluar to round, subidioblastic, with undulose extinction, grain size is 10 – 500 μm.
- Sericite: (metamorphic mineral), 30% of sample, defines foliation, ≤5 μm in size, only present in matrix.
- Graphite: (metamorphic mineral), 30% of sample, defines foliation, very fine grained elongate mineral (≤5 μm).
- Feldspars: (detrital grains), 5% of sample, common synthetic twinning and cross-hatch twinning in plagioclase and K-feldspar, grains are subidioblastci and sub-round, range from 20 – 30 μm.

Porphyroclasts:

- One type of porphyroclast present, Θ-type clasts, composed of quartz ranging in size from 50 – 100 μm, quartz have characteristic undulose extinction, and are sub-round.
- Pressure shadows are composed of very fine grained quartz and sericite (≤5 μm).

Structure:

- S_1 is a moderately rough disjunctive cleavage defined by alignment of graphite and muscovite.

a) 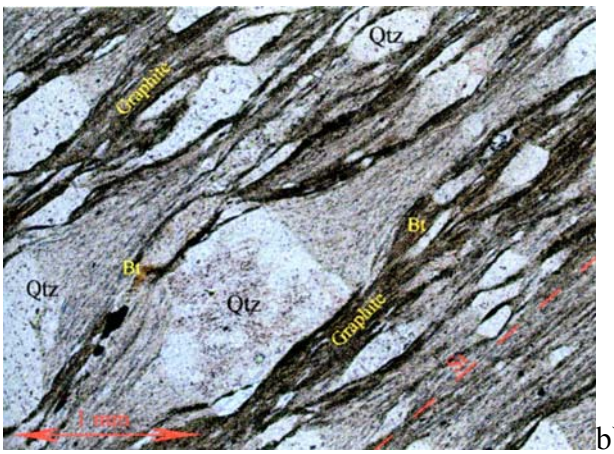

b) 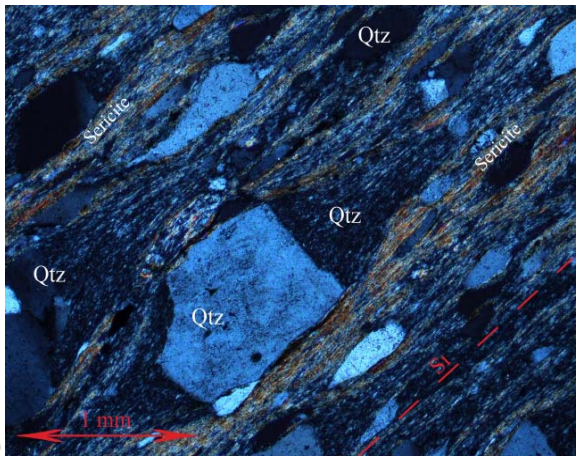

c) 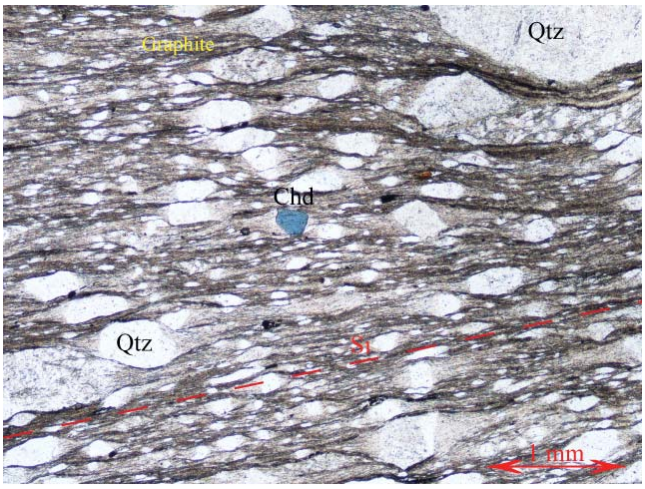

Micrographs for sample BH523. Micrographs a) and b) show the Θ-clasts of quartz and the fine grained pressure shadows, along with the moderately disjunctive cleavage. Micrograph c) is a zoomed out view and shows a single chloritoid grain along with the disjunctive cleavage.

Sample: BH524 – graphitic slate
Location: 27.0056551690N, 91.5288269520E
Rock Unit: Baxa Group

HAND SAMPLE

- Very fine grained sample, charcoal grey in colour. Wavy laminae are present as a form of relict sedimentary structure. Laminae are composed of light coloured mineral, possibly fine white micas. Very high graphite content visible from a semi-vitreous lustre. A foliation is present, however, it is weak and difficult to distinguish.

THIN SECTION
Mineralogy:

- Graphite: (metamorphic mineral), 45% of sample, very fine grained (≤5 μm), elongate, alignment of graphite defines foliation.
- Sericite: (metamorphic mineral), 40% of sample, occupies space between graphite, parallel to foliation.
- Biotite: (detrital grains), 14% of sample, very fine grained (≤5 μm), xenoblastic shape and elongate, parallel to foliation.
- Rutile: (accessory mineral), 1% of sample, occupies space along edge of micro-fractures, classic "beer-bottle brown."

Sedimentary Structure:

- Relictre texture of alternating laminae composed of graphite-rich and graphite-poor/quartz-rich zones.

Structure:

- S_o: relict sedimentary planar fabric.
- S_1: slaty cleavage defined by alignment of graphite
- S_c: cleavage refraction. Slaty cleavage is steeper in coarser and more competent quartz layers and at lower angle in finer grained, less competent layers.
- There is a small micro-fault present: shows displacement and curvature of graphite-rich laminae towards fault direct, also shows displacement of a cross-cutting fracture.
- Micro-fault is parallel to S_1.

a) 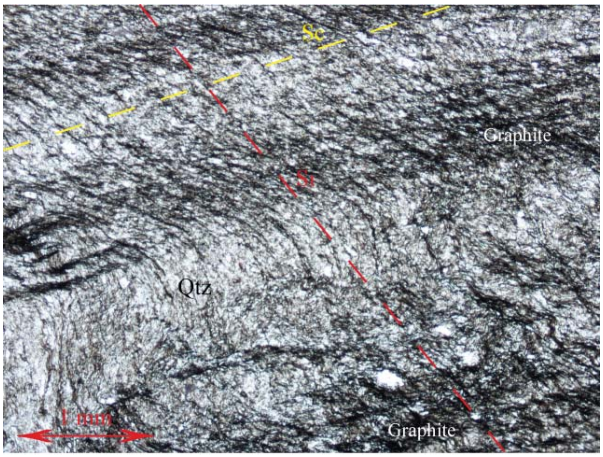

Micrograph for sample BH524. This micrograph shows the two domiant planar fabrics composed of alignment of graphite producing the slaty cleavage and the crenulation of S_1, producing S_c.

Sample: BH525 – calcareous slate
Location: 27.0403200390N, 91.4277774096E
Rock Unit: Daling Formation

HAND SAMPLE

- Very fine grained with light grey to dark grey laminae. Dark laminae are composed of biotite, light laminae are composed of white micas and quartz. Laminae are ~1 mm thick. Strong slaty cleavage is visible, defined by alignment of graphite and biotite.

THIN SECTION
Mineralogy:

- Calcite: (detrital grains/lithic fragments), 35% of sample, very fine to fine grained (5 – 50 μm), sub-angular to sub-round, and subidioblastic in shape.
- Quartz: (detrital grains), 35% very fine grained (≤5 μm), sub-round, subidioblastic to xenoblastic in shape, undulose extinction, subgrain boundaries formation in some grains.
- Sericite: (metamorphic mineral), 15% of sample, occupies space between quartz, calcite, and graphite, parallel to foliation.
- Graphite: (metamorphic mineral), 15% of sample, very fine grained (5 – 10 μm), elongate and irregular, defines foliation.

Structure:

- $S_{0:}$ relict sedimentary planar fabric.
- S_1 is a rough disjunctive cleavage defined by alignment of graphite.

a) 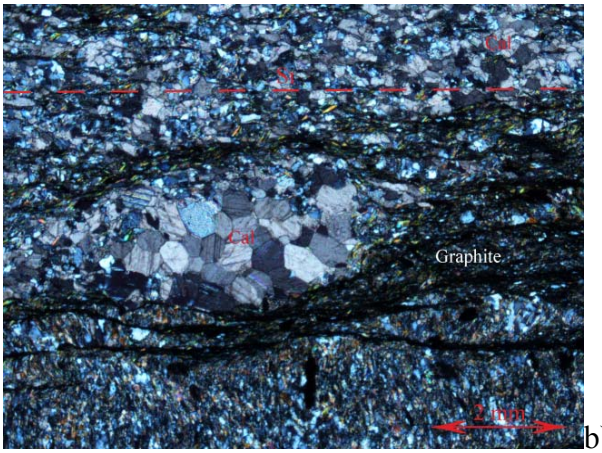

b) 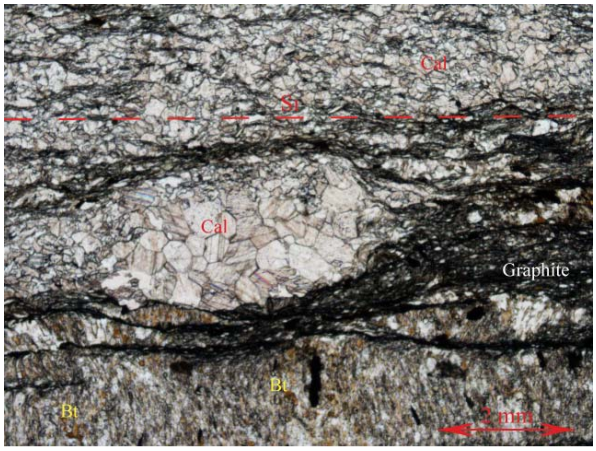

Micrographs for sample BH525. These micrographs show the large scale quartz and calcite lithic fragment (aggregate) with the rough disjunctive cleavage in the matrix.

Sample: BH526a – graphitic meta-siltstone
Location: 27.1779388190N, 91.5982478857E
Rock Unit: Daling Formation

HAND SAMPLE

- Very fine grained sample, light grey in colour. Relict sedimentary cross-bedding visible. Strong foliation throughout. Foliation is defined by alignment of white mica and graphite.

THIN SECTION
Mineralogy:

- Quartz: (detrital grains), 30% of sample, fine grained (10 – 20 μm), equigranular throughout sample, undulose extinction is common, xenoblastic shape with irregular grain boundaries, sub-angular to sub-round, parallel to foliation.
- Sericite: (metamorphic mineral), 30% occupies space between graphite and biotite, parallel to foliation.
- Graphite: (metamorphic mineral), 20% of sample, very fine grained (5 – 10 μm), elongate with irregular shapes, defines foliation.
- Biotite: (metamorphic mineral), 20% of sample, very fine grained (5 – 10 μm), irregular grain boundaries, defines foliation.

Sedimentary Structure:

- Relict sedimentary cross-bedding and thin (1 mm) relict laminae.

Structure:

- One foliation present: S_1.
- S_1 is a strong disjunctive cleavage defined by alignment of graphite and biotite.

a) 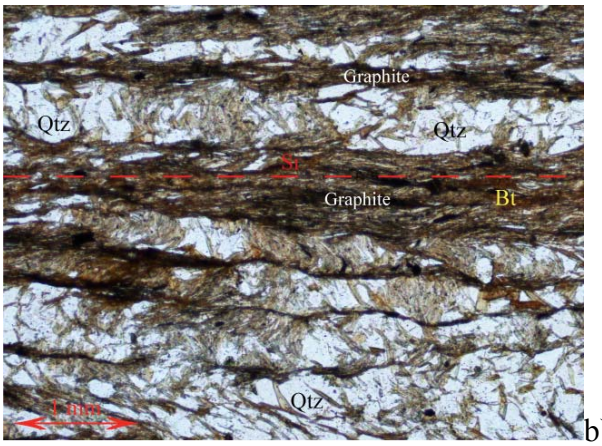

b) 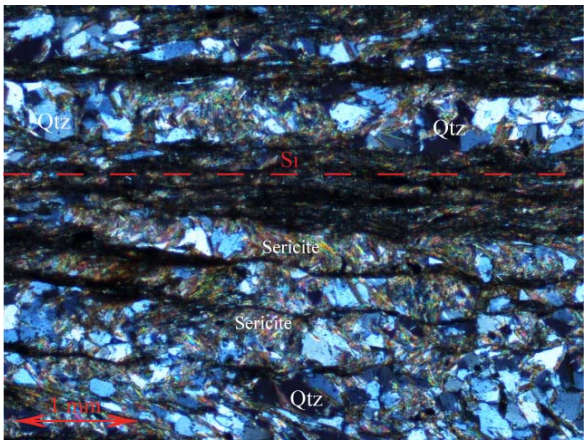

c) 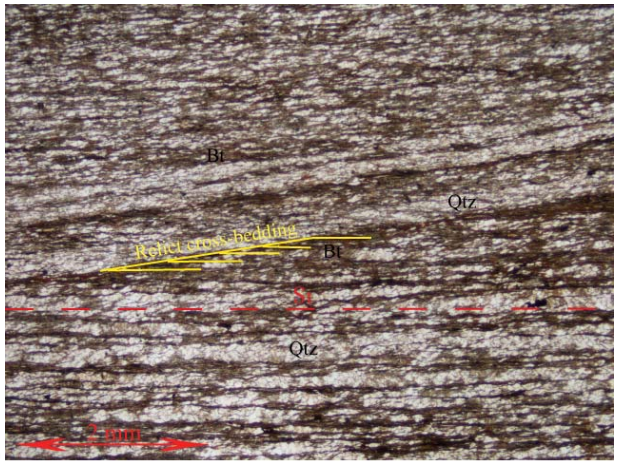

Micrographs for sample BH526a. Micrographs a) and b) show the strong disjunctive cleavage, and micrograph c) shows the relict cross-bedding.

Sample: BH526b – graphite bearing meta-quartzite
Location: 27.1779388190N, 91.5982478857E
Rock Unit: Daling Formation

HAND SAMPLE

- Very fine grained sample with distinct compositional banding composed of alternating graphite-rich/white mica-rich bands. Bands are relict sedimentary laminae. Compositional bands are planar. No porphyroclasts are present.

THIN SECTION
Mineraology:

- Quartz: (detrital grains), 60% of sample, fine grained (10 – 20 μm), equigranular, subidioblastic, sub-round to sub-angular, undulose extinction is very common.

- Graphite: (metamorphic mineral), 15% of sample, very fine grained (≤5 μm), not very common in mica-rich laminae, defines foliation.
- Biotite: (metamorphic mineral), 15% of sample, fine grained (10 – 20 μm), found in graphite-rich laminae, xenoblastic shape with irregular boundaries, also parallel to foliation.
- Sericite: (metamorphic mineral), 10% of sample, occupies space between quartz grains, parallel to foliation.

Sedimentary Structure:

- Planar alternating laminae of quartz/mica-rich bands and biotite/graphite-rich bands.
- Laminae are 2 – 5 mm thick.

Structure:

- One foliation present: S_1.
- S_1 is a complete disjunctive cleavage defined by alignment of graphite and biotite in graphite/biotite-rich layers, and parallel trending sericite in quartz-rich layers.

a) 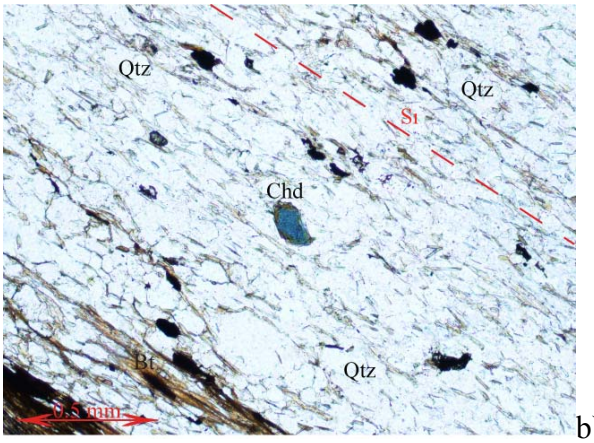

b) 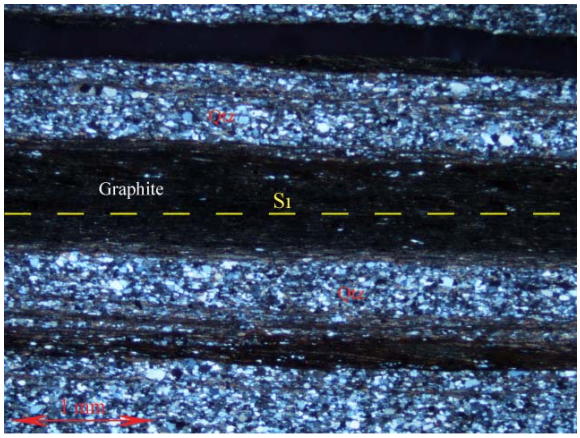

Micrographs for sample BH526b. Micrograph a) shows the high amount of quartz, along with the disjunctive cleavage and a single chloritoid grain. Micrograph b) shows the planar laminae of alternating quartz/mica-rich bands and biotite/graphite-rich bands.

Sample: BH527 – graphitic limestone
Location: 27.2191482780N, 91.5837049484E
Rock Unit: Daling Formation

HAND SAMPLE

- Very fine grained texture, light grey in colour. Sample is dominated by calcite, with graphite being relatively scarce. Multiple aggregates of calcite and quartz are present (not porphyroclasts) that range in size from 2 – 4 mm. Foliation is visible and defined by muscovite and biotite.

THIN SECTION

Mineralogy:

- Calcite/Dolomite: (detrital grains), 70% of sample, fine grained (10 – 20 μm), inequigranular with very irregular grain boundaries, xenoblastic texture, sub-round shape, along with quartz composes several large (2 – 4 mm) lithic fragments.
- Biotite: (metamorphic mineral), 10% of sample, fine grained (10 – 20 μm), irregular boundaries, subidioblastic, defines foliation.
- Quartz: (detrital grains), 10% of sample, very fine grained (5 – 10 μm), sub-round to sub-angular, undulose extinction is common, equigranular. Composes several lithic fragments throughout sample.
- Muscovite: (metamorphic mineral), 5% of sample, very fine grained (5 – 10 μm), irregular boundaries, defines foliation.
- Graphite: (metamorphic mineral), 5% of sample, very fine grained (≤5 μm), elongate, defines foliation.

Structure:

- S_1 is a moderate disjunctive cleavage defined by the alignment of muscovite, biotite, and graphite between calcite/dolomite grains.
- S_2 is a slight, not pervasive, crenulations of S_1 foliation.

a) 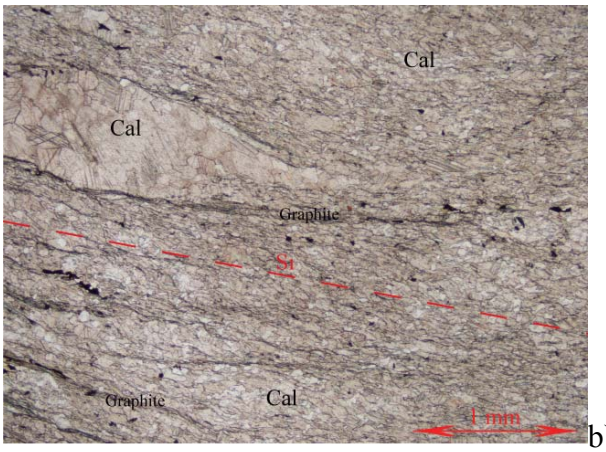

b) 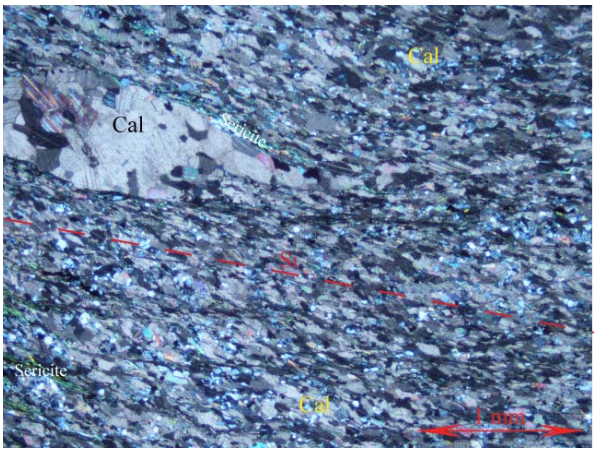

Micrographs for sample BH527. These micrographs show the high amount of calcite in both X-Nicols and PPL, and shows large scale calcite lithic fragments (aggregates).

Sample: BH528 – graphitic mylonite
Location: 27.2191482780N, 91.5837049484E
Rock Unit: Daling Formation

HAND SAMPLE

- Very fine grained sample, charcoal grey in colour. Difficult to determine if any structures are present. Some white mica along with quartz present. No porphyroclasts.

THIN SECTION

Mineralogy:

- Graphite: (metamorphic mineral), 60% of sample, grain size ranges from 5 – 200 µm, difficult to see any fabric composed of graphite.
- Quartz: (detrital grains), 30% of sample, grain size ranges from 10 – 100 µm, sub-angular to sub-round, subidioblastic shape, undulose extinction is common.
- Sericite: (metamorphic mineral), 10% of sample, parallel to foliation in graphite-rich areas.

Sedimentary Structure:

- Two distinctive layers in the sample.
  - 1) Defined by large amount of graphite.
  - 2) Defined by a more quartz-rich layer, with a presence of sericite.
- Relict sedimentary layering.

Structure:

- S_1 is a slaty cleavage defined by alignment of sericite within graphite-rich zones.
- Graphite-rich zones are massive and almost structureless, therefore S_1 is very difficult to distinguish.

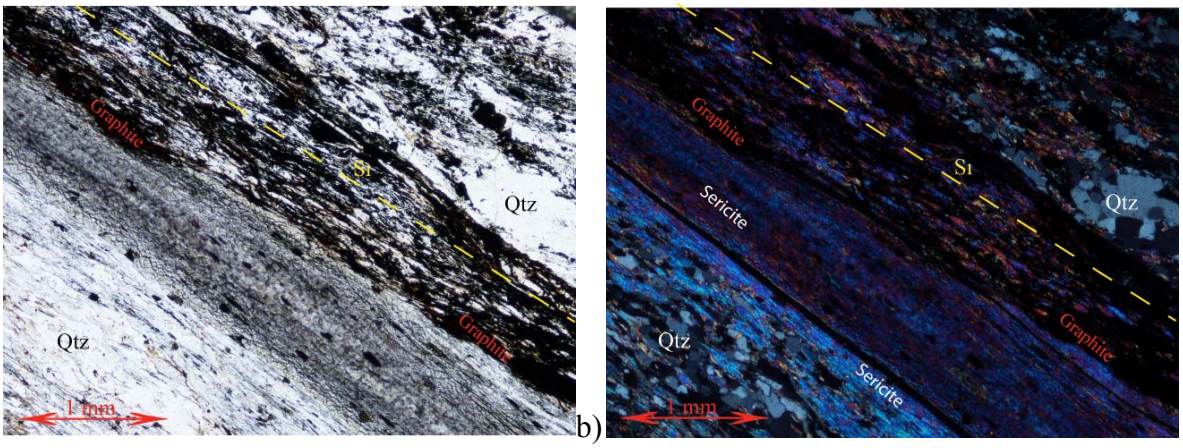

Micrographs for sample BH528. These micrographs show the slaty cleavage and the distinct alternating laminae of quartz-rich/graphite-rich laminae.

Sample: BH529 – graphitic slate
Location: 27.2238367800N, 91.5538251400E
Rock Unit: Daling Formation

HAND SAMPLE

- Very fine grained sample, charcoal grey in colour. Highly graphitic, which gives it a semi-lustrous shine. No or porphyroclasts visible.

THIN SECTION
Mineralogy:

- Graphite: (metamorphic mineral), 80% of sample, grain size difficult to determine, graphite is structureless (massive).
- Quartz: (detrital grains), 20% of sample, very fine grained (≤5 µm), occupies area between massive graphite, irregular grain boundaries, sub-round, xenoblastic shape, undulose extinction is common.

Structure:

- Sample is structureless.

a) 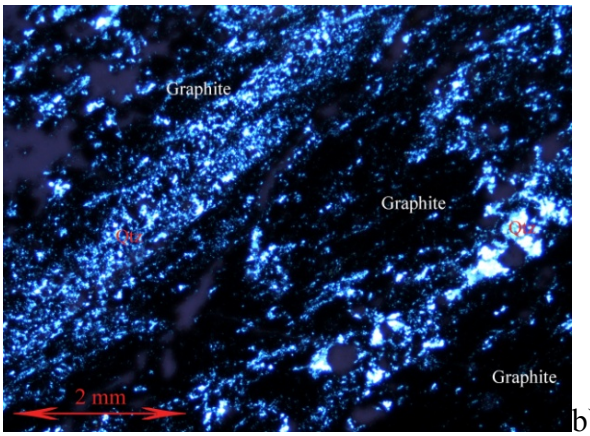

b) 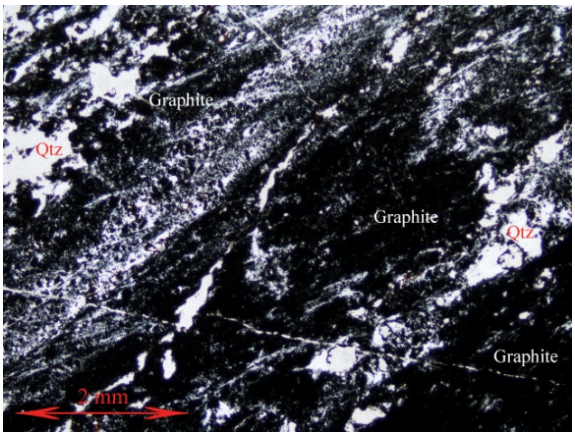

Micrographs for sample BH529. These micrographs show the overall massive (structureless) texture, and the very high amount of graphite within the sample.

APPENDIX B – RAMAN SPECTROSCOPY DATA

		Areas					Peak Heights			Temperatures	
	Analysis #	D1	D2	D3	G	R2	D1	G	R1	Temp. °C (Beyssac)	Temp. °C (Rahl)
BH507	1	31406.46	3596.52	0.00	65146.80	0.31	527.26	1790.39	0.29	501.45	489.94
	2	14118.08	1163.40	0.00	31242.69	0.30	296.85	1179.01	0.25	505.96	488.97
	3	55928.54	4376.81	0.00	51748.52	0.50	1028.65	1622.28	0.63	418.89	375.22
	4	40813.27	5082.71	0.00	35206.12	0.50	733.17	1151.31	0.64	417.06	371.43
	5	58213.21	5253.89	0.00	47419.42	0.52	1009.72	1436.84	0.70	407.38	362.20
	6	51581.34	5850.65	0.00	40248.55	0.53	916.16	1286.46	0.71	406.01	360.85
	7	46457.99	4105.84	0.00	61593.19	0.41	831.89	1960.90	0.42	456.67	416.57
	8	30983.57	3045.93	0.00	41691.21	0.41	581.15	1293.93	0.45	458.91	428.16
	9	56091.14	5694.88	0.00	75222.01	0.41	915.54	2286.11	0.40	458.82	415.69
	10	53771.49	5025.18	0.00	63383.95	0.44	889.35	1938.96	0.46	445.16	397.53
	11	25935.69	2259.50	0.00	24490.97	0.49	463.37	745.44	0.62	421.94	379.81
	12	74849.71	6420.28	0.00	116480.00	0.38	1436.37	4318.04	0.33	472.56	430.96
	13	48070.80	3933.78	0.00	58717.95	0.43	789.44	1826.88	0.43	447.80	397.28
	14	53328.94	5096.10	0.00	51402.60	0.49	968.04	1640.58	0.59	424.92	379.94
BH511	1	54212.71	5511.97	0.00	44668.07	0.52	1042.05	952.39	1.09	409.90	436.78
	2	103300.00	11016.50	0.00	88141.78	0.51	1534.87	1629.98	0.94	413.95	422.71
	3	72004.98	5467.11	0.00	55853.61	0.54	1354.47	1171.70	1.16	400.67	423.21
	4	104000.00	7222.04	0.00	74836.67	0.56	1840.76	1510.08	1.22	392.26	411.14
	5	53289.52	3826.50	0.00	42025.05	0.54	969.76	867.90	1.12	401.81	420.65
	6	57311.23	4939.79	0.00	41679.92	0.55	1055.44	902.12	1.17	395.61	412.93
	7	49791.98	1829.54	0.00	39774.79	0.54	774.66	650.71	1.19	398.57	422.68
	8	106790.00	6862.24	0.00	78542.50	0.56	1878.28	1510.77	1.24	393.74	417.64
	9	39455.62	3143.09	0.00	31711.12	0.53	789.09	702.36	1.12	404.72	428.50
	10	72590.08	5385.98	0.00	56790.95	0.54	1379.76	1218.92	1.13	401.31	421.48

BH513	1	27654.08	2115.51	0.00	34042.01	0.43	475.80	779.49	0.61	448.15	440.18
	2	125080.00	9324.48	0.00	157430.00	0.43	1921.53	3229.79	0.59	450.27	441.82
	3	47276.08	4331.25	0.00	61049.37	0.42	812.64	1431.89	0.57	454.26	445.17
	4	99590.24	8342.50	0.00	126390.00	0.43	1595.48	2755.06	0.58	451.87	442.08
	5	117100.00	7914.04	0.00	150250.00	0.43	1806.01	2903.09	0.62	451.69	451.25
	6	137990.00	11178.11	0.00	152240.00	0.46	2285.83	3435.68	0.67	437.27	426.02
	7	130940.00	7954.08	0.00	200650.00	0.39	1911.41	3655.11	0.52	469.39	471.59
	8	133000.00	8395.99	0.00	169630.00	0.43	2107.28	3517.98	0.60	450.71	444.32
	9	136100.00	10188.73	0.00	187390.00	0.41	2105.08	3802.73	0.55	459.49	455.03
	10	135650.00	9839.98	0.00	173620.00	0.43	2139.17	3479.35	0.61	451.84	450.54
	11	138060.00	8416.85	0.00	220940.00	0.38	1957.93	4155.03	0.47	473.79	469.67
BH516	1	225360.00	13041.99	0.00	115220.00	0.64	2997.63	1667.16	1.80	357.41	371.99
	2	187330.00	10922.19	0.00	96364.63	0.64	2669.06	1463.11	1.82	358.05	374.26
	3	197750.00	8490.05	0.00	103670.00	0.64	2660.81	1494.26	1.78	357.05	370.59
	4	121680.00	6960.20	0.00	63831.55	0.63	1545.46	952.76	1.62	359.67	369.64
	5	236830.00	15679.57	0.00	116770.00	0.64	3288.29	1771.22	1.86	355.61	369.16
	6	222140.00	19372.41	0.00	106400.00	0.64	2811.59	1487.58	1.89	356.87	372.78
	7	315550.00	12223.25	0.00	173050.00	0.63	4128.36	2390.30	1.73	360.62	378.72
	8	68641.36	5115.00	0.00	34011.02	0.64	904.27	510.43	1.77	357.56	373.10
	9	123340.00	7216.34	0.00	66182.29	0.63	1614.34	973.43	1.66	362.02	378.78
	10	112230.00	7704.74	0.00	58997.01	0.63	1396.41	845.44	1.65	361.89	378.09
BH518	1	623630.00	106370.00	93413.10	244720.00	0.64	6005.98	4122.22	1.46	356.29	349.68
	2	492550.00	81264.51	50137.83	205330.00	0.63	5372.82	3615.08	1.49	359.69	360.25
	3	428730.00	81061.28	39509.14	157650.00	0.64	4561.28	2801.68	1.63	355.15	359.16
	4	441910.00	67858.73	59388.48	155120.00	0.66	4759.16	3034.42	1.57	345.24	331.66
	5	267170.00	55279.59	28062.60	82638.99	0.66	2977.83	1525.44	1.95	347.51	350.96
	6	558600.00	100140.00	86426.24	169440.00	0.67	5357.68	3186.01	1.68	340.85	327.70
	7	234080.00	48494.65	22085.09	78581.51	0.65	2371.56	1318.28	1.80	352.58	360.44
	8	362240.00	66036.73	80881.08	91659.46	0.70	3320.37	1869.04	1.78	330.97	307.91

	9	366300.00	54938.35	66210.13	142330.00	0.65	3850.62	2306.57	1.67	351.77	353.27
	10	516820.00	82061.12	82108.19	205380.00	0.64	4584.86	3142.51	1.46	355.04	346.87
BH519	1	362670.00	42529.67	63294.82	167990.00	0.63	3174.27	2486.30	1.28	359.44	339.29
	2	288790.00	24940.49	42026.14	166840.00	0.60	2785.42	2118.47	1.31	373.59	377.45
	3	214240.00	26207.99	37109.95	79442.58	0.67	2091.00	1230.86	1.70	342.97	333.60
	4	324270.00	45025.03	82337.14	149000.00	0.63	2904.93	2223.01	1.31	362.59	350.20
	5	187580.00	19708.12	21557.00	94260.48	0.62	1775.40	1333.44	1.33	364.19	356.68
	6	458740.00	97084.53	95066.67	129820.00	0.67	4345.47	2356.06	1.84	343.27	339.30
	7	161260.00	29611.93	16065.81	63000.10	0.64	1868.11	1027.43	1.82	358.34	374.79
	8	379730.00	83739.93	40529.23	152100.00	0.62	3774.90	2245.49	1.68	366.49	389.16
	9	242740.00	35875.36	64469.94	86882.62	0.66	2240.84	1302.00	1.72	345.46	340.55
	10	553910.00	97807.59	61993.19	253950.00	0.61	5138.34	3565.47	1.44	368.84	378.41
BH520	1	252790.00	38104.79	20677.44	104850.00	0.64	2973.19	1576.42	1.89	356.75	372.42
	2	309750.00	58436.48	56227.33	84334.42	0.68	3625.17	1352.83	2.68	336.40	285.40
	3	409220.00	69007.54	55811.83	120330.00	0.68	4575.37	2020.25	2.26	336.76	318.94
	4	353370.00	47645.30	34877.58	132680.00	0.66	4222.89	2233.21	1.89	346.36	347.59
	5	292030.00	34847.98	35528.77	115410.00	0.66	3366.96	1867.29	1.80	347.18	347.62
	6	447830.00	64681.97	49736.96	161430.00	0.66	5188.74	2642.41	1.96	345.30	345.72
	7	356680.00	47032.57	48235.49	129010.00	0.67	3955.90	2016.86	1.96	343.05	340.33
	8	268580.00	52376.73	39410.54	81244.56	0.67	3136.08	1435.10	2.19	343.84	338.99
	9	207550.00	31157.34	26254.80	85982.59	0.64	2298.70	1253.63	1.83	356.54	370.89
	10	347630.00	58582.59	29616.21	124720.00	0.65	4033.15	2055.28	1.96	349.63	356.11
BH521	1	385690.00	61644.41	49460.76	126980.00	0.67	4212.31	2122.02	1.99	342.15	338.21
	2	373440.00	40827.25	35656.61	147470.00	0.66	4031.52	2339.75	1.72	345.17	339.93
	3	459700.00	68128.95	61875.18	152550.00	0.68	4871.91	2428.67	2.01	340.33	333.81
	4	277500.00	43003.84	29689.68	95647.12	0.67	3035.48	1645.24	1.85	344.26	341.70
	5	197160.00	26305.93	32983.58	57214.86	0.70	2246.67	1113.10	2.02	328.42	305.18
	6	254880.00	44416.88	39828.37	70908.59	0.69	2907.85	1403.63	2.07	334.63	319.54
	7	122860.00	18993.39	18039.28	41168.71	0.67	1368.39	740.68	1.85	342.28	337.00

	8	161420.00	25839.90	32361.72	42173.16	0.70	1843.15	872.42	2.11	327.92	302.74
	9	193280.00	25671.92	24972.06	68503.18	0.67	2085.36	1156.55	1.80	341.79	334.69
	10	300680.00	54326.20	60151.13	66733.02	0.71	3299.59	1339.95	2.46	323.74	275.60
	11	152900.00	27115.33	27499.26	43150.22	0.69	1673.66	740.95	2.26	336.11	317.64
BH523	1	188850.00	42510.58	30172.65	51978.48	0.67	1947.65	1109.43	1.76	344.40	339.38
	2	134760.00	22656.33	19744.51	44979.90	0.67	1398.13	794.48	1.76	344.71	340.28
	3	143440.00	22135.29	21396.74	49550.26	0.67	1474.95	896.66	1.64	344.29	334.04
	4	417950.00	57768.80	41689.05	147880.00	0.67	4207.05	2592.39	1.62	342.75	329.11
	5	185330.00	35985.03	19048.63	53282.64	0.67	2025.20	957.26	2.12	340.66	333.24
	6	90744.66	14669.41	9423.39	30333.06	0.67	982.25	581.76	1.69	343.53	334.44
	7	399000.00	44284.31	82234.42	119250.00	0.71	3977.69	2518.99	1.58	325.37	284.72
	8	268300.00	38182.18	25124.73	112350.00	0.64	2812.77	1927.52	1.46	355.94	349.04
	9	174070.00	30232.11	39553.72	37104.48	0.72	1847.75	971.45	1.90	320.13	284.85
	10	145510.00	34515.28	20959.90	35159.22	0.68	1511.31	616.18	2.45	340.09	315.55
BH524	1	233450.00	20933.48	0.00	136870.00	0.60	3012.30	1938.71	1.55	375.48	403.18
	2	227760.00	14964.79	0.00	132720.00	0.61	2864.83	1825.12	1.57	371.04	393.63
	3	227050.00	15918.53	0.00	126880.00	0.61	2670.27	1719.99	1.55	367.81	384.71
	4	584610.00	70311.13	97762.66	261990.00	0.64	7035.30	4506.84	1.56	357.27	360.02
	5	318890.00	45447.14	51801.62	109150.00	0.67	4030.74	2262.63	1.78	341.30	332.84
	6	238790.00	19995.26	0.00	133110.00	0.61	2673.05	1812.45	1.47	369.85	383.70
	7	309640.00	36342.09	38735.19	118720.00	0.67	3776.15	2208.21	1.71	344.49	337.75
	8	278660.00	40874.78	46802.98	98561.95	0.67	3480.46	2079.65	1.67	344.41	335.84
	9	222520.00	37000.79	25665.02	70937.03	0.67	2947.73	1501.51	1.96	341.35	336.25
	10	426250.00	49439.79	51234.83	173100.00	0.66	5800.31	3323.20	1.75	348.64	349.16
BH525	1	56360.09	4416.53	0.00	84930.88	0.39	940.22	1963.06	0.48	468.87	459.35
	2	80506.99	5889.40	0.00	153580.00	0.34	1135.42	2934.44	0.39	491.71	491.09
	3	78789.73	2593.11	0.00	108340.00	0.42	1167.83	1975.86	0.59	456.20	455.15
	4	33568.84	2105.59	0.00	40789.92	0.44	601.91	958.59	0.63	445.64	438.01
	5	88064.39	3694.26	0.00	152370.00	0.36	1406.70	2905.99	0.48	480.48	488.41

	6	70731.33	2915.85	0.00	126330.00	0.35	941.56	2307.05	0.41	483.60	477.07
	7	44351.70	4067.46	0.00	57186.59	0.42	710.95	1277.69	0.56	454.11	442.28
	8	48751.13	3601.74	0.00	66095.01	0.41	856.46	1578.08	0.54	457.85	448.06
	9	46986.98	2566.28	0.00	53346.28	0.46	776.33	1106.16	0.70	437.80	434.94
	10	40425.87	3575.71	0.00	42689.61	0.47	669.29	982.39	0.68	433.49	420.32
	11	53282.91	6630.57	0.00	45018.03	0.51	716.34	941.79	0.76	415.03	392.24
BH526a	1	15640.49	1505.83		37136.09	0.29	290.84	904.14	0.32	512.78	524.46
	2	69797.26	14084.88	10892.19	22420.84	0.66	556.60	457.48	1.22	348.82	306.69
	3	20282.62	1250.11	0.00	25438.08	0.43	329.35	686.14	0.48	448.84	411.58
	4	22240.55	1038.20	0.00	40397.16	0.35	339.04	935.89	0.36	485.57	469.96
	5	37621.29	6536.23	2627.68	11563.91	0.68	368.42	239.74	1.54	340.55	318.22
	6	25493.02	1193.18	0.00	29353.11	0.45	385.69	784.18	0.49	438.56	389.79
	7	33263.47	3001.46	0.00	42199.37	0.42	468.17	936.84	0.50	452.35	424.74
	8	23388.54	1973.80	0.00	36714.92	0.38	388.65	875.40	0.44	473.34	461.47
	9	20439.18	1882.15	0.00	34907.65	0.36	373.87	911.61	0.41	482.07	473.90
	10	18581.29	1444.71	0.00	27450.73	0.39	297.52	672.91	0.44	466.84	445.42
	11	27372.96	1677.27	0.00	44822.14	0.37	438.52	1142.38	0.38	476.11	452.89
	12	42758.57	321.24	0.00	83711.22	0.34	573.65	1564.69	0.37	490.93	483.95
BH526b	1	42779.79	1300.25		77172.02	0.35	737.74	1806.92	0.41	484.00	478.05
	2	52217.96	3769.47	3355.52	99155.35	0.34	784.08	2194.84	0.36	491.22	482.19
	3	27175.95	1491.47	0.00	42100.12	0.38	483.84	1062.55	0.46	470.11	456.55
	4	30595.00	2190.08	0.00	52536.64	0.36	533.37	1376.47	0.39	481.43	466.58
	5	41598.19	3794.03	6712.79	57662.96	0.40	546.43	1184.15	0.46	461.38	437.10
	6	26878.25	1739.18	0.00	51414.52	0.34	476.47	1205.04	0.40	491.55	492.87
	7	54885.77	2588.77	0.00	101650.00	0.34	800.00	2104.02	0.38	487.51	479.28
	8	39501.10	2222.87	0.00	77514.47	0.33	643.04	1740.97	0.37	493.58	491.02
	9	40847.09	2710.60	0.00	73755.40	0.35	674.19	1826.38	0.37	486.06	472.92
	10	29767.30	1352.91	0.00	61981.53	0.32	526.53	1575.07	0.33	498.72	494.11
	11	76859.32	5193.12	4053.72	110660.00	0.40	1232.81	2372.48	0.52	463.52	456.26

	12	22100.49	1717.03	0.00	40581.20	0.34	392.82	1048.44	0.37	488.28	479.70
BH527	1	13367.22	1932.91	0.00	24870.86	0.33	262.44	695.22	0.38	492.92	491.55
	2	24443.82	2749.00	0.00	37364.36	0.38	467.26	1042.92	0.45	472.51	460.48
	3	89348.65	9235.65	67848.10	140630.00	0.37	1009.35	2777.77	0.36	474.79	444.40
	4	21897.34	1625.40	0.00	44380.20	0.32	408.94	1228.95	0.33	497.50	490.77
	5	17657.21	1145.60	0.00	34137.21	0.33	337.33	929.53	0.36	492.58	486.93
	6	17939.23	1259.28	0.00	36102.00	0.32	335.69	968.50	0.35	496.64	492.40
	7	12062.38	597.82	0.00	24834.95	0.32	232.39	665.01	0.35	497.84	496.02
	8	26802.81	1544.18	0.00	53516.57	0.33	482.34	1463.38	0.33	495.30	484.67
	9	24535.74	1147.23	0.00	37494.92	0.39	430.29	1042.56	0.41	468.18	441.26
	10	19525.74	1383.26	0.00	41105.29	0.31	371.69	1111.62	0.33	500.89	499.33
	11	15254.02	1040.20	0.00	33218.98	0.31	313.07	895.59	0.35	503.90	510.59
	12	37475.47	2050.74	0.00	84383.10	0.30	712.90	2316.46	0.31	506.41	505.44
	13	31144.52	2497.59	0.00	71220.61	0.30	541.85	1858.64	0.29	508.83	506.83
BH528	1	52228.00	9787.02	11194.25	98625.37	0.33	728.43	2584.10	0.28	496.32	474.19
	2	12974.16	3123.46	0.00	27996.34	0.29	204.47	926.29	0.22	510.06	490.05
	3	39193.55	28669.25	70794.41	72738.75	0.28	481.71	1899.00	0.25	516.95	515.85
	4	42011.33	11544.05	30494.55	88414.19	0.30	640.28	2285.46	0.28	509.32	504.88
	5	60507.63	16317.78	58892.44	91799.48	0.36	753.07	2239.71	0.34	481.32	452.91
	6	32967.15	6210.76	3066.68	49359.90	0.37	384.74	987.96	0.39	475.30	452.39
	7	46354.15	12378.26	11361.14	99681.04	0.29	628.36	2371.62	0.26	510.79	504.20
	8	53173.30	28481.25	101120.00	101180.00	0.29	640.51	1963.82	0.33	511.58	522.78
	9	62303.42	7166.15	5929.93	135010.00	0.30	926.58	3329.25	0.28	505.41	495.01
	10	38650.06	16239.73	19518.80	84254.77	0.28	528.69	2321.45	0.23	517.39	509.62
	11	45883.50	13420.34	15408.02	88208.55	0.31	656.96	2126.19	0.31	502.58	496.59
BH529	1	73130.62	8374.71	0.00	153220.00	0.31	1019.91	3339.34	0.31	502.36	495.08
	2	42435.08	5405.79	0.00	96776.31	0.29	568.03	2255.39	0.25	510.42	499.69
	3	74795.56	8357.49	0.00	153370.00	0.32	1027.26	3339.82	0.31	500.28	490.68
	4	79945.83	8897.46	5576.11	142090.00	0.35	946.05	3055.37	0.31	486.95	459.27

5	41798.09	4681.13	0.00	101240.00	0.28	656.34	2710.56	0.24	515.08	508.14
6	70913.96	10259.38	12464.95	170080.00	0.28	1008.51	3779.66	0.27	515.40	515.79
7	56079.14	5930.26	0.00	159410.00	0.25	824.38	3703.75	0.22	528.29	534.29
8	43038.93	4621.97	0.00	117350.00	0.26	691.06	3300.33	0.21	524.93	522.47
9	56703.30	7752.66	0.00	151330.00	0.26	849.20	3314.95	0.26	524.06	533.60
10	59953.50	6352.67	0.00	135010.00	0.30	750.71	2857.88	0.26	508.48	498.03
11	62712.47	6780.76	0.00	145940.00	0.29	865.92	3201.65	0.27	511.46	507.35